MicroRNA Detection using Silver Nanoparticles and SERS

by

Laila Al-Maqbali

2018

Final thesis submitted to the Department of Pure and Applied Chemistry, University of Strathclyde, in part fulfilment of the requirements for the degree of Doctor of Philosophy

This thesis is the result of the author's original research. It has been composed by the author and has not been previously submitted for examination which has led to the award of a degree.

Signed:

Date:

ABSTRACT

MicroRNAs (miRNAs) are short non-coding RNA sequences with a length of 18 to 24 nucleotides and are known to modulate protein expression by binding to complementary sequences of messenger RNA (mRNA). Despite being discovered only recently, there is growing evidence that miRNAs are involved in key biological processes. Recent studies have shown a correlation between circulating miRNA biomarkers and many diseases including type 2 diabetes. The development of a method for miRNA detection is of great importance as it could allow for early detection of type 2 diabetes, and therefore may have the potential to reduce the number of people with undiagnosed diabetes. Many methods can be used for miRNA detection, however surface enhanced Raman scattering (SERS) is an ideal candidate as it is considered to be a fast, highly sensitive and an extremely effective technique for miRNA detection when applied with bio-functionalised metallic nanoparticles. In addition, it offers the capability for the simultaneous detection of multiple targets, which provides SERS with major advantages over other techniques.

The research began with the functionalization of silver nanoparticles using DNA oligonucleotide sequences and successive testing of their ability to detect miRNA biomarkers with a clinical relevance to type 2 diabetes in a solution-based assay. The silver nanoparticle conjugates were functionalised using thiol modified oligonucleotides and a Raman reporter to aid SERS detection. When the sample was exposed to a complementary strand of miRNA target, the nanoparticles aggregated and increased the SERS signal. Using a similar sandwich assay format, miRNA targets were also detected using a solid phase assay incorporating lateral flow strips. Lateral flow devices (LFDs) are already established for the detection of nucleic acids, and by using SERS, the detection sensitivity for targets in biological samples may be increased. Here we have been able to detect miRNA by direct visualisation of the lateral flow strips, and by SERS detection at very low concentrations difficult to see by the naked eye. These two approaches, towards using SERS for miRNA detection, are very promising and could allow biologists and clinicians to measure and monitor miRNA levels, for use in medical diagnosis and early detection of many diseases, not just type 2 diabetes.

ACKNOWLEDGEMENTS

I would like to express my sincere gratitude to my supervisors, Prof. Duncan Graham and Prof. Karen Faulds for giving me the opportunity to join their group, and for their continuous assistance, support and encouragement throughout my PhD study.

A big thank you to the Post Docs within the group, particularly Dr Sam Mabbot and Dr Kirsten Gracie for helping me enormously in the lab and with day-to-day problems and discussions. I would also thank all the Bionano group for being so kind and helpful, and giving me a hand whenever I needed it. Special mention to Pietro Gancitano for helping me with the lateral flow development, and Daniel Macdonald for his informative general discussions.

Thanks to my family; my mum for her continuous prayers, brothers and sisters, and Iman especially for her support and long, daily chats which always made me feel better. Thanks to all my friends here for the nice gatherings at the weekends that made me feel at home in Scotland.

A huge, big thank you to my beautiful shining stars; Eyad, Shahd and Asa'ad. Their smiles always make my tomorrows better. Thank you for understanding me during my difficult days, and trying to help me out with your sweet hugs and wishes. You always gave me the push to work harder so you will be proud of your mummy.

And most of all to my loving husband who I can't thank him enough because without his support this mission would be impossible. Thank you for putting up with me and for making my dream come true…. Thank you for everything.

This thesis is dedicated to the memory of my beloved father who passed away unexpectedly on 7th of April, 2008. He always believed in me and I still feel his impact in my life. I miss you dad and I hope you are proud of your girl.

ABBREVIATIONS

A	Adenine
C	Cytosine
Comp.	Complementary
Conc.	Concentration
DLS	Dynamic Light Scattering
DNA	2'-Deoxyribose Nucleic Acid
dsDNA	Double-stranded DNA
DTT	Dithiothreitol
E	Electronic state
EtOH	Ethanol
G	Guanine
h	hours
HEG	Hexaethylene glycol
HPLC	High Performance Liquid Chromatography
LSPR	Localised surface plasmon resonance
M	Molar
MGITC	Malachite green isothiocyanate
min	Minutes
mRNA	Messenger RNA
miRNA	MicroRNa

PBS	Phosphate buffered saline
PCR	Polymerase Chain Reaction
RNA	Ribonucleic acid
RBITC	Rhodamine B isothiocyanate
s	second
SEM	Scanning Electron Microscopy
SERS	Surface Enhanced Raman Scattering
SERRS	Surface Enhanced Resonance Raman Scattering
SPR	Surface Plasmon Resonance
ssDNA	Single-stranded DNA
T_m	Melting Temperature
tRNA	Transfer RNA
T1D	Type 1 diabetes
T2D	Type 2 diabetes
U	Uracil
UV	Ultra Violet
Vis	Visible

Table of Contents

CHAPTER 1: Introduction

1.1 Ribonucleic Acid (RNA)

1.1.1 Introduction to RNA

Ribonucleic acid (RNA) is involved in several key roles related to the transcription and translation of the genetic code that is stored in DNA and the assembly of proteins. RNA can be found in both the nucleus and the cytoplasm of cells. The main function of RNA is to provide an intermediate translational functionality between storage of genetic material within the nucleus, and protein synthesis within the ribosomes of the cytoplasm external to the nuclear membrane. This occurs through two main mechanisms; transcription and translation. To briefly summarise these two processes, the DNA nucleotide sequence is first transcribed into an RNA nucleotide sequence (mRNA) within the nucleus, and this sequence is then further translated into an amino acid sequence by the ribosomes. Thus, RNA plays a very significant role in converting the genetic code stored with DNA into functional proteins, which is the central dogma of molecular biology due to an additional hydroxyl group on the 2′ carbon group sugar.[1] RNA is highly comparable in structure to a single strand of deoxyribonucleic acid (DNA), but not identical as it differs in base composition, with RNA containing uracil as a replacement for thymine within DNA. Thymine is simply the methylated form of uracil. RNA is a linear polymer of ribonucleoside monophosphate moieties that are linked by phosphodiester bonds.

1.1.2 RNA Structure

RNA is composed of structural unit nucleotides with a high degree of similarity to DNA. Each nucleotide consists of three main components; the nitrogenous base, a phosphate group and a ribose sugar which is a five-carbon sugar with designated numbering from 1′ to 5′. The nitrogenous bases are bound to the ribose sugar at the 1′ carbon and may be composed of any one of the following four bases; adenine (A), guanine (G), uracil (U) or cytosine (C). The nucleobase structures are shown in

Figure 1.1. Adenine and guanine are known as the purine bases, whilst uracil and cytosine are known as the pyrimidine bases.

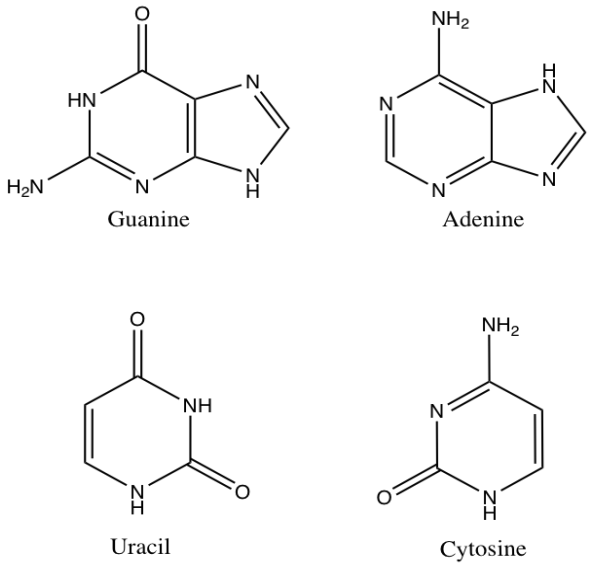

Figure 1.1: *The structures of the four bases in RNA: guanine, adenine, uracil and cytosine.*

The bases are bound together via phosphodiester linkages. They bind to the ribose sugar at the 1′ position of the pentose ring, which additionally binds to the proceeding ribose of the polymer chain through the 3′ position (Figure 1.2).

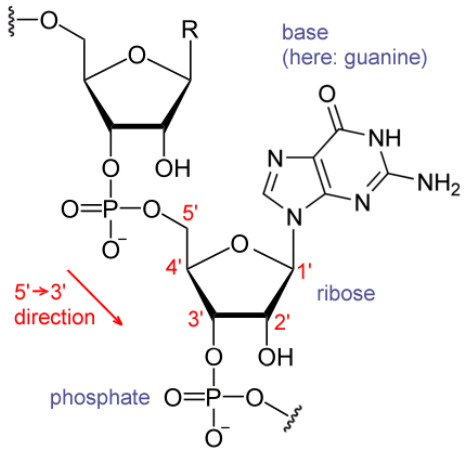

Figure 1.2: *Chemical structure of RNA, R is a nitrogen base.*[2]

An RNA monomer composed of a five-carbon sugar (pentose) and nitrogenous base is called a nucleoside and with a phosphate group present is known as a nucleotide. The phosphate group carries a negative charge, designating RNA as a polyanionic molecule. The presence of the hydroxyl group at the 2′ position in the sugar is a significant characteristic of R.[3] The presence of this hydroxyl group renders RNA less stable due to the likelihood of nucleophilic attack on the phosphodiester bond by the neighbouring 2′ hydroxyl group, and therefore RNA requires freezing or lyophilisation for long-term storage. The addition of the 2′ OH group increases the melting temperature (T_m) and stability by locking an RNA duplex into a compact A-form helix that is more stable than DNA's standard B-form helix.

In 1953, Watson and Crick discovered the double helix structure of DNA and after this defining discovery, researchers turned their attention to the structure of RNA.[4-5] Although RNA is a single-stranded molecule, it can form double-stranded structures, with DNA-RNA hybrid helices first demonstrated by Rich in 1960.[6] The single strand of RNA can hybridize with a single strand of DNA to form a double helix. Knowing the solution structure of DNA-RNA hybrids is of notable importance due to their role in the transference of genetic information from DNA to RNA during transcription.

The bases present in single strands of DNA can form hydrogen bonds with the complementary bases on the RNA strand. This is known as complementary base pairing. The nitrogenous base, uracil—as present within RNA, is a pyrimidine that is structurally comparable to thymine—as present within DNA, and like thymine it can base-pair with adenine. Adenine forms two hydrogen bonds with uracil whilst guanine bonds to cytosine with three hydrogen bonds (Figure 1.3).

(a)

(b)

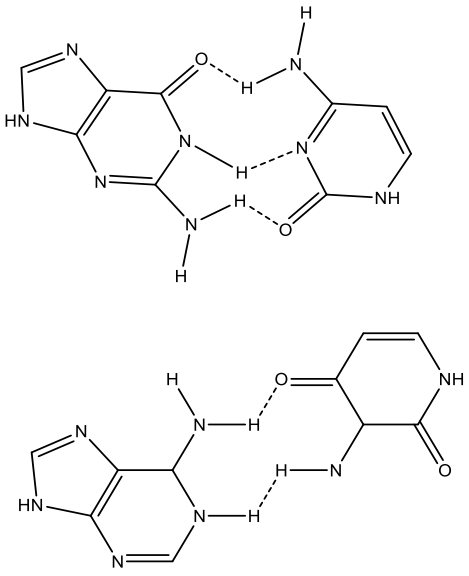

Figure 1.3: *Hydrogen bond formation between the purines and pyrimidines. (a) Guanine and cytosine have three hydrogen bonds (b) adenine and uracil have two hydrogen bonds.*

As the bonding is specific between the two strands due to specific base-pairing between adenine (A) and uracil (U), or guanine (G) and cytosine (C), duplex formation between two opposing strands is reliant upon the complementary of the base composition of the individual strand sequences. One of the strands is 5′ to 3′ oriented and whilst the complementary strand is 3′ to 5′ orientated. A single-stranded RNA molecule may also form many internal secondary structures by folding and forming hairpin loops (Figure 1.4). These structures are stabilized by intramolecular hydrogen bonds between the complementary bases. The base-pairing of RNA is critical for many RNA functions.[7] The duplex regions are vital in providing stability. The remaining single-stranded regions rely on the reactive 2′ OH groups to bind to proteins, creating RNA-protein complexes that have critical roles in processes such as DNA and protein synthesis.

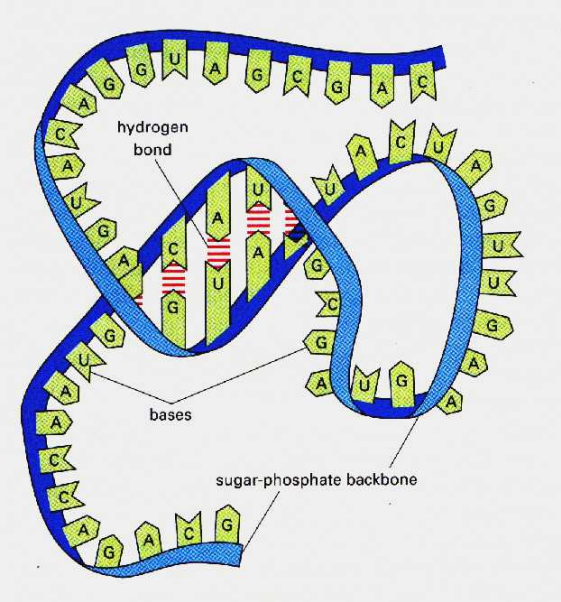

Figure 1.4 *Schematic depicting RNA secondary structure formation. The RNA strand can loop back and form intrastrand base-pairs from self-complementary regions within the polymer sequence.*[8]

1.1.3 Differences between RNA and DNA

DNA and RNA are highly similar and are composed of the same structural units but with three key differences (Table 1.1). The most significant difference is the presence of a hydroxyl group (-OH) on the 2′ carbon of the RNA ribose ring. The hydroxyl group is absent within the DNA structure at the 2′ carbon of the ribose ring and is therefore referred to as deoxyribose. Secondly, RNA exists in single-stranded form while DNA exists as a double-stranded helix. The third main difference is the substitution of thymine with uracil within RNA. However, there are some cases where uracil might be found within DNA, such as instances in which direct mis-incorporation of uracil occurs in place of thymine when DNA polymerase catalyses the process of DNA replication and repair.[9]

Table 1.1: *Main differences between DNA and RNA*

	RNA	**DNA**
Nitrogenous bases	A, G, C, U	A, G, C, T
Sugar type	Ribose sugar	Deoxyribose sugar
Strand type	Single strand	Double strand
Hydrolysis	More prone to hydrolysis due to presence of hydroxyl groups	Less prone
Structure	Consists of short internal secondary structures	Consists of long double helixes

1.1.4 RNA Synthesis

Synthesis of RNA during the transcription process is significant for the conversion of genetic information contained within a DNA sequence into proteins. RNA transcribed from DNA will have different sequence lengths in relation to the amino acid sequences that form the resulting protein structures. Differencing proteins present within in the cellular machinery are synthesised from differing messenger RNA (mRNA) as transcribed from a specific gene within the genetic makeup contained within DNA.

The transcription process consists of five steps: pre-initiation, initiation, promoter clearance, elongation and termination. During the pre-initiation stage, activated transcription factors bin directly to the DNA at either the promoter region itself, or nearby regions that are referred to as enhancer regions. These transcription factors provide an anchor for protein complexes (referred to as coactivators) to form. The coactivators do not bind directly to the DNA, but bind to the transcription factors instead. The coactivators have been associated with enzymatic activity in a complex process that involves acetylation and methylation of the histone proteins that compact DNA within nucleosomes for genetic preservation. Nucleosomes are the monomer units of chromatin, which in turn forms the chromosomes of eukaryotic genomes. In

summary, transcription factors and coactivator proteins remodel chromatin to allow progression of the initiation stage.

Following chromatin remodelling, the promoter has been "opened" and is now accessible for the basal initiation machinery. A series of further transcription factors now assemble on the promoter during the initiation stage. Most importantly, a protein complex called TFIID (transcription factor for type II genes) that contains an essential protein called TBP (TATA-box-binding protein). The TBP protein connect the TFIID complex to the promote, which in turn binds to further TBP-associated factors (TAFs) and the RNA polymerase. Finally, a further complex referred to as the "mediator" complex binds to the polymerase and the transcription factors associated with the promoter and enhancer regions, providing a regulatory mechanism for gene expression. The promoter clearance stage then begins with phosphorylation of serine residues contained within the C-terminal domain (CTD) of the RNA polymerase. The polymerase melts the DNA duplex as it proceeds to leave the promoter region, pausing to cap the 5' end of the transcript with a modified guanine monophosphate to protect from exonucleases. The polymerase is then free to proceed with elongation. Further modification takes place after transcription such as the addition of a 5′ cap. Transcription is then terminated when the CTD of the RNA polymerase is dephosphorylated allowing the process to repeat.[10]

1.1.5 Types of RNA

RNA performs various functions in cells and may be synthesised by different RNA polymerases in regard to the different roles performed within the cell. Thus, there are many types of RNA molecules that can exist. They have been broadly classified into two main categories; coding and non-coding RNA. The coding RNA is messenger RNA (mRNA) which is a large family of RNA molecules that convert genetic information from DNA for transport to the ribosome and subsequent synthesis into various proteins. Ribosomal RNA (rRNA) and transfer RNA (tRNA) are non-coding RNA as they have infrastructural roles but they do not encode proteins. Recently, RNA molecules have been also being broadly defined as either large or small RNA. Among

these types, the small RNA molecules such as microRNA (miRNA) have been subject to intense interest by researchers due to their significant regulative role in many biochemical processes within the cell.[11]

1.1.5.1 Introduction to microRNA (miRNA)

MicroRNA (miRNA) molecules are termed non-coding as they do not directly partake in protein synthesis, but rather, perform regulatory functions and have a base length of approximately 22 nucleotides. They have been identified as key biomarkers for the early detection of various diseases. The up-regulation or down-regulation of miRNA expression levels can be related to the onset and progression of many diseases.[12-14] They were first discovered in 1993 by Victor Ambros and his fellow researchers during a study on the lin-4 gene in the Caenorhabditis elegans (*C. elegans)* species, however they were not recognised as a class of RNA until 2000.[13] Since this discovery, research has increasingly been performed with an emphasis on miRNAs and their role in the biological system. It has been estimated *via* computational studies that over 60 % of total genes can be regulated by miRNAs.[12] Each miRNA has the ability to target many messenger RNAs, and one messenger RNA can be targeted by many miRNAs. miRNA binds to the 3′ untranslated region (3'-UTR) of the targeted mRNA transcripts *via* Watson-Crick complementary base pairing and this can inhibit or repress the translation process, with this activity relatable to the onset of many diseases. The stability and ubiquitous presence of miRNAs in the cells of various tissues as well as the blood and general circulatory system makes them ideal targets for disease diagnosis. Although the mechanisms of release of cellular miRNAs to extracellular environment remain mostly unknown, recent studies suggest that the expression of miRNAs in circulting system can be associated with patho-physiological condition. Moreover, miRNAs may deliver to the recipient cells via certain pathways where they can regulate translational activity of target genes.[15]

There are several studies that have established links between miRNA levels in the blood and tissue samples, with their presence or expression levels indicative of disease onset or lack thereof.[16-17]

1.1.6 microRNA in Type 2 Diabetes

Diabetes is a chronic, lifelong condition associated with severe complications such as heart disease and kidney or eye damage and is diagnosed when the patient has a high level of glucose present in the blood. It has two main types: type 1 for which the body doesn't produce a hormone called insulin because the cells designated for this function within pancreas attacked and destroyed by the body itself (autoimmune response). However, recently it has been proposed to classify diabetes into five types to improve patients' treatment which are severe autoimmune diabetes (T1D), severe insulin-deficient diabetes, severe insulin-resistance diabetes, mild obesity related diabetes and mild age-resistance diabetes (older age).[18]

The understanding of this process remains uncertain but has not been associated with lifestyle. Conversely, type 2 diabetes is associated with the body continuing to produce insulin, but the process is dysfunctional and may not consume enough or all the glucose in the blood, or the body may not react properly allowing glucose levels to increase within the bloodstream. Type 2 diabetes accounts for about 80 % of all diabetes cases and can be prevented or even delayed if early diagnosis is made for high-risk individuals with a predisposition for this disease.[19-20]

miRNA was recently linked to many diseases[21] including type 2 diabetes, and has since become an important area of great research interest as miRNAs provide robust diagnostic targets for clinical diagnosis. Alteration in their gene expression levels in the tissue or blood were linked with the presence or the developmental stage of the disease. In addition, miRNA is present within the circulatory system and blood plasma for which miRNAs are notably stable, even under harsh conditions.[22] This is likely to be due to endogenous miRNA being protected from RNase enzymes and resistant to RNase degradation[3], which is not the case for the synthetic miRNAs which are easily degraded as they are not synthesised in the same manner. Their stability in body fluids presents them as ideal targets for disease diagnosis. They are consistently and reproducibly associated with specific diseases with expression correlating with the onset or progression of disease.[23]

Since 2000, there have been numerous reports that link miRNA biomarker expression levels with the onset of various different diseases.[17, 24-25] However, Lawrie *et al.*, were the first to reproducibly detect miRNAs in serum samples in 2008 and demonstrated elevated levels of miRNA-21 and miRNA-155 in patients with B-cell lymphoma as compared to healthy groups.[26] In 2010, a study by Weber *et al.*, successfully detected more than one hundred miRNAs in 12 different biological fluids including plasma, saliva, tears and urine from healthy individuals.[27] In the same year, the first study to demonstrate the relation between plasma miRNA gene expression and type 2 diabetes was published.[28] It revealed that 13 plasma miRNAs including miRNA-126 were down-regulated in patients with type 2 diabetes. The circulating plasma miRNA displayed altered expression in diabetes type 2 patients, with this discovery providing potential for the development of miRNA-based therapeutics or diagnostics (theranostics) for complications associated with the disease. Following the publication of these findings, further studies showed that miRNA biomarker expression levels changed for people at high risk of developing type 2 diabetes.[19] This stage is referred to as the pre-diabetes stage, and therefore miRNA expression could be useful for prevention of diabetes rather than diagnosis of patients who have already developed diabetes. Amongst the various miRNA biomarkers reported in the literature that have been associated with type 2 diabetes, miRNA-29a and miRNA-126 have been consistently reported to be credible targets.[19, 28-29] Therefore, these targets were selected for investigation with the aim to develop an optimised SERS assay demonstrating a high degree of specificity and sensitivity.

1.1.7 Current Detection Methods for miRNA

miRNA detection is particularly challenging because they are small in size and since most detection methods for nucleic acids rely upon hybridisation, this requires designing of probes that are limited to equally short lengths, and additionally miRNAs from the same family are very similar in structure.[30] Specific miRNA biomarkers must first be identified and correlated to the presence and progression of a specific disease. The current methods for miRNA detection fail to meet the ideal standard for detection of multiple miRNA sequences in a rapid manner with high sensitivity, specificity and

reproducibility. In addition, such methods are usually expensive, time consuming and require skilled operators to perform assays using specialist equipment.[31]

One of the most common methods for miRNA detection and quantification is reverse transcription polymerase chain reaction (RT-PCR).[32-35] However, because a miRNA sequence is ~22 nucleotides and naturally single-stranded, this method requires intricate primer design criteria to be implemented, and a reverse transcriptase conversion of RNA into complementary DNA (cDNA) prior to amplification by DNA polymerase. Thus, reverse transcription PCR for miRNA detection is a two-step process. Firstly, a stem-loop reverse transcription (RT) primer needs to be designed for hybridisation to the miRNA target. The reverse transcriptase then reverse transcribes the miRNA into complementary DNA form in the RT stage of the reaction.

Secondly, the RT product is amplified as per standard PCR by a DNA polymerase using a miRNA-specific forward and reverse primer (Figure 1.5). The method can effectively detect and quantify miRNA but it is lengthy process (approximately 2-3 hours) requiring skilled operators for application and additionally, is a costly methodology due to the multiple primers, enzymes and probes required (unless substituted with an intercalator such as Sybrgreen I which can eliminate probe requirements).

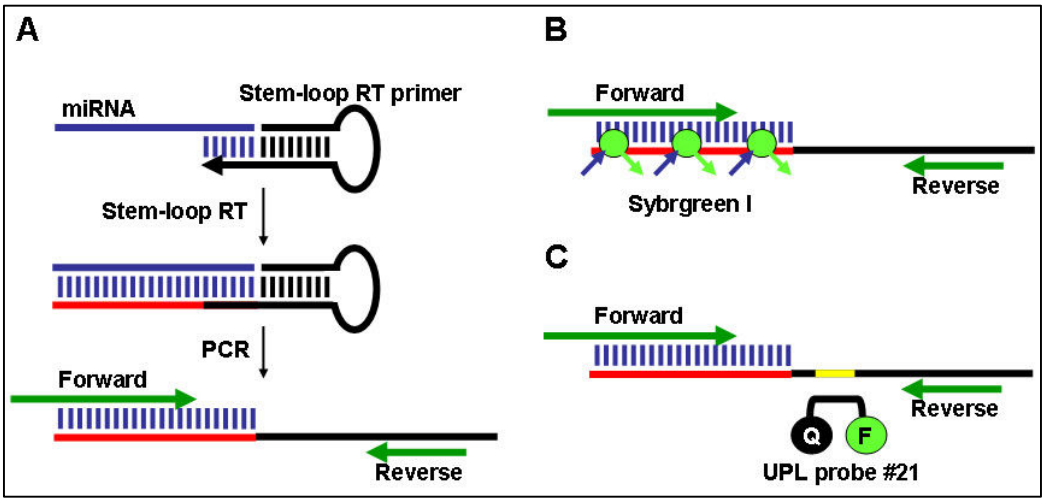

Figure 1.5: *A schematic representation shows RT-PCR method used for miRNA detection and quantification. The reverse transcription initiated by binding the stem-loop RT primers to the miRNA molecule. Then, the RT product is amplified by using a miRNA forward primer and the reverse primer.*[36]

miRNAs may also be detected with the application of a microarray, which is a powerful method for miRNA detection and quantification and is dependent on hybridisation between probes and complementary target sequences.[37] The probes used for microarray analysis are usually amine-modified probes that are immobilized on glass slides to form a miRNA microarray, with many different probes immobilised on a single slide. A key advantage of the microarray is the high-throughput multiplexing capability that can provide the benefit of detecting and quantifying many miRNA expression levels within a single slide applied for analysis. Figure 1.6 briefly explains how microarrays are used for miRNA detection. miRNAs are isolated from samples and their cDNA transcripts are labelled with a fluorescent dye during the amplification process. These amplicons are then hybridised to the miRNA probes immobilised on the microarray. Following a wash step, only labelled miRNA will have hybridised to the complementary probes and the fluorescence emitted from the incorporated label within the target will be detected at different positions on the slide. The fluorescence signal intensity can then be analysed, quantified and related to the original miRNA target content in the samples studied.

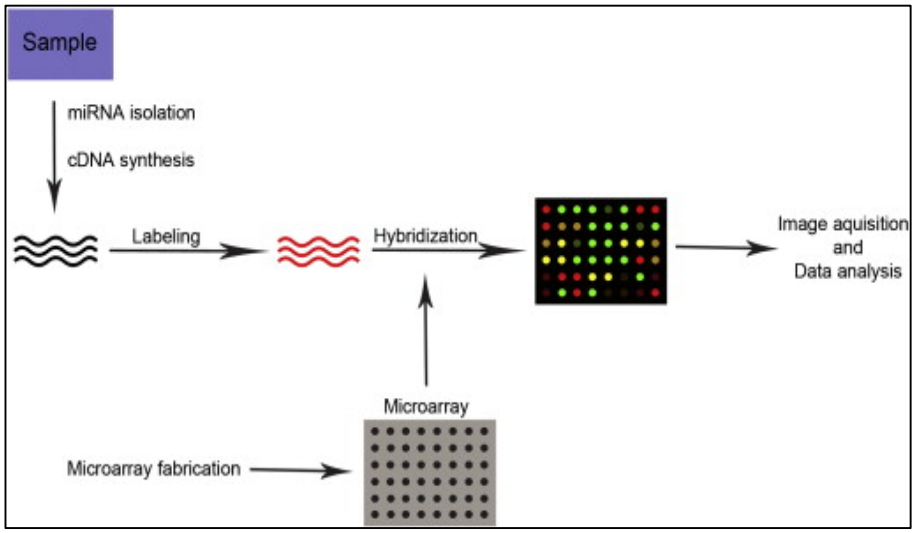

Figure 1.6: *A schematic representation showing the microarray method for miRNA detection. The method involves miRNA isolation and labelling and then hybridisation to the corresponding probes on the chip. The fluorescence signal is then analysed.*[38]

Over the past decade, a variety of new and improved assays have been developed for miRNA biomarker detection. However, these methods have considerable limitations due to cost, speed, reproducibility or technical application limitations. There is still a significant requirement to find a robust and effective method for miRNA detection that can be applied by practitioners in clinics in a time and cost effective manner, thus increasing the implementation of miRNA detection for diagnostic, prognostic and therapeutic purposes. Most recently, novel diagnostic methodologies have been proposed and developed based upon the use of nanotechnology and Raman spectroscopy as detection tools for nucleic acids, and specifically miRNA detection. Some examples will be shown later in this chapter.

1.2 Raman Spectroscopy

The main spectroscopic techniques used to detect vibrations in molecules are based upon the processes of infrared absorption and Raman scattering. They provide information on the chemical structure and physical forms for identification of substances from their characteristic spectral patterns. The analyte of interest could be

Raman active or IR-active depending on the type of vibration. If the vibrations result in alterations to the polarization of the molecule then it will be Raman active. For example, a CS_2 molecule has a centre of symmetry, and the molecular vibrations will therefore be symmetric which changes the molecular polarizability and this will not be visible in the infrared. However, to be IR active the molecular vibrations should result in a change to the dipole moment of the molecule. Therefore, the most significant Raman scattering occurs for symmetrical molecules in which a change in polarisation occurs so generally only symmetrical molecules are Raman active. The vibrational mode could be either Raman active or IR active but not both according to the rule of mutual exclusion.

1.2.1 Basic theory of Raman

Raman scattering is the inelastic scattering of a photon. It was first discovered by Adolf Smekal in 1923 and it was not until 1928 that it was observed in practice by Raman and Krishnan. This phenomenon has since been called the Raman effect and can be identified by Raman Spectroscopy.[39]

Raman won the Nobel Prize for physics in 1930 as he was the first to demonstrate the Raman effect experimentally. For this original experiment, sunlight was focused by a telescope onto a sample and a second one was placed by the sample to collect the scattered radiation. A system of optical filters was used to show the existence of scattered radiation with an altered frequency as compared to the incident light.[40] The shift in wavelength depends upon the chemical structure of the molecules responsible for the scattering.

The basic characteristic of Raman spectroscopy is the shift in the frequency between the incident and scattered light. When a beam of light interacts with a molecule, the photons within the beam can either be absorbed, scattered or pass straight through with no interaction. If the energy of an incident photon corresponds to the energy gap between the ground state of the molecule and an excited state, the photon may be absorbed and the molecule promoted to the higher energy excited state. This change in the photon's energy is measured using absorption spectroscopy. However, light

which interacts with a molecule and is scattered with no loss in energy can be detected by Raman spectroscopy. In this case, the energy of the incident photon and the energy gap do not need to be similar and the scattered photon can be observed by collecting the light at an angle to the beam of the incident light.[40] When the light interacts with the molecule and distorts the cloud of electrons around the nuclei, short-lived virtual states are formed. These states are not stable and the photon is quickly re-radiated by scattering.

There are two types of scattering, elastic and inelastic scattering. Elastic scattering, also called Rayleigh scattering, is the dominant form of scattering. Inelastic scattering occurs when the energy of the scattered photon differs from the energy of the incident photon and this is called Raman scattering. Raman scattering has two forms: Stokes and anti-Stokes scattering. In Stokes scattering, the molecule absorbs energy and goes from the vibrational state *m* to *n* which is a higher energy state and is known as the excited vibrational state. However, when the molecule is present in the *n* vibrational state, and is scattered to the lower vibrational state *m,* anti-Stokes scattering occurs (Figure 1.7).

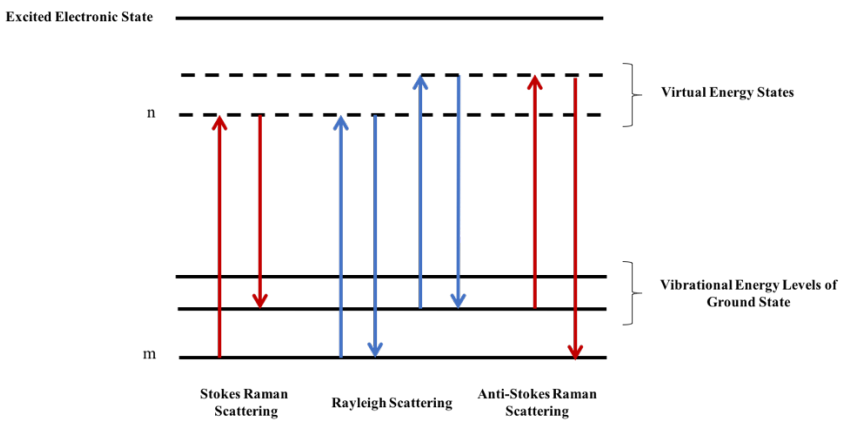

Figure 1.7: *Diagram of the Rayleigh and Raman scattering processes.*

The intensity of Stokes and anti-Stokes scattering is dependent upon the Boltzman distribution. The Stokes scattering is the most abundant form of scattering as most of the molecules will be in the lower energy states at thermal equilibrium.[41]

$$N_i = \frac{\mathrm{N}e^{-E_i/kT}}{\mathrm{q}}$$

Where;

N_i = number of particles in a sample of N particles found in a state with energy E_i when present in a thermal equilibrium system at temperature T.

k = Boltzmann constant = 1.381×10^{-23} J K^{-1}

$\mathrm{q} = \sum_i e^{-E_i/kT}$

Raman shifts are always expressed in wavenumbers, which have units of inverse length. To convert between spectral wavelength and wavenumbers of shift in the Raman spectrum, the following formula can be used:

$$\Delta w = \left(\frac{1}{\lambda_0} - \frac{1}{\lambda_1}\right)$$

Where Δw is the Raman shift expressed in wavenumber, λ_0 is the excitation wavelength, and λ_1 is the Raman spectrum wavelength.

There are several factors affecting the intensity of the electron scattering such as the intensity of light source, wavelength of the source, concentration of the sample and scattering properties of the sample. Different ranges of excitation frequencies can be used for Raman measurements to increase the sensitivity of Raman spectroscopy. The intensity of Raman scattering is directly proportional to the fourth power of the excitation frequency. However, increasing the excitation energy could result in sample decomposition or fluorescence. In addition, the analyte itself could be a weak scatter such as observable for water, or could give strong scattering as observed for molecules with aromatic rings.[42] However, Raman scattering is known to be a very weak process as only one in 10^6 photons are Raman scattered and detecting such a weak phenomenon needs a highly sensitive experimental detection set up. However, advanced modern techniques such as surface enhanced Raman scattering (SERS) can enhance the Raman scattering intensities significantly by several orders of magnitude.

1.2.2 Surfaced Enhanced Raman Scattering (SERS)

In 1974 Fleishman and co-workers initially observed considerable enhancement of the Raman signal when pyridine was absorbed onto a roughened silver surface.[43] The enhancement was thought to be due to the large increase in surface area, allowing more pyridine molecules to be adsorbed on the surface. In 1977, proposed mechanisms for this enhanced Raman signal were reported independently by Albrecht and Creighton, and Jeanmarie and Van Duyne.[40] This technique is now called surface enhanced Raman scattering (SERS) and can increase the Raman signal up to 10^4 orders of magnitude as compared to the Raman technique.[40] It is believed that there are two mechanisms behind the SERS effect; electromagnetic enhancement and chemical enhancement. Electromagnetic enhancement, outlined by Jeanmarie and Van Duyne, was a result of the interaction of the oscillating electrons on the surface, known as surface plasmons, with the analyte molecule. When incident light interacts with the surface, the localised surface plasmon of the metal exist in an excited state in resonance and can increase the number of photons that are scattered. This electromagnetic enhancement is the main causative effect for the Raman signal enhancement. The greatest enhancement can be achieved when the plasmon frequency is in resonance with the laser radiation; this technique is known as surface enhanced Raman resonance scattering (SERRS).

Another mechanism that is involved in Raman enhancement but considered to contribute to the enhancement factor to a lesser extent is the chemical enhancement mechanism. It involves the induction of a charge transfer through the bond formation between the molecule and the metal surface. This increases the polarisability of the molecule and enhances the Raman signal.

There are many suitable surfaces that can be used in SERS but the most common metals are silver and gold due to their stability and the presence of surface plasmons within the visible region of the electromagnetic spectrum. The analyte is adsorbed onto the roughened metal surfaces such as roughened electrode surfaces or colloidal suspensions that may be aggregated. The fluorescence which is produced during Raman scattering is quenched by the metal and this allows for detection of sharp and specific peaks in the SERS spectra, without fluorescence interference. This presents

SERS as a sensitive detection tool for molecular identification as compared to other optical detection methods and allows for the use of a wide range of fluorescent dyes for application as SERS labels.

1.2.3 Surfaced Enhanced Resonance Raman Scattering (SERRS)

The SERRS technique may be a combination of both the chemical and electromagnetic enhancement contributions to the Raman signal, as for SERS, but additional enhancement is obtained by introducing a chromophore with an electronic transition close to that of the excitation frequency of the laser used. In 1983, SERRS was first reported by Stacy and Van Duyne.[44] They adsorbed a chromophore onto a roughened metal surface that has a molecular vibration close to the excitation wavelength of the laser used. The enhancement factor was increased by a factor of 10^{10} as compared to the conventional Raman technique. Thus, SERRS has many advantages over SERS due to the considerably increased enhancement.[40] Figure 1.8 shows the difference between normal Raman and resonance Raman scattering.

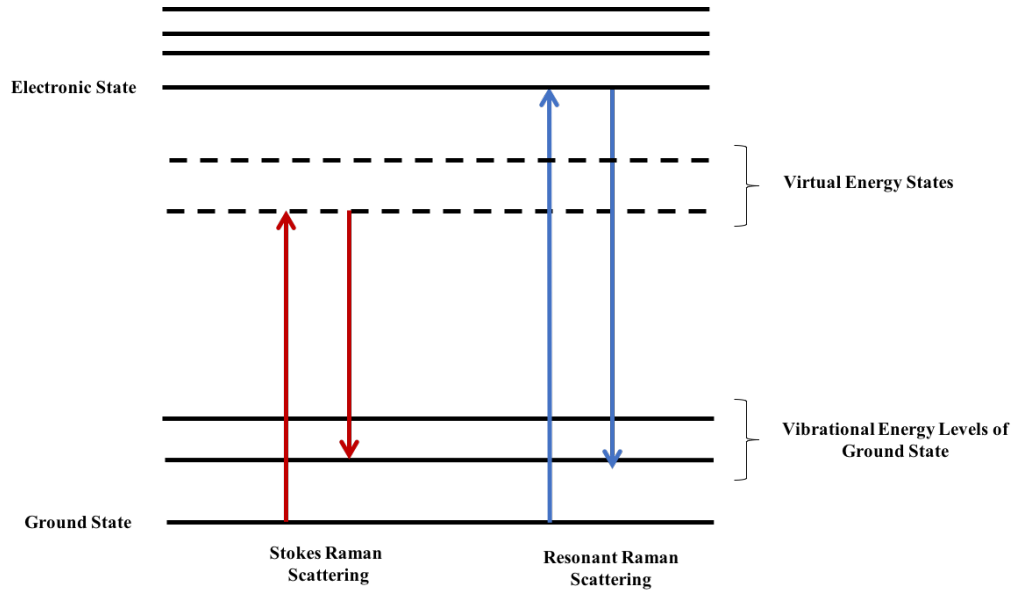

Figure 1.8: *Difference in energy transitions involved in normal Raman and resonance Raman scattering.*

The analyte molecule must have a chromophore or Raman reporter associated if the molecule is not inherently an efficient Raman scatter on the metal surface, and the excitation frequency of the incident light must be very close to the molecular frequency of the chromophore or Raman reporter, to obtain intense SERRS spectra. With use of SERRS, samples can be subjected to photodecomposition due to self-absorption of the scattered light by the analyte of interest. Additionally, fluorescence is another problem associated with SERRS and may result in spectra with significant background interference, although fluorescence is often quenched sufficiently. A suitable surface for enhancement is needed to obtain sufficient SE(R)RS, and as such, the surfaces of noble metal nanoparticles were selected for use within this investigation.

1.3 Nanoparticles

A nanoparticle is defined as a particle with one or more dimensions in the size range of 1-100 nm. They display unique chemical and physical properties as compared to the bulk material because they have a small size and large surface to volume ratios. These differing properties can be tuned by altering the size and shape to suit different applications. Recently, this has been widely used in the fields of fluorescence and Raman spectroscopy in bio-detection.[45]

1.3.1 History of Nanoparticles

Nanoparticles have been used for thousands of years to colour glass and ceramics. The most well-known example is the ancient Lycurgus Cup.[46] The cup was made of ruby glass containing gold and silver nanoparticles which allow to change colour under different lighting. The glass appears green under normal lighting but become ruby red when light changes because of the different scattering electrons by the green and red nanoparticles that are in the glass (Figure 1.9). In addition to this interesting example, there are many examples recorded throughout history for the use of gold nanoparticles as a medicinal solution for drinking as recommended by physicians to their patients.[47]

Figure 1.9: *The Lycurgus cup. Green in reflected light (left) and red in transmitted light (right). It was made by the Romans and on display in the British Museum.*[46]

The first scientific synthesis of gold nanoparticles occurred in 1857 as conducted by Michael Faraday.[48] He formed a red solution of gold colloid by the reduction of an aqueous solution of chloroaurate ($AuCl_4^-$) and then he investigated the optical properties of the gold nanoparticles. Faraday outlined in his scientific application the formation of a deep-red solution of the gold colloid and he showed the various reversible colour changes of the dried colloidal gold thin films when he applied mechanical compression upon them.

1.3.2 Synthesis of Gold and Silver Nanoparticles

Several metals can be used to form nanoparticles but the most commonly used are the noble metals such as gold and silver, due to their stability. Colloidal solutions of metals have been used for a long time and a large variety of preparative techniques are now available. Generally, nanoparticles can be prepared by the reduction of metal salts using reducing agents. For example, gold nanoparticles are produced by the reduction of chloroauric acid ($H[AuCl_4]$). The synthesis of gold nanoparticles using citrate as a reducing agent has three main steps; they are nucleation, growth and coagulation. Nucleation is the creation of nuclei upon which growth can occur. The nuclei are created via a redox reaction. Gold ions coordinate amongst each other and with the chosen capping agent—such as sodium citrate. When it reaches a critical mass greater than its thermodynamic stability, reduction to metallic gold occurs yielding the nuclei.

The growth step occurs when gold particles are added to the existing nuclei. Growth stops when all the gold has reacted. The creation of larger gold particles occurs due to the coagulation of multiple twins of various shapes. It is the control of coagulation which determines the sizes, shape and distribution of the particle in the suspension.

The first report for use of sodium citrate as the reducing agent was by Turkevitch in 1951.[49] However, in 1973, Frens reported the synthesis of gold nanoparticles ranging in size from 16-147 nm by changing the ratio of reducing and stabilizing agents.[50] Afterwards, many advanced and precise methods were demonstrated to stabilize the gold nanoparticles allowing them to be produced with different sizes and shapes.

Silver nanoparticles are also synthesised using similar methods as for gold nanoparticles with the reduction of silver nitrate ($AgNO_3$) using a reducing agent. The most common procedure for the synthesis of silver nanoparticles was first reported by Lee and Meisel in 1982.[41] They used citrate to reduce the aqueous solution of $AgNO_3$ and produce silver nanoparticles. It is a straightforward method for the synthesis of silver nanoparticles; the solution of $AgNO_3$ is boiled and stirred vigorously followed by the addition of sodium citrate solution. The stirring is continuous until the expected colour of the silver colloid is observable and then the nanoparticle suspension is left to cool. The citrate works as a reducing agent as well as a stabilizer for the synthesised nanoparticles. However, citrate is not a particularly effective stabilizing agent and can be easily displaced from the surface. In addition, the synthesised nanoparticles using the citrate reducing method tend to have a large size distribution and different shapes exist within the colloidal suspension.[51]

Different synthesis methods for silver nanoparticles were developed over the years using a variety of reducing agents including the borohydride reduction of $AgCl_4$,[52] and the ethylenediamineteraacetic acid (EDTA) reduction of $AgNO_3$[53] and the reduction of $AgNO_3$ by hydroxylamine hydrochloride[54]. The synthesised nanoparticles are monodispersed and have a negative surface charge reducing aggregation due to the repelling surface charges.

Gold and silver nanoparticles have been used most commonly by researchers as they have unique optical properties that are controlled by their size and shape. The most

important feature of gold and silver nanoparticles is the localized surface plasmon resonance band in the visible region of the electromagnetic spectrum due to the oscillation of conduction electrons.

1.3.3 Surface Plasmon Resonance (SPR)

Suspensions of gold and silver nanoparticles are known for their distinctive colouration, which arises from a combination of absorption and scattering of light depending on the particle size.

When light (the electromagnetic waves) interacts with nanoparticles, the free electrons in the metal particle move back and forth inducing an oscillating cloud of electrons at the nanoparticle surface called surface plasmon resonance (Figure 1.10). When the surface plasmon resonance is confined by the spherical nature of the gold and silver nanoparticles, it is termed localized surface plasmon resonance (LSPR). The LSPR effect produces the red colouration in gold nanoparticles and the green colouration in silver nanoparticles. The plasmon peak is easily seen in the extinction spectrum of the nanoparticles. The surface plasmon band for gold (15 nm diameter) and silver (35 nm diameter) nanoparticles gives an absorbance at 520 nm and 400 nm respectively. The optical properties are largely dependent on the nanoparticle size, shape and the dielectric constant of the surrounding medium.[55]

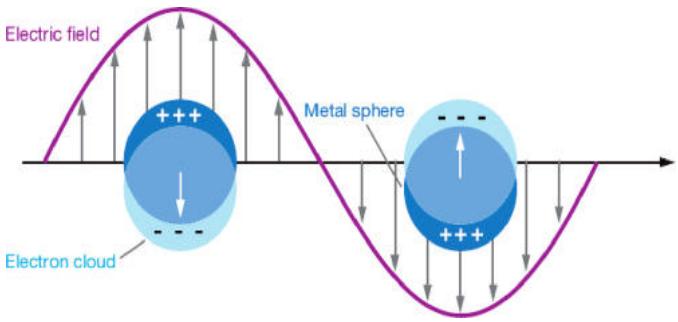

Figure 1.10: *A schematic illustration of a localised surface plasmon of the metal nanoparticles.*[56]

Localized surface plasmon resonance (LSPR) spectroscopy of metallic nanoparticles is a powerful technique for biosensing experiments. When two or more nanoparticles come into close proximity of each other, this results in the coupling of their surface plasmons and a red shift of the nanoparticle absorbance band to longer wavelengths.[57] The plasmon coupling results in a colour change within the nanoparticle suspension that can be seen by the naked eye. For example, the colour of the silver nanoparticles changes upon aggregation and can be detected by extinction spectrometry as depicted in Figure 1.11.

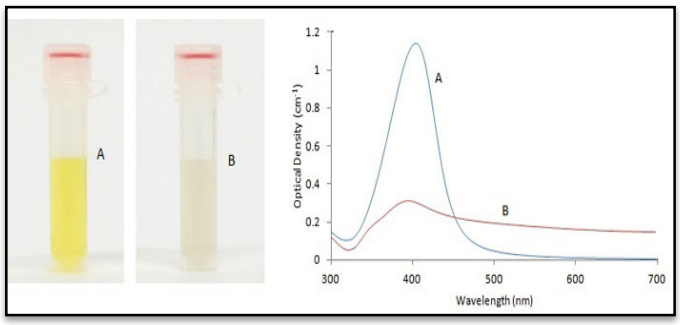

Figure 1.11: *The colour and absorbance change associated when two or more silver nanoparticles come into close proximity to each other.[58] In solution A, the nanoparticles are monodispersed and the sample has a yellow colour and a distinct plasmon band in the UV-extinction. As the nanoparticles aggregated, the solution colour has changed as can be seen from solution B and the Plasmon peak red-shifted and damped.*

Moreover, the LSPR is responsible for the electromagnetic-field enhancement that leads to surface-enhanced Raman scattering (SERS) and other surface-enhanced spectroscopic processes such as infrared absorption.[59]

1.3.4 Nanoparticle Hot Spots

Individual nanoparticles have a localised surface plasmon but the field strength is weak and this does not give large Raman enhancement. However, when the nanoparticles are aggregated and come in to close proximity of each other, additional field

enhancement is obtained by the coupling of their surface plasmons. In this case, hot spots are created for which the electric field intensity is very high at regions between the nanoparticles (Figure 1.12). A previous study by McMahon et al. showed electromagnetic enhancement increased from 10^8 to 10^{10} when the edge-to-edge distance in 90 nm gold nanoparticles decreased from 1 to 0.5 nm and when this distance decreased to 0 nm, the surface enhancement increased to 10^{14}.[60] A following study by the same group demonstrated that sub-nanometre separation between nanoparticles was necessary to obtain maximum SERS enhancement.[61]

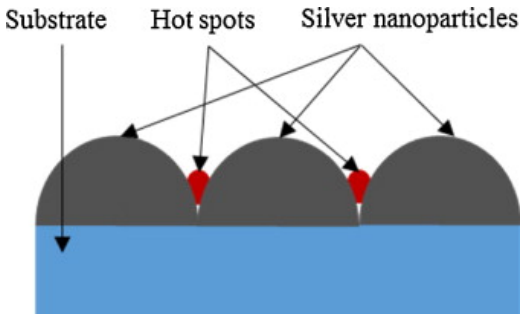

Figure 1.12: *A schematic representation showing the hot spots between nanoparticles.*[62]

Nanoparticles can be aggregated in various different ways such as the addition of aggregating agent including salts (NaCl, Mg_2Cl), nitric acid and spermine hydrochloride. The aggregates should be stable for a longer time frame than the time required to take the spectrum for reproducible spectral accumulations. The aggregation process can be controlled using either chemical or biological linkers between the nanoparticles. In the work presented, nucleic acid (DNA and miRNA) linkers were used for nanoparticle assembly.

1.3.5 Nucleic acid detection: Nanoparticle LSPR

Localised surface plasmon resonance (LSPR) of noble metal nanoparticles has attracted significant attention and has created a new field of research regarding the application of nanoparticles as biomolecular sensors. Over the years, gold and silver

nanoparticles have emerged as a promising analytical tool for the detection of nucleic acids via the hybridisation of oligonucleotide nanoparticle conjugates with DNA and RNA targets.

In the mid-1990s, two different groups (Mirkin and Alivisatos) individually reported the functionalisation of gold nanoparticles with thiol-modified oligonucleotides sequences in the *Nature* journal.[63-64] The gold nanoparticles were 13 nm in size and the surfaces were functionalized with short single-stranded DNA oligonucleotides via a terminal thiol group. The method employed by Mirkin's group was to add an excess of 3′-alkane thiol-modified oligonucleotides to gold nanoparticles, so that oligonucleotides would adhere to the surface of each nanoparticle. Upon addition of the DNA target to the oligonucleotide functionalised gold nanoparticles, the nanoparticles aggregated and formed large structures through DNA hybridisation. Watson-Crick DNA base pairing occurred between the complementary DNA strand and the oligonucleotides, resulting in duplex formation of the DNA. The hybridisation that brought the nanoparticles into close proximity reduced the plasmon energy and induced a colour change from red to blue-purple (Figure 1.13).

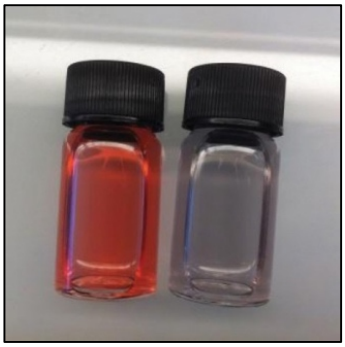

Figure 1.13: *The colour change observed when a non-complementary sequence of DNA is added to the gold nanoparticles conjugates (left) and the colour change obtained when the complementary sequence is added to the gold nanoparticle conjugates (right).*

The hybridisation process is a reversible process. At high temperatures, they remain unaggregated but at lower temperatures hybridisation occurs and the aggregation of nanoparticles is evident (Figure 1.14).

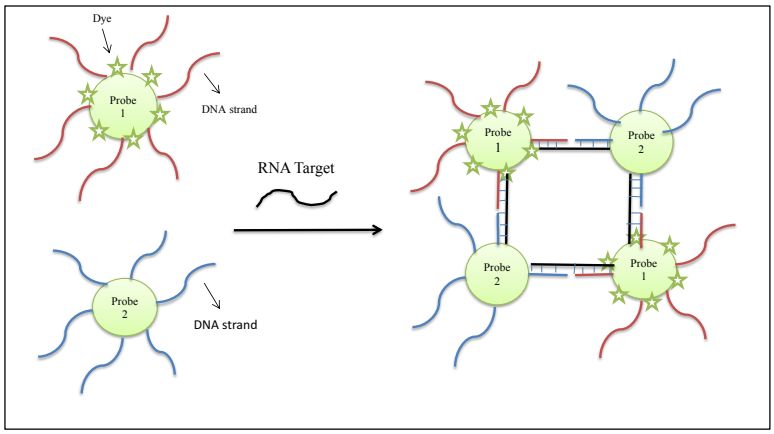

Figure 1.14: *Illustration of hybridisation occurring upon addition of complementary target sequence at low temperature to the gold-nanoparticle conjugates.*

In the following years, Elghanian *et al.* and Storfoff *et al.* reported the use of the thiol-modified oligonucleotide nanoparticle conjugates for the detection of multiple base pair mismatched oligonucleotides based upon the melting profiles of the conjugates. The DNA target melting profile was sensitive enough to discriminate matched DNA from the single-mismatch variants in a short time. This provided a new approach for the detection of DNA sequence variation as it is significant to detect the presence of defects in a nucleic acid target.[65-66]

Gold nanoparticles can also be used for RNA detection. Conjugates composed of gold nanoparticles were functionalised with multiple molecular beacons containing hairpin structures, and upon target addition, these hairpins were displaced and the oligonucleotides acted as hybridisation probes. This coordinated the fluorophores away from the nanoparticles, thus eliminating the quenching effect, and fluorescence was used to identify four types of intracellular mRNA transcripts who could distinguish cancerous cells from healthy cells rapidly and with a high degree of specificity. The multiplexing capability improved the reliability of the results with

consideration that some mRNAs may be overexpressed within normal healthy cells, and multiplexing provided improved certainty regarding confirmatory diagnosis. This approach provided accurate and reliable information for early cancer detection and avoided false positive results associated with detection of just one or two mRNAs that may reflect natural variation in mRNA expression levels.[67]

Most previous work has involved the application of gold nanoparticle conjugates for nucleic acid detection. However, silver nanoparticles conjugates have also been used recently for biosensing in a comparable manner to that of gold nanoparticle conjugates. Thompson *et al.* reported the use of silver nanoparticle conjugates for DNA detection. The conjugates aggregated upon addition of the DNA target *via* hybridisation. As nanoparticles come in to closer proximity during aggregation, their surface plasmon changes resulting in a colour change within the suspension.[68]

The synthesis of RNA-functionalised gold nanoparticles has also been reported recently. Giljohann et al. reported the synthesis of RNA functionalised nanoparticles using citrate-capped gold nanoparticles.[69] It is increasingly challenging to load RNA oligonucleotides on to the surface of the gold nanoparticles due to the chemical instability of RNA as compared to DNA. However, the surface of the gold nanoparticles—densely functionalised with RNA oligonucleotides, increased the stability and efficacy of the bound RNA. The gold nanoparticles were treated before functionalising them with RNA oligonucleotides to be free of nucleases and prevent the degradation of the RNA which could result in unstable RNA-gold nanoparticle conjugates. RNA duplexes were formed via hybridisation with RNA targets. RNA gold nanoparticle conjugates are promising tools for use in diagnostic applications.

1.3.6 Nucleic acid detection: SE(R)RS

As reported by Mirkin[63] and Alivisatos,[64] target DNA can be detected using localised surface plasmon resonance. An alternative approach was demonstrated later by Kneipp for the detection of target DNA by SE(R)RS.[70] This approach has proven to be an effective technique, providing greater sensitivity, specificity and allowing for multiplexed detection of Raman active oligonucleotide conjugates.[71-72] Fluorescent or

non-fluorescent dyes are adsorbed to the oligonucleotide-nanoparticle conjugates to act as functional hybridisation probes for detection of nucleic acid targets by SE(R)RS. The SE(R)RS assay for DNA detection relies upon the formation of "hotspots'' that are required for the generation of SE(R)RS signals. The "hotspots'' are generated during the assembly of the nanoparticles coordinated by the hybridisation event. As they come into close proximity, this induces a large electromagnetic enhancement (Figure 1.15).[73] Aggregation of a colloidal suspension of nanoparticles can also be achieved with the addition of salts. This disturbs the negatively charged layer surrounding the nanoparticles and reduces the repulsion between the nanoparticles leading to the formation of large structures of nanoparticles. Additionally, some dye molecules may function as aggregating agents for the nanoparticles.[74]

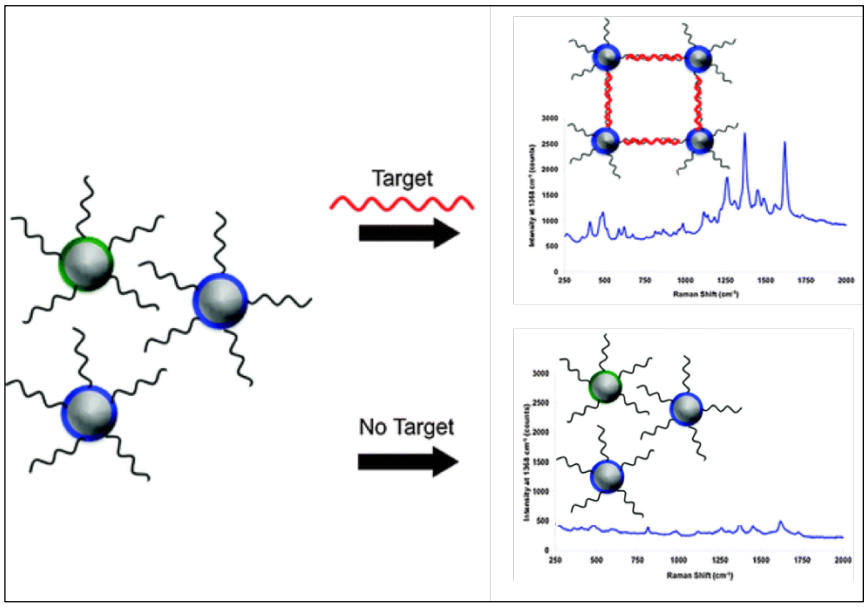

Figure 1.15: *Enhanced SERRS signal obtained as the nanoparticles aggregate in the presence of the target (top image) and low SERS signal generated from the monodispersed nanoparticles when the target is absent (bottom image), adapted from reference 73.*[75]

As mentioned previously, many methods have been recently reported for nucleic acid detection. Mirkin has used the surface array approach for the detection of DNA targets. This work described gold nanoparticles modified with thiolated DNA oligos and

Raman-active dyes that were used to achieve multiplexed SERS detection of oligonucleotide targets. Six different DNA targets with six different Raman reporters were used in the assay and they were distinguished with a detection limit of 20 femtomolar.[76] Furthermore, the detection of mRNA with application of SERS in the same manner as applied to DNA has been reported.[71] SERS provides a powerful alternative for the detection of miRNA detection and specific profiling for discrimination between the short sequences with a high degree of similarity (homology) between the miRNA family members.[71]

Silver nanoparticles are known for greater enhancement of the labels than gold nanoparticles. Thompson et al. reported the use of the silver nanoparticles conjugated for DNA detection[68] and Graham et al. showed how the SERRS effect could be tuned with select use of dye Raman tags, silver nanoparticles and functionalised DNA oligonucleotides. Nanoparticle assemblies formed from silver nanoparticles result in significantly lower limits of detection and this improves upon the sensitivity of DNA detection by SERS analysis as compared to gold nanoparticles.[77]

1.4 Project Aim

The aim of this project was to develop a robust, sensitive and multiplexed method for miRNA biomarker detection with the use of SERS and silver nanoparticles. The concept is founded upon the aggregation of nanoparticles following a hybridisation recognition event between oligonucleotides functionalised conjugates and the target sequence. This will in turn induce a significant enhancement of the SERS signal produced by the Raman reporter positioned within the assembled hotspot regions.

The developed method should be sensitive enough to be able to detect the target at low concentration and should also allow for multiplexing with the ultimate objective that this approach will prove amenable to future clinical application. Thus, the developed approach should be sensitive, specific and reliable with the capacity to detect and discriminate miRNA targets within a biological sample matrix. This will require the synthesis of nanoparticles and DNA oligo functionalised conjugates with additional testing and selection of suitable Raman reporters. Furthermore, development and optimisation of different assay formats will be conducted with further evaluation of assay performance when miRNA detection is implemented with the use of SERS analysis.

CHAPTER 2: Experimental

2.1 Chemical Reagents

All chemical reagents were supplied by Sigma-Aldrich (Gillingham, UK). Oligonucleotide sequences were purchased from ATDBio (Southampton, UK) and miRNA target sequences were purchased from IDT (Leuvan, Belgium). Lateral flow strips were obtained from BBI Solutions (Cardiff, UK).

2.2 Instrumentation

Extinction spectroscopy was carried out using a Cary 300 Bio UV-Vis spectrometer fitted with a 6 × 6 cell changer and Peltier temperature controller. Before the spectra were collected, a baseline measurement was recorded from a blank solution of the solvent used for sample dilution, prior to analysis of the samples. Dynamic light scattering (DLS) measurements were performed on a Malvern Zetasizer NanoZS (Malvern, UK). SERS was performed on an Avalon plate reader (PerkinElmer, Waltham, USA) using a stabilized 532 nm external cavity diode laser, with an Echelle spectrograph and Andor Technology CCD detector (Belfast, UK). In addition, Raman spectra from samples were taken using a Snowy Range Sierra 2.0 spectrometer (Laramie, USA) with a 532 nm laser wavelength. Lateral flow strips were analysed by SERS using the Snowy 532 nm spectrometer and a Renishaw InVia Raman microscope (Gloucestershire, UK) with a 532 nm laser wavelength and 5x lens. For all SERS spectra, data analysis was carried out using the Matlab software application. A Sirion 200 Schottky field-emission electron microscope (FEI, Hillsboro, USA) was used for acquiring SEM images.

2.3 Preparation of Buffers

2.3.1 Phosphate Buffered Saline (PBS)

PBS buffer was prepared at 0.1 M and 0.3 M concentrations using Milli-Q water. At both concentrations, the phosphate was maintained at 10 mM whilst the NaCl was adjusted to achieve either 0.1 M or 0.3 M concentration as required. The pH of the buffer solution was confirmed to be within the range of 7.2 to 7.4. Both buffer solutions were stored in the fridge prior to use.

2.3.2 0.4 M NaCl Buffer with 40 mM Phosphate

0.4 M NaCl buffer was composed of NaCl (0.4 M) phosphate (40 mM) and prepared using Milli-Q water. The pH of the buffer solution was pH 7.4.

2.3.3 Citrate Buffer

250 mM citrate buffer was prepared by dissolving sodium citrate dihydrate in Milli-Q water. The pH of the buffer was adjusted to pH 2.9 using concentrated HCl acid.

2.3.4 Dextran Sulfate Buffer

Dextran sulfate buffer was routinely prepared prior to experimentation by dissolving the polymer in 0.3 M PBS for the required % concentration (w/v).

2.4 Nanoparticles Synthesis and Characterisation

2.4.1 Preparation of Silver Hydroxylamine Reduced Colloid

All glassware was cleaned with aqua regia (HCl: HNO_3 3:1 *v/v*) for two hours prior to synthesis of nanoparticles. The glassware was then rinsed thoroughly with distilled water. Washings were collected and neutralised with sodium carbonate before disposal. Hydroxylamine reduced silver colloid was prepared using Leopold's

method.[54] Distilled water (90 mL) was added to a conical flask containing a magnetic stir bar and this was placed upon a stir plate (no heat required).

Sodium hydroxide (12 mg) and hydroxylamine hydrochloride (10 mg) were then added and dissolved in solution with rigorous stirring. Separately, silver nitrate (17 mg) was dissolved within a Sterilin tube containing distilled H_2O (10 mL). While the contents of the flask were stirring vigorously, the silver nitrate solution was added to the flask dropwise and the stirring was continued for a further 15 min. The resulting silver nanoparticles were green/yellow in colouration. The quality of the colloid was assessed by extinction spectroscopy. The synthesised colloid was found to have an absorption maximum of 408 nm. The concentration of the silver nanoparticles was estimated using the Beer-Lambert law and the extinction coefficient of 2.8×10^{10} mol^{-1} cm^{-1} as associated with the λ_{max} for the silver nanoparticles synthesised.[78]

2.4.2 Characterisation of the Colloid

The synthesised nanoparticles were characterised using the following techniques:

2.4.2.1 Extinction Spectroscopy of Silver Nanoparticles.

Silver nanoparticle samples were analysed using an extinction spectrometer. The samples were diluted 1: 20 in water and transferred into plastic cuvettes. The concentrations of the nanoparticles were obtained using the Beer-Lambert law:

$A = \varepsilon lc$

Where,

A = Absorbance

ε = Molar extinction coefficient (mol^{-1} cm^{-1})

I = Path length (cm)

c = Concentration (mol l^{-1})

The molar extinction coefficient used in this equation for calculation of the concentration was 2.8×10^{10} mol^{-1} cm^{-1} and the path length of the cuvette was 1 cm.[8]

2.4.2.2 Hydrodynamic Radius

The hydrodynamic radius of the nanoparticles was determined using a Malvern Zetasizer NanoZS. Prior to sample analysis, a size reference standard consisting of 40 nm polystyrene beads was measured to confirm accurate calibration of the Zetasizer, followed by analysis of 500 μL samples that were pipetted into plastic cuvettes. All measurements were carried out in triplicate.

2.4.2.3 Zeta Potential

Zeta potential measurements were performed using a Malvern Zetasizer Nano ZS and 500 μL samples were added to plastic cuvettes. Before each measurement, a reference standard solution with a zeta potential of −42.2 mV was analysed to confirm accurate calibration.

2.5 Conjugation of Silver nanoparticles with Oligonucleotides and Raman Reports

2.5.1 Oligonucleotides Purification

The thiol modified oligonucleotides were purified by HPLC prior to use for functionalisation of the nanoparticles. The disulfide bonds of thiolated oligonucleotides were reduced into the active sulfhydryl form for anchorage to the solid surface of the silver nanoparticles. Thus, dithiothreitol (DDT, 1 M, pH 8.5) was added to the conjugate and left for 1 h. The sample was then purified by HPLC on a Sephadex Superfine desalting column, with conductivity detection monitored for capture of the purified oligonucleotides and subsequent elimination of the DTT

fraction. Milli-Q water was used for eluent with a flow rate of 3 mL/min. The samples collected were then analysed by UV-Vis spectroscopy for determination of the concentration.

2.5.2 Oligonucleotide Concentration

Purified oligonucleotide sequences were analysed by absorption spectroscopy to determine the concentration. Oligonucleotides absorb light in the UV region with an absorption maximum or $\lambda_{max,}$ at 260 nm. The absorbance is caused by electronic transitions in the purine and pyrimidine bases and varies depending on many factors such as the base sequence and base-pair interactions. The concentration of oligonucleotides was determined using the Beer-Lambert law and the extinction coefficient of the oligonucleotide was calculated from the extinction coefficients of the individual bases, which are listed as follows:

A = 15,200 mol^{-1} cm^{-1}

C = 7,050 mol^{-1} cm^{-1}

G = 12,010 mol^{-1} cm^{-1}

T = 8, 400 mol^{-1} cm^{-1}

The extinction coefficients for the individual bases in the sequence were added together and the value obtained was multiplied by 0.9—a factor that accounts for hypochromicity due to base-stacking interactions. The final value represented the calculated extinction coefficient for the whole oligonucleotide sequence. Oligonucleotide modifications such as HEG spacers and thiol groups did not have an attributed ε value. The concentration of the oligonucleotide was calculated to determine the volume of oligonucleotides required for subsequent nanoparticle conjugation.

2.5.3 Preparation of Oligonucleotide-Nanoparticle Conjugates

Thompson *et al.* were the first to report the synthesis of silver nanoparticle conjugates.[68] Rapid facilitation of oligonucleotide loading onto the nanoparticle surface was performed using a pH adjusted citrate buffer (pH 2.9) as published by Zhang et al.[79] The volume of thiol modified oligonucleotides required for addition to the silver nanoparticles was calculated, and 5000 oligonucleotides per nanoparticle was assumed as sufficient to achieve the surface coverage necessary for maintaining stability and functionality. The suspension was left to equilibrate for 5 min. Two sequential aliquots of 250 mM citrate buffer were dispensed with an initial 25 μL aliquot added followed by shaking for 15 min, then a second 25 μL addition was dispensed followed by a further 45 min of shaking. 250 μL of NaCl buffer containing phosphate (0.4 mM NaCl and 40 mM phosphate) was added to the suspension as it will make the conjugation process between oligonucleotides and nanoparticles easier by reducing the repulsion between DNA backbones. Milli-Q water was then added to ensure a final volume of 1 mL. The sample was left to shake for 45 min and was then centrifuged at 3000 × g for 15 min. The supernatant was removed and the nanoparticles were resuspended in 500 μL PBS buffer (0.1 M NaCl, 10 mM phosphate). The λ_{max} was determined by extinction spectroscopy and concentration of silver nanoparticle conjugates was estimated with use of the Beer-Lambert law and the extinction coefficient of 2.8×10^{10} mol^{-1} cm^{-1} for silver nanoparticles.[8] The silver nanoparticle conjugates were stored in the fridge at 4 °C.

2.5.4 Dye Labelling of Oligonucleotides-Nanoparticle Conjugates

The concentration of dye required for addition to the conjugates was calculated assuming 3000 dye molecules adsorbed per silver nanoparticle. The required volume of malachite green isothiocyanate (1×10^{-5} M) was added to the silver nanoparticle conjugates and left overnight. The conjugates were centrifuged at 3000 × g for 20 min and the supernatant removed to eliminate any unbound dye from the matrix. Conjugates were then resuspended in 500 μL PBS buffer (0.1 M NaCl,

10 mM phosphate) and the concentration of the dye functionalised conjugates were then determined using UV-Vis spectroscopy.

The same method was used to prepare the thiolated oligo conjugates for application within the lateral flow assay but differed in the final resuspension step. After the second centrifugation cycle following dye addition, conjugates were instead resuspended in 50 µL of 0.1 M PBS. Additionally, 2.5 µL of 1 x 10^{-5} M dye was added for to conjugates used for lateral flow analysis.

2.6 Assembly of Oligonucleotide-Nanoparticle Conjugates

2.6.1 Oligonucleotide-Nanoparticle Conjugate Hybridisation

Hybridisation was initiated with the addition of the complementary or non-complementary oligonucleotide sequences to the probe conjugates (probe 1 and probe 2). The final concentration of the conjugate probes was 10 pM whereas the final target and nonsense control concentration was 5 nM. The total volume of the samples prepared in 0.3 M PBS was 400 µL and the samples were left for 2 h at room temperature whilst hybridisation occurred.

2.6.2 Oligonucleotide-Nanoparticle Conjugate Hybridisation: Kinetic Properties

Extinction spectroscopy was performed using a Varian Cary 300 Bio UV-Vis spectrophotometer to obtain the scanning kinetics of conjugates hybridising to the complementary target within the spectral range of 300 nm to 800 nm. Prior to sample analysis, blanks containing Milli-Q water were pipetted into 500 µL micro cuvettes and placed into different slots of the UV spectrometer. The blanks were used for automated baseline correction of the samples which were then analysed following this step. Each sample contained oligo- silver nanoparticle conjugates (probes 1 & 2) and target at the required concentrations within 0.3 M PBS buffer, with a total sample volume of 500 µL. The spectra were collected every 10 min over a specific time frame (usually 120 min) and measurements were taken immediately after target addition.

Hybridisation experiments were conducted at 25 ºC and the results obtained were converted to an Excel format for subsequent data analysis.

2.6.3 Oligonucleotide-Nanoparticle Conjugate Hybridisation: Melting Properties

Melting analysis was implemented by extinction spectroscopy as performed using a Varian Cary 300 Bio UV- Vis spectrophotometer with Peltier thermal control and the 'Thermal' software application. The temperature was cycled from 20 $^{\circ}$C to 70 $^{\circ}$C at 1 $^{\circ}$C per min and the extinction value was measured at 415 nm. Samples were initially prepared in 1.5 mL Eppendorf tubes and left to hybridise for 2 h or more before transferring to microcuvettes for melting analysis. The same volumes and concentrations were used as for the previous kinetics experiment. Data were then collected in an Excel format prior to analysis.

2.6.4 Oligonucleotide-Nanoparticle Conjugate Hybridisation: SEM Analysis

Silicon wafers were cleaned with acetone, water and then acetone again, then placed in an oxygen plasma chamber before being modified for 30 min by surface adsorption of PDDA (50 µL) with NaCl (1 mL, 1 mM) dissolved in MQ water. After 30 min, the wafers were rinsed with MQ water and dried with N_2 flow. The hybridised conjugate suspension (50 µL) was then pipetted onto the surface and left to adsorb for 30 min. The surface was then rinsed with MQ water and dried under N_2. Imaging was performed on a Sirion 200 Schottky field-emission electron microscope operating at an accelerating voltage of 5 kW. Images were then analysed with use of ImageJ software.

2.7 SERS Analysis of Oligonucleotide-Nanoparticle Conjugates

2.7.1 Monoplex Detection of Each Target by SERS

Probe1-AgNPs (with Raman reporter) and Probe2-AgNPs were mixed within a single tube with a final concentration of 10 pM and total sample volume of 150 µL made up

with the further addition of 0.3 M PBS hybridisation buffer. Hybridisation was initiated with the addition of either complementary target sequence or non-complementary negative control sequence and samples were left for 2 h or more at room temperature. Three replicates were analysed for each sample condition and the average was calculated from the triplicate samples. SERS analysis was performed using an Avalon plate reader with an Argon 532 nm laser with 3 × 3 s accumulations and a Snowy range instrument with 10% laser power using the same excitation wavelength. All spectra obtained were background corrected using Matlab software.

2.7.2 SERS Measurements of Hybridisation Kinetics Over Regular Time Intervals

Hybridisation experiments with complementary and non-complementary targets were performed on a Renishaw plate reader with a 532 nm laser wavelength at regular time intervals for observation of the hybridisation rate. Spectra for all samples were collected every 30 min. Experiments began immediately after target addition with 3 × 3 s accumulations made for four replicates of each sample. All spectra were then background corrected using Matlab software.

2.7.3 Multiplexing Experiment

Multiplexing experiments were performed for detection of both miRNA-29a and miRNA-126 targets within a single sample. Thus, two Raman reporters were selected; MGITC was used to functionalise probe 1 specific to miRNA-29a and RBITC was used to functionalise probe 1 specific to miRNA-126. For all of the samples analysed, the final probe concentration was maintained at 10 pM with a complementary target or non-complementary control sequence concentration of 5 nM. Samples were prepared in Eppendorf tubes, with probes and target dispensed initially followed by addition of 250 μL of 0.3 M PBS buffer, which was then mixed, and left to hybridise for 2.5 h within the Eppendorf tubes. After the hybridisation step, a further addition of PBS was dispensed to make up a total sample volume of 750 μL. The sample set up for the experiment is shown in Table 2.1. Four aliquots of 150 μL were taken from

each sample condition for replicate sampling and analysed using a Renishaw plate reader. SERS spectra were obtained at a wavelength of 532 nm with 3 × 3 s exposure times. Matlab software was then used to correct the background of the spectra and implement PCA for all of the sample conditions investigated.

Table 2.1: *Sample Set up for the Multiplexing Experiment*

Sample No	29a-Prob1 (µL)	29a-Prob2 (µL)	126-Prob1 (µL)	126-Prob2 (µL)	miRNA 29a Comp (µL)	miRNA 126 Comp (µL)	miRNA Non-Comp (µL)	0.3 M PBS (µL)
Sample 1	47	43	53	41.5	0	0	0	565.5
Sample 2	47	43	53	41.5	15	0	0	550.5
Sample 3	47	43	53	41.5	0	15	0	550.5
Sample 4	47	43	53	41.5	15	15	0	535.5
Sample 5	47	43	53	41.5	0	0	30	535.5

2.8 Preparation of Lateral Flow Strips for Analysis

The total volume of samples prepared for lateral flow strip analysis was 100 µL. Lateral flow strips were functionalised with deposition of streptavidin (2mg/1m) on the test line region of the nitrocellulose membrane. The streptavidin dried on the nitrocellulose membrane prior to analysis. Strips were then placed in glass vials containing the sample consisting of 0.3 M PBS running buffer, with target and capture probe (biotinylated-oligo conjugate) added to the running buffer prior to strip addition. Different target concentrations were used and capture probe (1 µl, 5 µM) was added

to the sample. The detection probe (thiolated oligo conjugate, 2.5 µl, 2.5 nM) was deposited on to the conjugate pad and dried. The lateral flow strip was placed in a glass vial containing a total sample volume of 100 µL, and this was absorbed by the sample pad and then flowed through the strip toward the absorbent pad. After 15 min, a wash step was performed using 0.1 M PBS washing buffer (100 µL).

2.9 Analysis of Lateral Flow Strips by SERS

Lateral flow strips were analysed using a Renishaw InVia Raman microscope (5x lens) with a 532 nm wavelength and Snowy range spectrometer at the same wavelength. Three strips were analysed in replicate for each sample and the replicate spectra generated were then averaged. All spectra obtained were background corrected using Matlab and Wire software applications.

CHAPTER 3: Development of a Solution-Based Assay for RNA Detection using Silver Nanoparticles and SERS

Mirkin *et al.* and Alivisatos *et al*. independently reported the self-assembly of nanoparticles by DNA hybridisation using gold nanoparticles functionalised with thiol-modified oligonucleotide sequences in 1996.[63-64] Since then there has been significant interest in using metallic nanoparticles functionalised with oligonucleotides for biomedical applications. Researchers have designed, synthesised and studied the hybridisation of specific DNA sequences to nanoparticle conjugates and their findings have resulted in a better understanding of hybrid nanostructures.[80]

The aim of this project was to design and develop methods for RNA detection and to use these methods for further detection of different miRNA biomarkers related to differing diseases. This will build upon previous results for DNA detection using metallic nanoparticles, and initially a solution-based assay was developed to detect a short RNA sequence. This chapter describes an assay that has been prepared for the detection of specific RNA sequences and an account of the method applied for the assembly of nanoparticles via RNA hybridisation will be explored. Silver nanoparticle conjugates were synthesised and functionalised with thiol modified oligonucleotides and a Raman reporter to aid SERS detection.

3.1 Introduction to the Assay

The proposed multi-target assay for RNA detection is illustrated in Figure 3.1. Silver nanoparticles provided the roughened surface required for SERS, and were functionalised with DNA sequences which were not complementary to each other, but complementary to half of the target sequence. Hybridisation should only take place upon addition of the complementary target, resulting in enhancement of the SERS signal. A synthetic model RNA sequence was used initially to validate the capability of the assay to detect a short RNA sequence.

For this research, silver nanoparticle conjugates were prepared by functionalisation with thiol modified oligonucleotides and a Raman reporter to facilitate SERS detection. The nanoparticles aggregated upon formation of self-assembled structures after exposure to the complementary sequence of RNA. During aggregation, the nanoparticles come into proximity with each other and this positions the Raman reporter molecules within the enhanced local electrical field regions between the nanoparticles termed hotspots.[81] This is a result of nanoparticles having localised surface plasmon resonances, which couple when the nanoparticles aggregate in close proximity and this enhances SERS dramatically.

Following conjugation of the nanoparticles and probe sequences, they are mixed together with the complementary target sequence, which in this instance, is a single-stranded oligonucleotide. The assembly of the nanoparticles takes place via Watson Crick base pairing as the target sequence is complementary to the probe sequences. In the case of having a non-complementary target sequence (nonsense sequence), no base pairing occurs and this is used as a negative control.

The concept of detecting the presence of target relies upon the aggregation of the nanoparticles via hybridisation which allows for the coupling of the surface plasmons in resonance. This results in an increased Raman scattering intensity as shown in Figure 3.1 and will be referred to as 'SERS ON'. If the probes are mixed with a nonsense sequence, no hybridisation occurs and no aggregation of the nanoparticles occurs, thus there is no increase in the Raman scattering intensity observed, and this will be referred to as 'SERS OFF'. The discrimination factor of Raman scattering intensity between SERS ON: OFF can be related to the presence or absence of a target sequence.

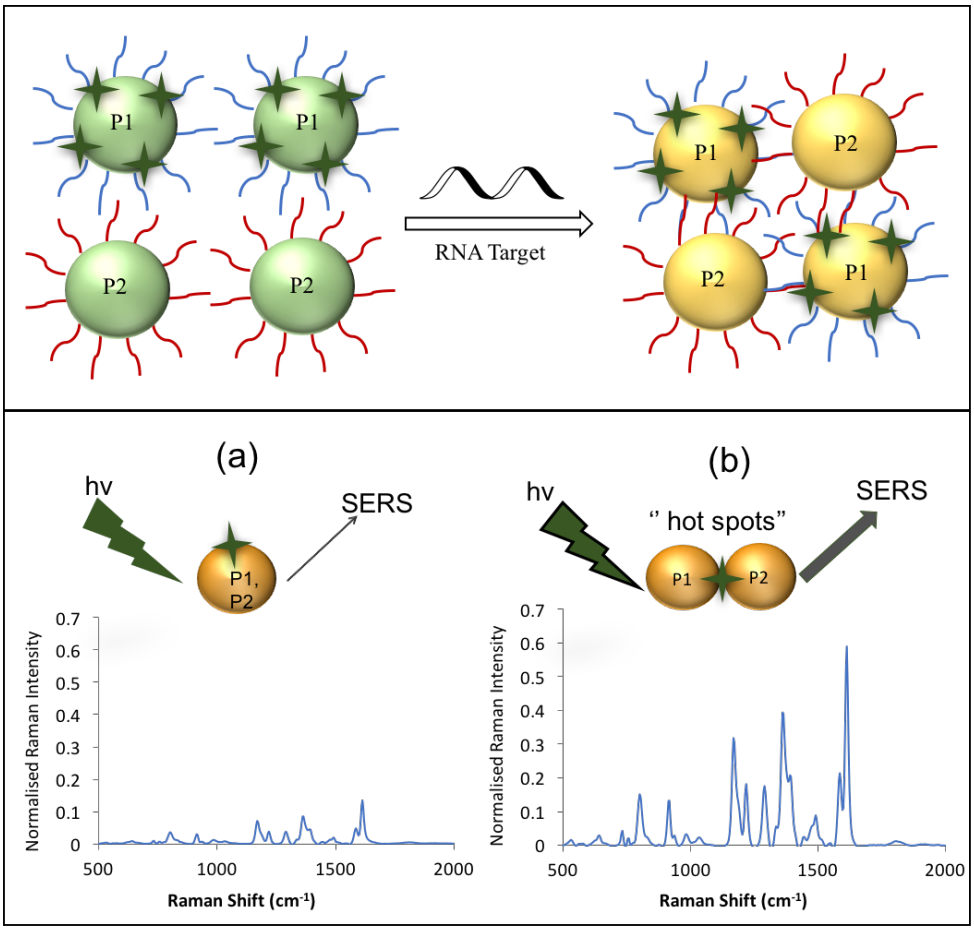

Figure 3.1: *A schematic representation of the solution-based assay developed to detect RNA sequences. Probe 1 (blue) and 2 (red) were functionalised with oligonucleotides, where the Raman reporter (displayed as green stars) is added to probe 1 only. Aggregation occurs upon addition of the target sequences as each half of the target is complementary to each probe. SERS signal is enhanced and a good discrimination between the presence and absence of target should be obtained. (a) No aggregation of the nanoparticles was observed as the target was not present, and there was no obvious increase in SERS signal designated "OFF". (b) hybridisation occurred as the target sequence was present, and SERS signal from the Raman reporter was enhanced as designated "ON". The spectra were obtained using an Avalon plate reader at a laser wavelength of 532 nm with 3s accumulation times.*

3.2 Nanoparticle and Conjugate Synthesis

3.2.1 Nanoparticle Synthesis and Characterisation

Batches of silver nanoparticles were synthesised by two different synthesis methods; citrate and hydroxylamine reduced nanoparticles were synthesised for use in the assay and for comparison of the results obtained by these methods. The results shown within

this chapter were obtained using hydroxylamine reduced nanoparticles as they provided more intense SERS signals and less variation from batch-to-batch which improved the reproducibility of results in addition to the simplicity of application.

The Leopold and Lendl method of hydroxylamine reduction was used to synthesise silver nanoparticles. This method allows for the highly reproducible synthesis of monodispersed nanoparticles.[54] The nanoparticles were characterised using extinction spectroscopy and dynamic light scattering (DLS) analysis to ensure their stability and size. The main extinction peak shown in Figure 3.2 of the silver nanoparticles is a result of the interaction between the light and the surface plasmon. The concentration of nanoparticles can be estimated using the Beer-Lambert law; where A = absorbance, ε = molar extinction coefficient, c = concentration and l = path length using the following equation:

$$A = \varepsilon lc$$

The size of the nanoparticles gained from the nanosizer was measured to be 39.5 nm, so the molar extinction coefficient value was estimated to be $2.87 \times 10^{10}\ \mathrm{mol^{-1}dm^3cm^{-1}}$ in accordance with the estimated size.[8] Thus, the calculated concentration of silver nanoparticles used was 320 pM. However, the nanoparticles were diluted in water to 200 pM for the purpose of conjugation.

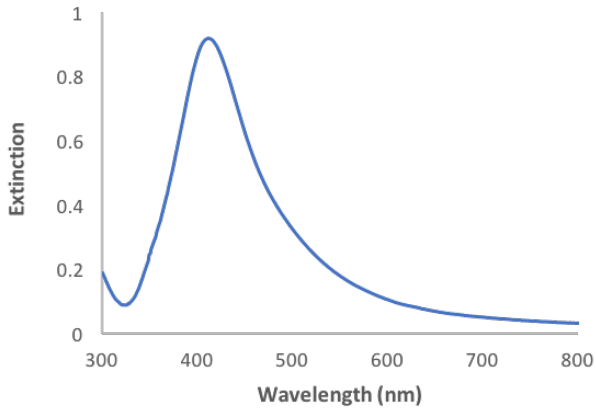

Figure 3.2: *Extinction spectrum for hydroxylamine silver nanoparticles measured using a UV-vis spectrometer, with a λ_{max} value of 408 nm.*

The size of the nanoparticles was measured to be 39.5 nm on average as obtained from DLS. The zeta potential is the potential difference between the dispersion medium and the stationary layer of fluid attached to the dispersed particle, providing an indication of the stability of the nanoparticles, and was measured at -37.7 mV. This indicated that they are stable nanoparticles as they were below -30 mV which is considered to be a standard threshold for colloidal suspensions.

3.2.2 Oligonucleotide Sequences

The assay probes are silver nanoparticles functionalised with oligonucleotides which can then be used as biosensors for confirming the presence or absence of target DNA sequences. The DNA sequences used for the nanoparticle functionalisation were modified with a thiol terminal group as they have a high affinity for anchorage to metal surfaces, resulting in a strong attachment of the biomolecule onto the nanoparticle surface. In addition, the probes had three hexaethylene glycol (HEG) units attached at the 5′ end of the oligonucleotide prior to the thiol modification. These act as spacer groups to minimise steric crowding during the hybridisation as it provides extra distance between the nanoparticle and the oligonucleotide sequence.[68] Also, spacers composed of HEG groups have been shown to improve oligonucleotide loading onto nanoparticle surfaces.[82] The 12-base and 24-base oligonucleotide probe sequences and associated complementary target sequences used in the preliminary experiments are set out below.

Table 3.1: *Details of the probes and targets sequences used for the assay*

Sequence Name	Sequence Details
Probe 1	5'THIOL-(HEG)3-TCT CAA CTC GTA3'
Probe 2	5'THIOL-(HEG)3-CGC ATT CAG GAT3'
Model DNA Complementary	TAC GAG TTG AGA ATC CTG AAT GCG
Model RNA Complementary	UAC GAG UUG AGA AUC CUG AAU GCG
DNA Non-Complementary (nonsense)	CGC ATT CAG GAT TCT CAA CTC GTA
RNA Non-Complementary (nonsense)	CGC AUU CAG GAU UCU CAA CUC GUA

The nanoparticles can assemble in different ways during the hybridisation event depending on the position of the thiol modification in the oligonucleotide sequence. In this work, the thiol group is at 5′ end for both probes, so the result is a "head-to-tail" orientation of the nanoparticle—see Figure 3.3.

There are two alternative nanoparticle orientations referred to as "head-to-head" and "tail-to-tail". However, 3′-thiol modifications have been found to produce less stable conjugates with silver nanoparticles.[68]

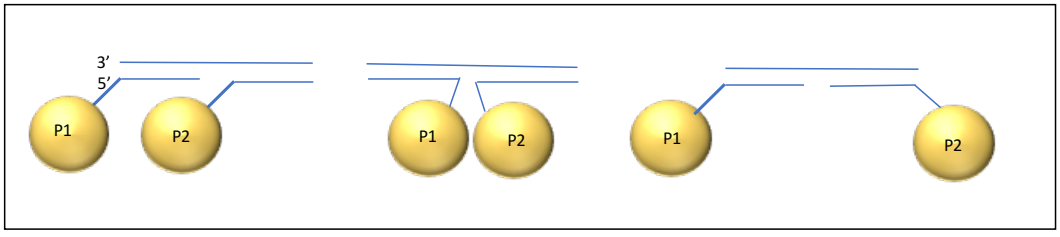

Figure 3.3: *Schematic representation showing different orientations of nanoparticle assembly. Head-to-tail (left), head-to-head (middle) and tail-to-tail (right).*

3.2.3 Oligonucleotide-Nanoparticle Conjugates

To prepare the conjugates, a thiolated oligonucleotide was added to the silver nanoparticle suspension at low pH. The charge density of the nanoparticles is reduced as some of the DNA bases are protonated at low pH such as cytosine-N3.[83] This significantly reduces the charge repulsion between DNA and silver nanoparticles and DNA attachment to silver-nanoparticles occurs in just a few minutes, (pH 2.9, citrate buffer).[79, 84] This method is much faster as compared to the salt-aging method which requires the addition of salt and phosphate buffer to the thiolated oligonucleotides in a slow and controlled stepwise manner over several days. This ensures that the conjugates are stable in a high concentration of salt because sodium chloride addition is important to negate charge repulsions, thus facilitating and maximising oligonucleotide loading onto the nanoparticle surface.[85] Sodium ions effectively minimise inter-strand repulsion between neighbouring oligonucleotides by interacting with the DNA backbone. This method provides enough time for the oligonucleotides to attach to the nanoparticles before the next incremental increase in salt concentration and protects the nanoparticles from non-specific aggregation. Although this method was reported to synthesise stable silver and gold conjugates,[68, 85] it was associated with wastage of the oligonucleotides due to inefficiency and the necessity for saturation with probe sequences. Additionally, this approach was time consuming as the nanoparticles could irreversibly aggregate during the addition of the salt aliquots. The low pH method was selected as the method of choice, and oligonucleotide-nanoparticle conjugates were subject to several rounds of centrifugation for removal of any excess oligonucleotides from the suspension.

The silver-oligonucleotide nanoparticles were also analysed by extinction spectroscopy to determine the concentration. Silver nanoparticles display subtle differences when functionalised with oligonucleotides as compared to bare nanoparticles, with conjugates exhibiting a slight red-shift in the plasmon absorption peak. The extinction spectrum of the conjugated nanoparticles is shown in Figure 3.4. The peak is slightly red-shifted for the probes as compared to the Ag nanoparticles, as expected[68] (from 408 nm to 411 nm).

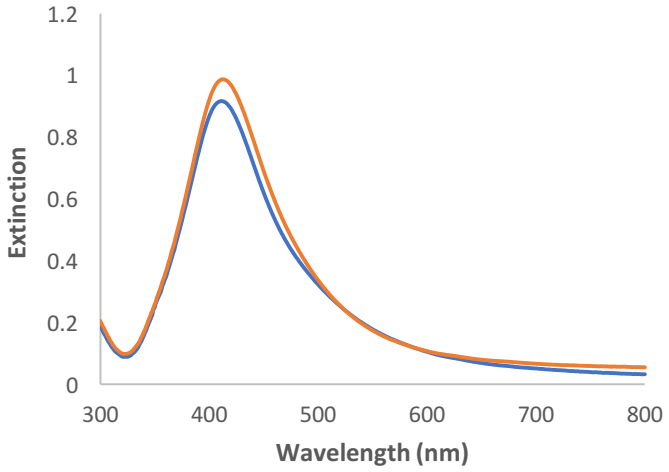

Figure 3.4: *Combined UV-Vis extinction spectrum of unmodified silver nanoparticles (blue* λ_{max} *= 408nm) and silver nanoparticles modified with a 5'-thiol-modified oligonucleotides (red* λ_{max}*=411nm)*

3.2.4 Raman Reporters (dye): Malachite Green

During this research, a study was carried out to select an appropriate Raman reporter to be used in the subsequent assay development, with oligonucleotide-nanoparticle conjugates including both fluorescent and non-fluorescent dyes. A Raman reporter is added to the nanoparticle conjugates to act as a tag for the detection of analytes by SERS. This is due to the inherently weak signal from DNA alone and is referred to as extrinsic detection. Throughout the study, different Raman reporters were investigated and characterised prior to the selection of the optimally suited reporter. The stability with the nanoparticles was an integral factor as some reporters could aggregate the nanoparticles. In addition, a suitable reporter should have a strong and distinctive SERS signal and provide a discriminatory ON: OFF ratio with the potential for multiplexing with other reporters. Malachite green (MGITC) was selected for this assay based upon the research carried out. It incorporates an isothiocyanate surface (- N=C=S) seeking group which is used for adsorption onto the nanoparticle surface (structure shown in Figure 3.5). It attaches to the nanoparticles through the isothiocyanate group to produce a strong Ag-S bond with the nanoparticle.

The extinction of MGITC shows a maximum absorbance at 621 nm. The laser wavelength used throughout this work was selected at 532 nm and therefore the technique is referred to as SERS rather than SERRS within this report as the dye is not in resonance with the laser wavelength applied.

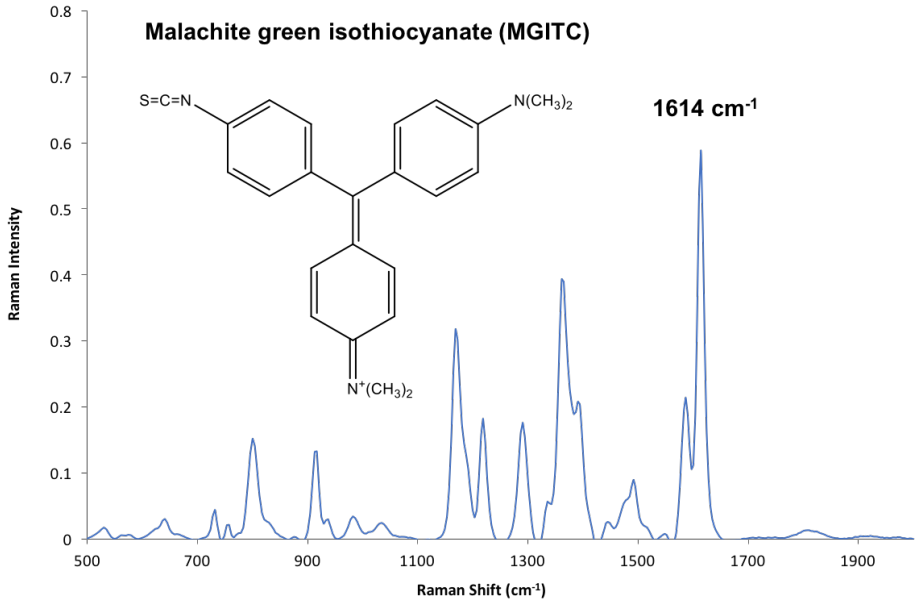

Figure 3.5: *Schematic showing the chemical structure of Malachite Green Raman reporter used for the assay and a background corrected SERS spectrum for 1 x 10^{-6} M MGITC. The distinctive peak at 1614 cm^{-1} relates to the C-H ring rotation and vibration.*

A range of dye-labelled Ag-oligonucleotide conjugates functionalised with probe 1 (P1) and probe 2 (P2) were prepared throughout this work. The P1 probe was functionalised with both the oligonucleotide probe and the MGITC dye, while the P2 probe was functionalised with the oligonucleotide probe sequence only. The dye was added after the silver nanoparticles were conjugated with the oligonucleotides rather than before as the nanoparticles would already be stabilised by the steric and electrostatic protection provided by the adjacent oligonucleotide strands.[82]

This method was devised by McKenzie *at al.* who added the dye after the oligonucleotides with the advantage that a large number of dye labels, which would

normally cause irreversible aggregation of the nanoparticle conjugates, can successfully be adsorbed because they are already stable from the surface immobilised oligonucleotides.[86]

However, the dye can be added before the oligonucleotides to the suspension of nanoparticles. This method requires a dye that has a structure that will not infer any non-specific aggregation of the nanoparticles, as any clusters that are indirectly formed will be highly SERS-active.[77]

3.3 Assembly of Oligonucleotide-Nanoparticle Conjugates via DNA/RNA Hybridisation

Before any hybridisation experiments were implemented using the model RNA target, a DNA target was utilised to evaluate preliminary results as model DNA hybridisation experiments were previously proven to work and provide a good ON: OFF signal ratio.[77] This allowed for comparison of the results of duplex DNA-DNA hybridisation experiments with duplex RNA-DNA hybridisations, and evaluation of effectiveness prior to moving on to the next step with use of miRNA biomarkers, which was the ultimate target for investigation.

So, all the results in this chapter will be describe the use of model DNA and RNA targets only with comparisons of the results under the same experimental conditions, and with replicate sampling to evaluate the experimental reproducibility.

During this work, the prepared AgNP-oligonucleotide conjugates were mixed with the target or non-complementary DNA/RNA oligonucleotides in a ratio of 10 pM final concentration of each nanoparticle conjugate to 10 nM target/nonsense sequence. The hybridisation of silver nanoparticle probes with complementary target sequence was investigated. The primary method of investigation was performed using extinction spectroscopy with an overall focus to develop an assay for detection of specific miRNA sequences related to disease using SERS.

3.3.1 Reaction Kinetics

Reaction kinetic studies were performed using extinction spectroscopy to determine the extent of any aggregation within the sample after the addition of target/non-complementary sequences to the two probes. Aggregation could be detected by the colour change; however, this does not provide any information regarding the aggregation process. Extinction spectroscopy allows the monitoring of the DNA/RNA hybridisation effect on the surface plasmon coupling of the silver nanoparticles at allocated times.

To achieve hybridisation, conjugates of P1 and P2 were mixed at 10 pM final concentrations with 10 nM target/non-complementary oligonucleotides in PBS (0.3 M, pH 7.4). The blue spectrum of the nanoparticles in Figure 3.6 (a) shows no aggregation and the silver nanoparticles are monodispersed and have a surface plasmon peak at 431 nm. Over time, the plasmon peak decreases as DNA hybridisation occurs. The changes in the plasmon profile indicate the formation of aggregated nanoparticles.

Under the same experimental conditions, a non-complementary oligonucleotide sequence was used in place of a complementary sequence (target) to investigate sequence specificity and to confirm that hybridisation occurs with the target sequence due to the base pairing of the complementary oligonucleotides. The spectrum in Figure 3.6 (b) was obtained using the non-complementary DNA sequence. The blue spectrum is observed after the addition of a non-complementary sequence with a peak at 431 nm. The spectrum indicates the progress of aggregation after 120 min which is the same time period in Figure 3.6 (a). Adding the non-complementary DNA sequence did not change the plasmon and the silver nanoparticles remained monodispersed and green in colour. The results confirmed that addition of the target aggregated the nanoparticles sequence specifically and this changed the plasmonic properties of the nanoparticles, while no effect was observed after adding the nonsense sequence.

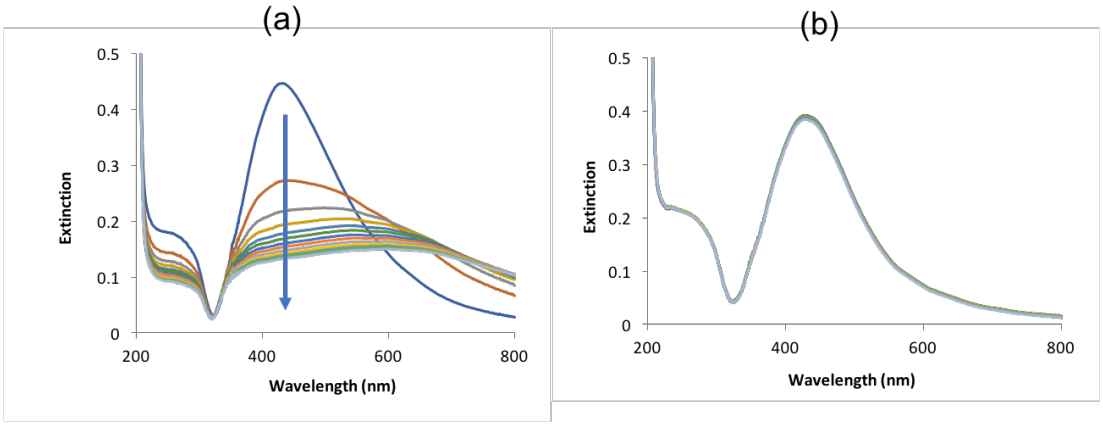

Figure 3.6: *Reaction kinetics spectra of a mixture of dye-labelled nanoparticle conjugates with complementary DNA sequence (a) and non-complementary DNA sequence (b) collected every 10 min over 120 min. The final concentration of each probe was 10 pM and 10 nM for the targets.*

For comparison, the same experimental conditions were applied to an RNA target instead to identify if the assay could detect this alternative. Aggregation was again indicated by a red shift in wavelength frequency and a reduction in absorbance of the main peak, complemented by the appearance of a plasmon peak at a longer wavelength in with the addition of a colour change in the suspension that could be seen by the naked eye.[87]

When target RNA was added to the dye-labelled nanoparticle conjugates, hybridisation occurred. The plasmon peak dampened due to the nanoparticle assembly; i.e. aggregation of the nanoparticles by hybridisation. When adding the non-complementary sequence to the assay, no noticeable changes were observed to the plasmon peak indicating that the particles were stable and unaggregated (Figure 3.7).

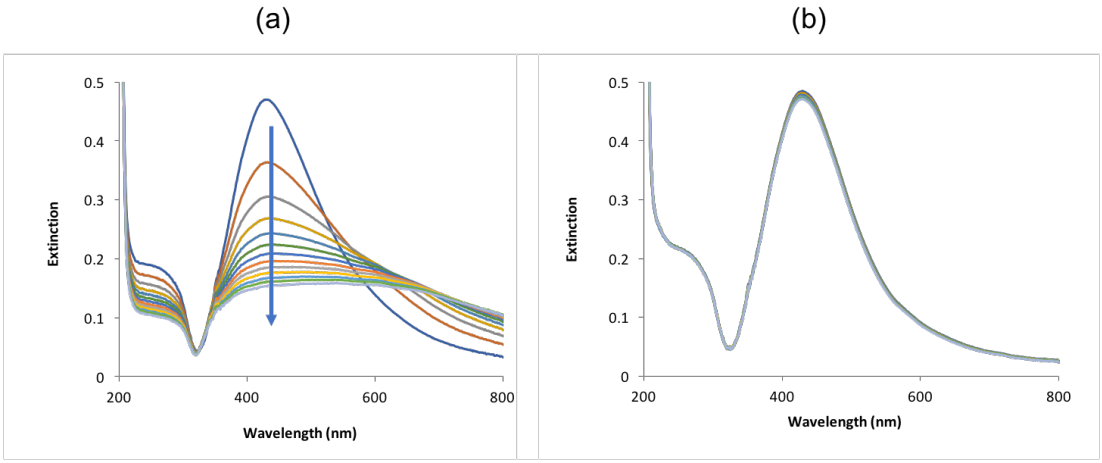

***Figure 3.7**: Reaction kinetics spectra of a mixture of dye-labelled nanoparticle conjugates with complementary RNA sequence (a) or non-complementary RNA sequence (b) collected every 10 min over 120 min. The final concentration of each probe was 10 pM and 10 nM for the targets.*

The hybridisation event coordinated the nanoparticles aggregation in suspension and changed their plasmonic properties. During aggregation, the distance between the nanoparticles changed due to the plasmonic coupling. The resulting colour change in the presence of target was very efficient and a simple method for RNA detection. In figure 2.8b, there were three sample suspensions investigated but only (i) had a complementary RNA target, for which hybridisation occurred causing the nanoparticles to come within proximity to each other and allowing for plasmonic coupling. The extinction spectra of each suspension are shown in Figure 3.8 and it is clear that the suspension that has no target (control) and the suspension with non-complementary target (nonsense) maintain their plasmonic peak at the same wavelength. In addition, the SPR peak height and width remain the same in the suspensions with non-complementary target and this demonstrates the stability of the probes within the hybridisation buffer (0.3 M PBS).

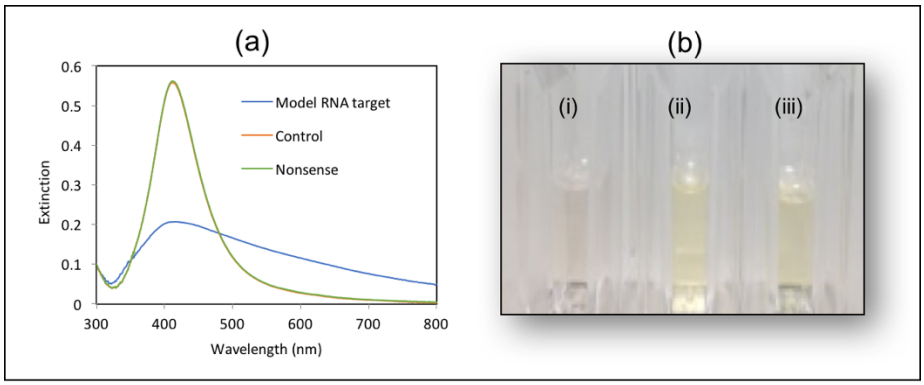

Figure 3.8: *(a) Extinction spectra of silver nanoparticle conjugates hybridising to a fully complementary strand (model RNA target), non-complementary target (nonsense) and no target (control). The final concentration of each probe was 10 pM and 10 nM for the target. (b) Visual image of (i) silver nanoparticle conjugates with the complementary RNA target (ii) with the non-complementary RNA target and (iii) No target addition.*

A number of repeats were carried out to confirm the results and investigate the reproducibility of the assay for the detection of RNA targets and the results yielded showed the great promise for use of this method for miRNA sequence detection. All the suspensions that contained a complementary RNA target in figure 3.9 had a colour change due to the aggregation of nanoparticles upon hybridisation.

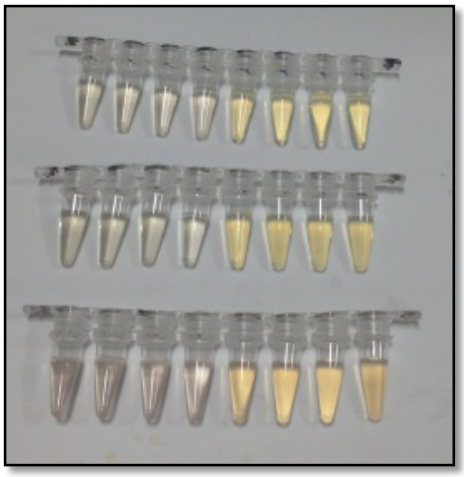

Figure 3.9: *Visual image shows different replicates of silver-oligonucleotide conjugates, with samples containing model RNA target sequence coloured grey (left) and silver-oligonucleotide conjugates with non-complementary target sequence remaining yellow (right). All the replicates had the same final concentration for each probe (10 pM) and target (10 nM).*

A plot of the absorbance ratios at 429 nm and 550 nm versus time is shown in Figure 3.10 to further highlight the difference in aggregation rates between the RNA and DNA targets added to the oligonucleotide-silver nanoparticle conjugates. The ratio approach used in this graph can be used to determine relative hybridisation rates due to the plasmonic dampening at 429 nm and associated increase at 550 nm. An absorbance ratio value of one indicates an aggregated state and it can be seen from the graph in Figure 3.10 that both the RNA and DNA targets hybridise to the probes in a similar manner and reach a fully hybridised state within the first 20 min.

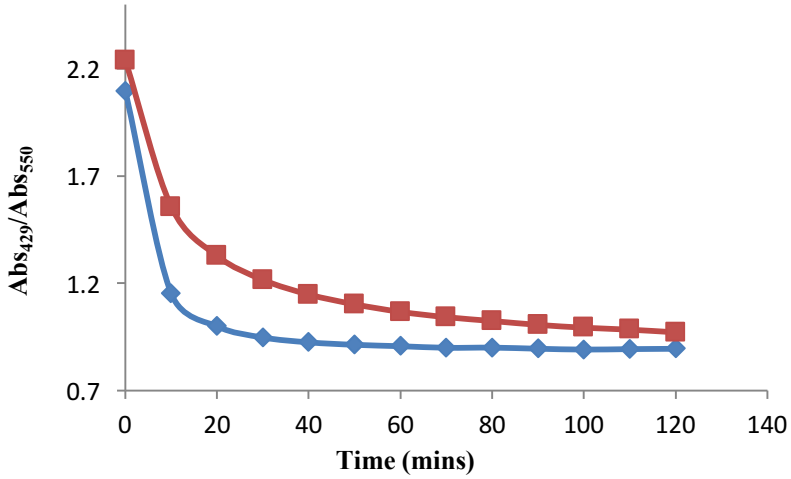

Figure 3.10: *Ratios between absorbance values at 429 nm (λ_{max} for monodispersed oligonucleotide-silver nanoparticle conjugates) and 550 nm (emergence of red-shifted secondary plasmonic profile) versus time (minutes) for DNA (red) and RNA (blue) target sequences with silver nanoparticle conjugates. Conjugate and targets final concentrations were the same for each sample which were 10 pM for each prob and 10 nM for targets.*

3.3.2 Dynamic Light Scattering (DLS)

Since the silver nanoparticles aggregated upon hybridisation, this meant that nanoparticle formations should increase in size. Thus, DLS measurements were taken to compare the sizes between suspensions that contained silver conjugates with complementary and non-complementary (nonsense) RNA targets, and a suspension with no target present. The nanoparticles aggregated upon the addition of the target sequence. The silver nanoparticle conjugates with a non-complementary sequence of

RNA demonstrated approximately the same sizing as the unaggregated nanoparticles. The data in Figure 3.11 suggested that hybridisation with RNA coordinated the aggregation event as the the size increased dramatically upon target addition only, and this was not evident for any of the negative controls.

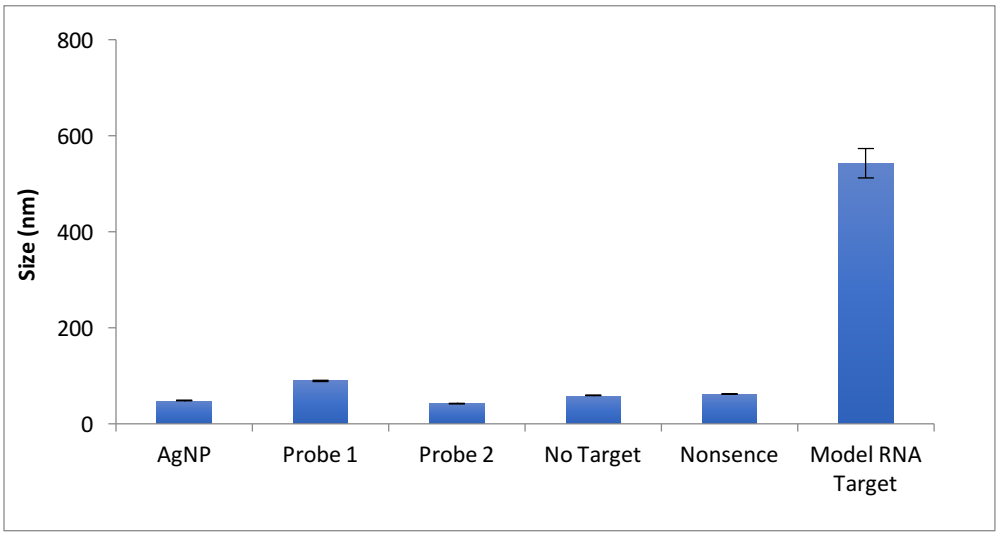

Figure 3.11: *Size measurement of the silver nanoparticles, probes and oligonucleotide silver nanoparticle conjugates with no target, a non-complementary (nonsense) RNA target and a complementary RNA target sequence. The final concentration of each probe was 10 pM and 10 nM for the targets. Error bars represent ± one standard deviation from 3 replicate analyses.*

The results obtained from DLS are in good agreement with further results gained from the application of scanning electron microscopy (SEM). Images of the probes with RNA complementary target and non-complementary (nonsense) oligonucleotide sequence, are shown in Figure 3.12. There are some smaller particles and rods clearly visible in the SEM image of the nanoparticles. The second image shows there are large aggregates formed by the hybridization of the conjugates to the RNA target.

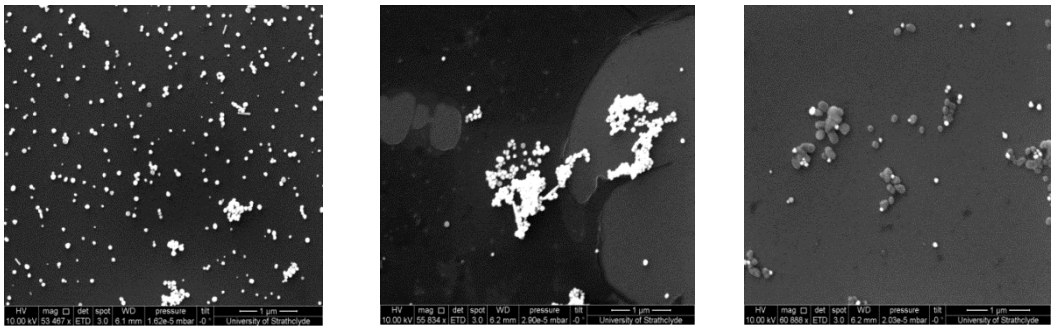

(a) (b) (c)

Figure 3.12: *(a) SEM images for hydroxylamine nanoparticles (b) silver oligonucleotide conjugates with target RNA (c) silver oligonucleotides conjugates with nonsense RNA.*

3.3.3 Melting Transitions

The point at which half of the RNA is in a duplex state and half is in a ssRNA state is called the melting temperature or T_m. Heating the oligonucleotide-silver nanoparticle RNA duplex at high temperature will break the hydrogen bonding between complementary base-pairs and reduce the base stacking, resulting in the formation of ssRNA. Thus, the hybridisation-induced aggregation of the nanoparticles can be reversed by heating above the melting point of the RNA /DNA duplex. This process can be monitored by extinction spectroscopy. Concentrations of conjugates used were 10 pM final concentrations mixed with 10 nM complementary sequence in PBS (0.3 M, pH 7.4). The temperature was cycled between 10 ^{o}C and 70 ^{o}C by heating and cooling the samples four times and the extinction values recorded at 415 nm (Figure 3.13).

The DNA/RNA peak at 260 nm will not be visible as they are present in a very low concentration relative to the nanoparticles. Monitoring of melting transition was carried out at the conjugate extinction peak maximum. The melting curves are sharp for the conjugate and target duplex, with target samples for both DNA and RNA remaining consistent throughout the 4 heating/cooling cycles which demonstrated that the conjugates structures formed were stable.

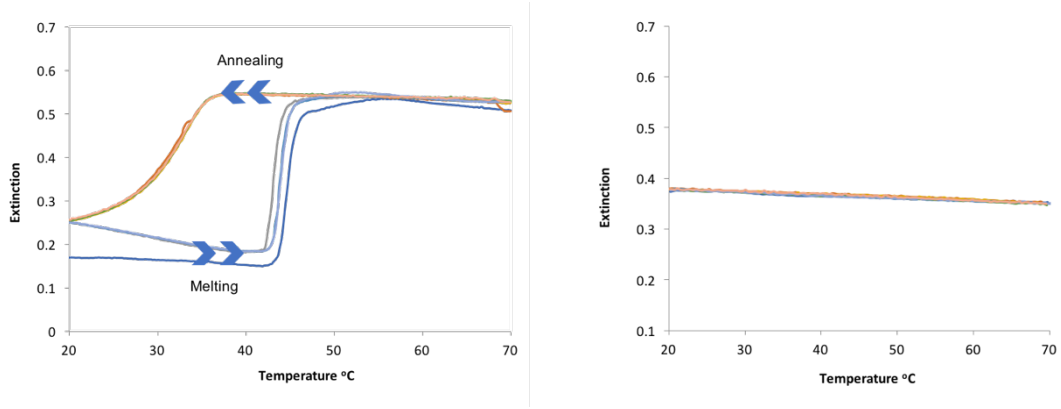

Figure 3.13: *Melting curve analysis: Melting profiles (40 °C – 50 °C) and annealing profiles (20 °C – 37 °C) of a mixture of dye-labelled AgNP-olignucleotide conjugates with RNA target sequence (left) or RNA nonsense sequence (right), samples were monitored using the extinction at 415 nm against temperature (°C). The final concentrations of each probe was 10 pM and 10 nM for the RNA target.*

The melting curve plot following RNA nonsense sequence addition to the oligonucleotide-silver nanoparticle conjugates displays a linear absorbance profile. This confirmed the melting curve is a result of sequence specific RNA hybridisation and it was indicated that no hybridisation takes place with the addition of nonsense sequence. Melting curves obtained when DNA target was added for comparative purposes are displayed in Figure 3.14 and demonstrate similar behaviour. The RNA-linked Ag-NPs exhibit a sharp melting transition similar to the characteristic behaviour of the analogous DNA-linked Ag NP aggregates, indicating that RNA-linked Ag conjugates also exhibit highly cooperative binding properties.

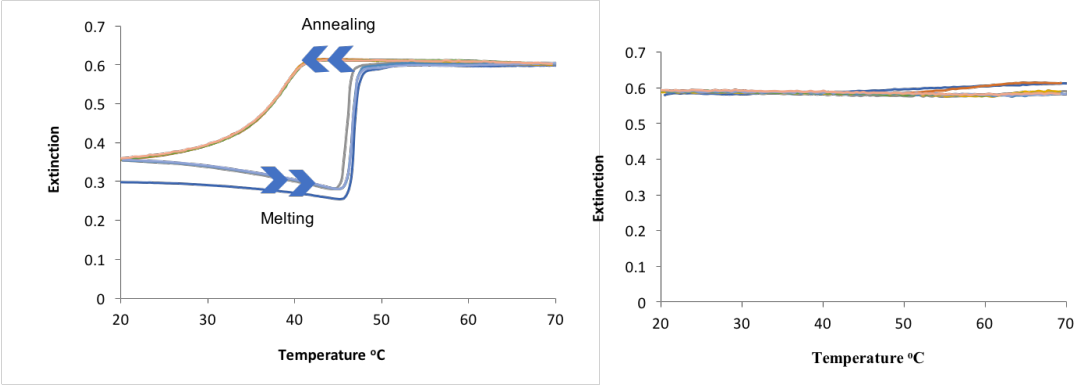

Figure 3.14: *Melting curve analysis: Melting profiles (40 °C – 50 °C) and annealing profiles (20 °C – 41 °C) of dye-labelled AgNP-oligonucleotide with a DNA target sequence (left) or DNA nonsense sequence (right), monitoring the extinction at 415 nm against temperature. The final concentrations of probes are 10 pM and 10 nM for DNA target*

Most importantly, these melting transitions were found to be highly reproducible and this is strong evidence that the modification of the silver nanoparticles with oligonucleotides was thermostable upon heat cycling.

Heating the conjugates past the melting temperature of the RNA/DNA duplex results in an increase in extinction values because the base-pairing is disrupted and the silver nanoparticles return to the monodispersed state. Having established the plasmonic properties of the DNA-RNA conjugates the SERS response was subsequently investigated.

3.4 Detection of an RNA Target using Surface Enhanced Raman Spectroscopy (SERS)

SERS offers many advantages for DNA detection due to its sensitivity and capability for multiplexing.[88] It has been found to be an effective analytical technique for the quantitative detection of DNA.[89] The functionalisation of silver nanoparticles with a SERS-active dye and thiol-modified oligonucleotides, followed by hybridisation with a complementary DNA sequence can result in an increase in the SERS intensity generated by the "hotspots" formed upon DNA hybridisation.[77]

The dye label is responsible for providing the Raman signal, rather than the RNA. RNA does not contain a chromophore, so it is difficult to observe Raman peaks easily. Fluorescent dyes can be used for Raman-tagging, as the fluorescence is quenched at the nanoparticle surface, thereby minimizing possible interference with the Raman signal.

SERS detection provides a spectroscopic signal output for discriminating between the presence or absence of specific nucleic acid sequences in a sandwich assay format. Upon hybridisation of dye-labelled oligonucleotide-nanoparticle conjugate probes to the RNA/DNA target, SERS may be "switched ON". In this assay, SERS was used to detect a specific RNA/DNA sequence. The conjugates and target/nonsense sequences were mixed in the same ratio as previously used, and the suspension was analysed by SERS using a 532 nm laser excitation with 5 × 5 s accumulations. The averaged results gained with use of both RNA and DNA targets are shown in Figure 3.15, obtained from four replicates. It is clear from the spectra shown that adding a complementary target to the assay enhanced the Raman signal and "switched ON" SERS.

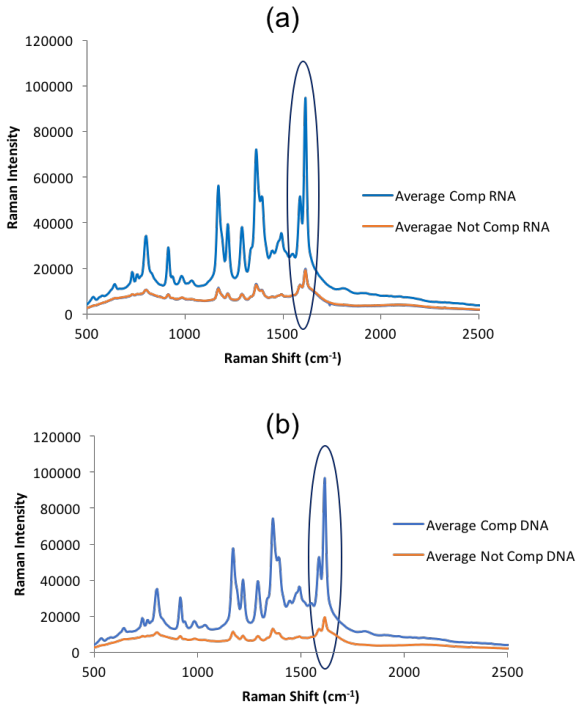

Figure 3.15: *SERS analysis for RNA/DNA assembly using MGITC-labelled oligonucleotide-hydroxylamine reduced silver nanoparticle conjugates at 532 nm excitation wavelength with 5 × 5 s accumulations. Blue line: suspensions with complementary RNA/DNA target sequence, Red line: suspensions with non-complementary (nonsense) DNA and RNA sequences. Final concentration was 10 pM for each probe and 10 nM for target. (a) with RNA target sequence. (b) with DNA target sequence.*

The peak observed around 1614 cm^{-1} was used for comparison of peak heights. In the presence of DNA/RNA nonsense sequences, a low SERS signal was observed and upon addition of the complementary target, an increase in SERS was observed with the coupling of the nanoparticle surface plasmons inducing a local field of high electromagnetic intensity commonly referred to as hot spots, which resulted in an increased SERS intensity. Figure 3.16 highlights the enhancement of the peak when a complementary target is present as compared to the suspension that has no target or a nonsense target sequence.

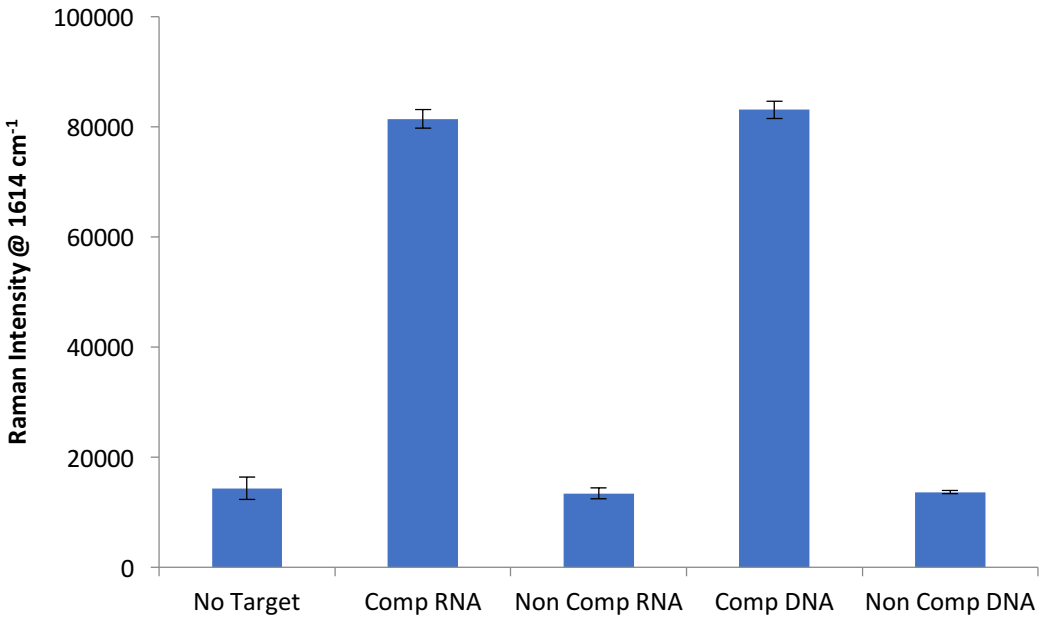

Figure 3.16: *SERS intensities of five suspensions that have silver conjugates with no target, complementary RNA target, non-complementary RNA target, complementary DNA target and non-complementary DNA target sequences as identified using the 1614 cm^{-1} peak after all the spectra were baslined. Final concentration of suspensions was 10 pM for each probe and 10 nM for targets in 0.3 M PBS. The SERS spectra were obtained using a 532 nm laser wavelength and 5 × 5 s accumulations. Error bars represents ± one standard deviation from 4 replicate analyses.*

3.5 Concentration study of model RNA sequence using SERS

Further investigation into the effect of target concentration on SERS signal intensity was performed. A concentration range between 0 and 10 nM of complementary target was studied whilst the concentration of non-complementary target (10 nM) and probes remained the same (10 pM) for control purposes. The bar chart in Figure 3.17 demonstrates that as the complementary target concentration increased, the discrimination ratio between complementary and non-complementary target improved. However, beyond a certain target concentration, the suspension became saturated and even with an increase in complementary target concentration, the SERS signal didn't increase much and even resulted in a minor decrease in SERS signal beyond a certain threshold as seen in Figure 3.18.

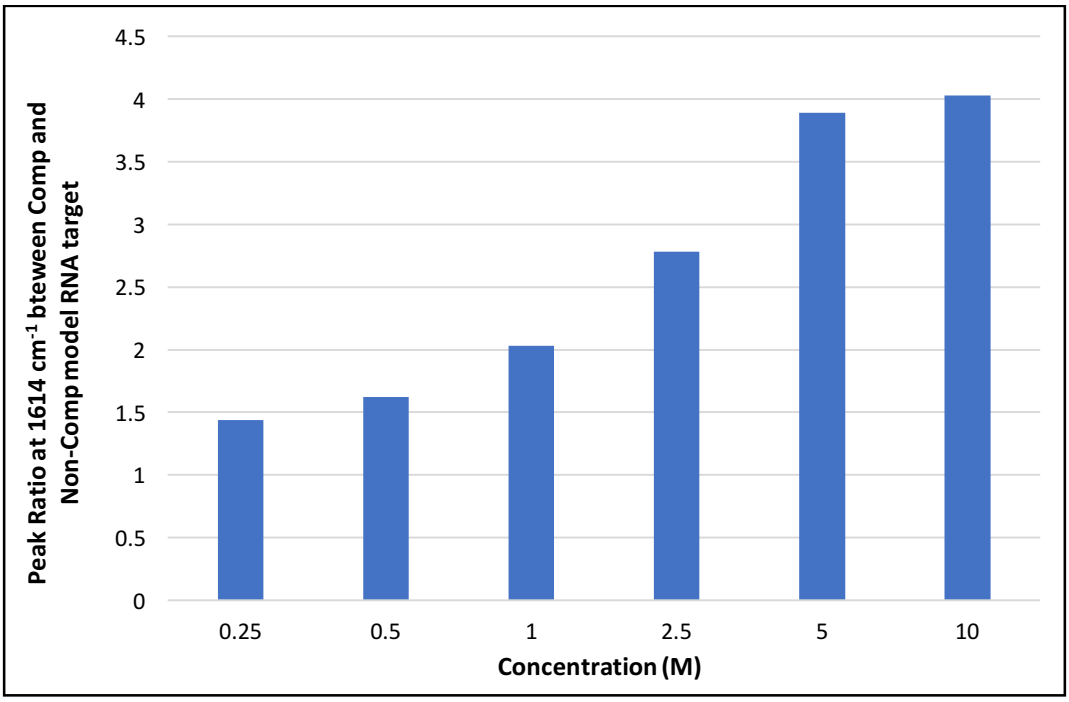

Figure 3.17: *The spectra of all the suspensions were taken using 532 cm^{-1} laser wave length and 3 * 3 s accumulations using a Renishaw plate reader. The concentration of each probe was 10 pM and for the non-complementary target was 10 nM. The concentration of the complementary target was varied between 0.25 and 10 nM. The samples were left for two hours at room temperature prior to analysis.*

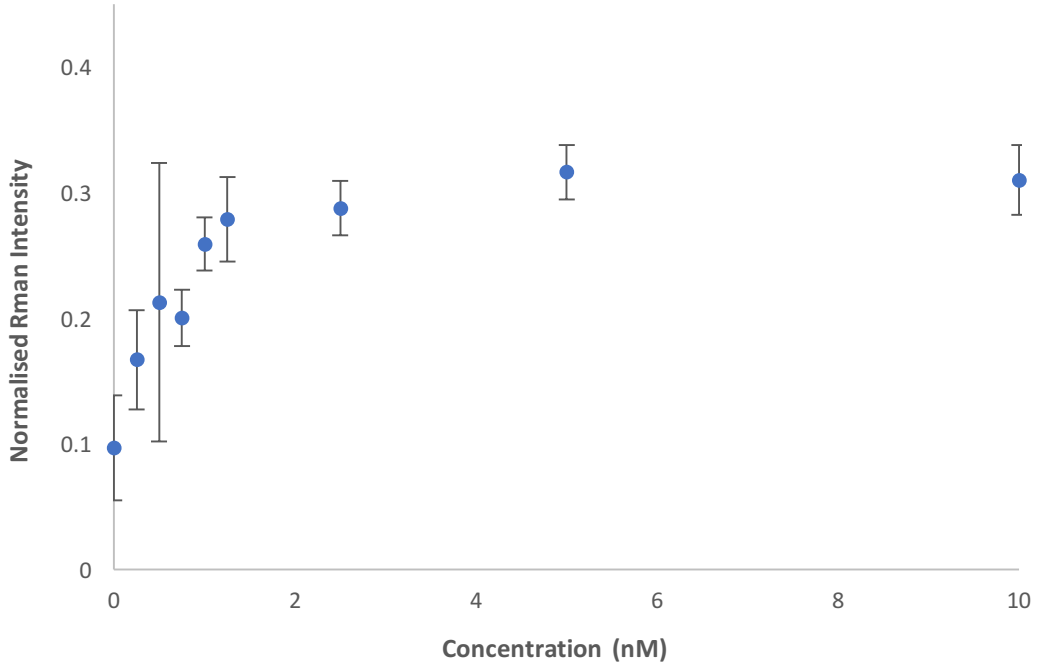

Figure 3.18: *Each spectrum is average of four replicates and were taken using 532 laser wave length and 3 × 3 s accumulations in a Renishaw plate reader. The final concentration of each probe was 10 pM and the final concentration of complementary target was varied between 0 and 10 nM.*

The graph shows a linear relationship between the complementary target at low concentrations and SERS signal intensity. A calibration curve was constructed for model RNA target using 0, 0.25, 0.5, 0,75, 1, and 1.25 nM final concentrations in Figure 3.19 and lower limit of detection (LOD) was calculated using the graph's equation to be 1 pM . At low concentration, there will likely be fewer aggregates formed with a wider degree of distribution throughout the sample suspension. Therefore, data accumulations taken from a single point may be prone to further variation due to the probability of the incident light scattering upon an aggregate, or transmitting through the sample suspension if aggregates were not present within the single laser wavelength. One possible solution would be the use of a raster effect upon future analysis at low concentration, to account for distribution throughout the sample.

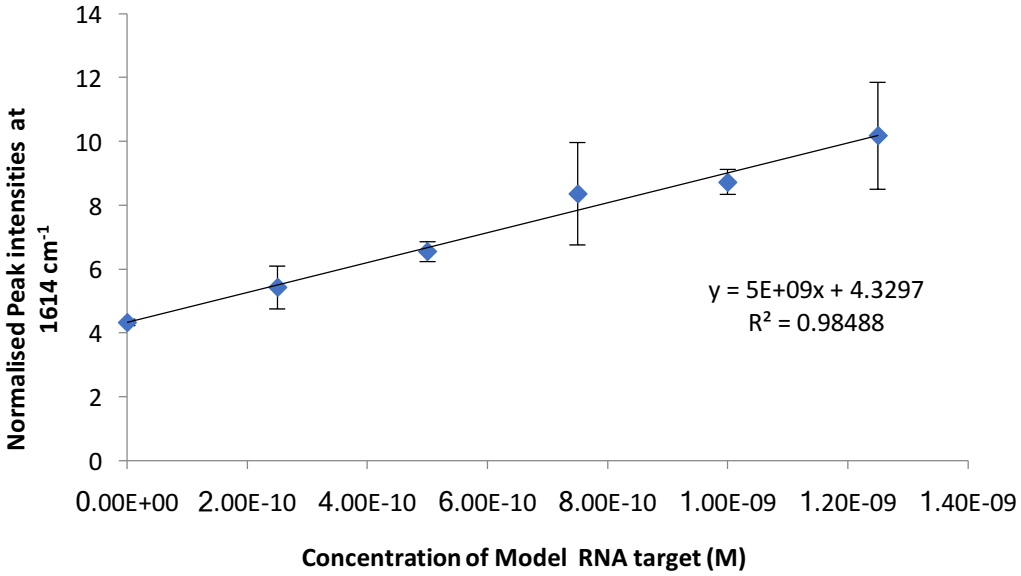

Figure 3.19: *Each spectrum is an average of four replicates. They were taken using 532 nm laser wave length and 3 × 3 s accumulations using a Renishaw plate reader. The concentration of each probe was 10 pM and the concentration of the complementary target was varied between 0 nM and 1.25 nM.*

This chapter has demonstrated the results gained from the development and application of a solution-based assay for the detection of RNA targets. The application was successful and supports the great promise of SERS for the progression of disease diagnostics and the use for the detection of miRNA biomarkers that have a clinical relevance for type 2 diabetes diagnosis.

3.6 Summary of the Assay

In this work, two probes were synthesised: probe 1 consisted of silver nanoparticles conjugated to a 12-base oligonucleotide sequence and a Raman-active dye; probe 2 consisted of silver nanoparticles conjugated to a different 12-base oligonucleotide sequence with a Raman functionality. The oligonucleotide-silver nanoparticle conjugates hybridised to a complementary RNA target sequence that was exactly the length of the two probe conjugates combined, *i.e.* 24-base pairs. This resulted in the aggregation of nanoparticles via hybridisation and changed the kinetic and melting properties of the hybridised nanoparticle conjugates. The dampening and broadening of the surface plasmon band (λ_{max}), due to the coupling of individual nanoparticles during aggregation, resulted in a colour change of the suspension as observed by the naked eye. Melting analysis of the oligonucleotide-nanoparticle conjugates in the presence of the RNA target demonstrated the reversibility and reproducibility of the aggregation process and the stability of the conjugates at high temperature. Adding a non-complementary RNA sequence to the DNA nanoparticle conjugates resulted in no observed optical and melting transitions as no hybridisation induced aggregation occurred.

The oligonucleotide-silver nanoparticle conjugates functionalised with MGITC were assembled via RNA hybridisation and analysed by SERS. An observable discrimination in the SERS intensities of the complementary and non-complementary targets was observed but there was not a large difference between the 'off' to 'on' SERS signal. An investigation into reducing the background signal from the non-complementary samples could be an important step in future work to improve discrimination between the complementary and non-complementary RNA targets.

The nanoparticle assembly process is influenced by the amount of complementary RNA target available for hybridisation. Changing the target to probe concentration ratio would result in a difference of the complementary to non-complementary peak ratio given that the target RNA sequence is always added in excess to the conjugate probes. The proof-of-principle was validated using a model RNA target sequence and the project then progressed towards the use of RNA that was both representative in

length and sequence composition of recognised miRNA biomarkers. This aligned the assay development with the idealised aim of ultimately detecting natural miRNA from a biological sample, with the use of a homologous oligonucleotide target sequence described within the next chapter.

CHAPTER 4: Solution-Based Assay for the Detection of miRNA related to type 2 diabetes using Silver Nanoparticles and SERS

The previously developed assay successfully detected a model RNA sequence and provided significant ON: OFF discrimination, which meant it could easily discriminate between complementary and non-complementary target sequences. As the main objective of this research was to develop a method for miRNA biomarker detection, further experimental development toward detection of miRNA sequences that related to type 2 diabetes was conducted. Since 2010, there has been evidence to suggest that the gene expression of many miRNA biomarkers can be indicative of the onset of type 2 diabetes and affecting insulin production in β-cells in pancrias.[28] Pancreatic β-cells play a fundamental role in glucose homeostasis by releasing insulin according to glucose levels in the bloodstream. Insulin then triggers glucose uptake in its target tissues, such as the liver, kidney and skeletal muscle. Absence of β-cells leads to diabetes due to lack of insulin producing cells (T1D), or to the inability to increase insulin levels to sufficiently consume glucose in bloodstream (T2D). The role of miRNAs in the function of β-cells in T2D patients has been extensively studied but is not yet fully understood. However, miRNAs were proven to be involved in the pathogenesis of diabetes mellitus by affecting pancreatic β-cell functions, insulin resistance, or both. They are differentially expressed in insulin target organs or circulating blood in diabetic patients compared to normal individuals. Recently, it was demonstrated possible functions of different miRNAs in regulating insulin sensitivity and glucose utilisation activity in insulin target tissues, including pancreatic β cells [90] it is known that there are specific roles of miRNAs in controlling insulin activity and maintaining normal physiology of insulin target organs under diabetes mellitus condition.

This evidence demonstrated that the genetic expression of circulating miRNA was altered in patients with type 2 diabetes, and this could therefore lead to development of targeted miRNA-based therapeutics for the treatment of complications associated with this disease. There are many circulating miRNA sequences that have displayed

altered expression levels in patients with type 2 diabetes, and for this work two specific miRNA biomarkers were investigated; miRNA-29a Homo Sapien (miR- 29a HS) and miRNA-126 Homo Sapien (miR-126 HS).[19]

4.1 Hybridisation Experiments with miRNA Biomarkers as Targets.

4.1.1 miRNA Biomarker Sequences Selected for Assay Development

It is known that miRNA sequences are usually between 18 and 22 nucleotides in length with miRNA-29a and miRNA-126 both being 22 bases long and the sequences used to validate the method are shown in Table 4.1. As the miRNA target is shorter than the model RNA by two bases, the probes were designed to have 11 oligonucleotides each for full complementarity to the 22-base targets. Having a short sequence as a target is one of the challenges associated with miRNA biomarker detection because it is difficult to design the probes whilst maintaining the melting point above that of room temperature.

Table 4.1: *Details of the probes and miRNA targets sequences used for the assay*

Sequence Name	Sequence Details
miRNA-29a Probe 1	5'THIOL-(HEG)3-TAA CCG ATT TC 3'
miRNA-29a Probe 2	5'THIOL-(HEG)3-AGA TGG TGC TA 3'
miRNA-126 Probe 1	5'THIOL-(HEG)3- CGC ATT ATT AC 3'
miRNA-126 Probe 2	5'THIOL-(HEG)3-TCA CGG TAC GA 3'
miRNA-29a Complementary Sequence	UAG CAC CAU CUG AAA UCG GUU A
miRNA-126 Complementary Sequence	UCG UAC CGU GAG UAA UAA UGC G
miRNA Non-Complementary Sequence (nonsense)	ACU GAC GAC GGC ACA UAU CUA C

Initially it was important to determine if the proposed approach would be able to detect the presence of miRNA target by experimental investigation of the hybridisation kinetics especially that the melting temperature of the probes needed to detect the miRNA targets are considered to be low as can be seen from Table 4.2. so, confirmation of the hybridisation event occurring between the conjugates and complementary target was required

Table 4.2: The melting temperature for the miRNA targets probes

Probe	T_m (^oC)
miRNA-29a P1	18.4
miRNA-29a P2	22.2
miRNA-126 P1	18.4
miRNA-126 P2	25.9

4.1.2 Kinetic Studies for Hybridisation Confirmation

Reaction kinetic studies were performed using extinction spectroscopy to determine the extent of any aggregation within the sample after the addition of target sequence to the two probes. When the target was added to the probes, hybridisation took place and thus the nanoparticles aggregated, which resulted in an increase in particle size. This in turn altered the optical properties of the particles, which could be observed as a decrease in absorbance intensity and a shift in wavelength. Figure 4.1 shows the kinetic results obtained when the silver conjugates were exposed to the complementary miRNA sequence. The spectra were collected every 10 min for 120 min at 25 $^{\circ}$C. Under the same experimental conditions, a non-complementary target sequence was used in place of a complementary target sequence as a negative control for investigation of specificity. This confirmed that hybridisation only occurred due to the base pairing of the complementary oligonucleotides. Adding the non-complementary miRNA sequence did not change the plasmon peak and the silver nanoparticles remained monodispersed and green in colour. These results confirmed that addition of the target had induced sequence-specific aggregation of the nanoparticles, with an associated change in the plasmonic properties of the nanoparticles, whilst no effect was observed following addition of the non-complementary (nonsense) sequence. Despite the low melting temperature of the probe that can make the hyberdisation process between the probes and the target difficult at room temperature, the assay was successful as shown by kinetics results in Figure 4.1 which was carried at room temperature. This is because the cooperative melting effect from short range duplex to duplex interactions is independent of the nucleic acid base sequences when it forms a nanostructure probe that is heavily functionalised with oligonucleotides. Thus, DNA-nanoparticle system is stable due to the multiple DNA links between the particles and to the high loading of DNA on the nanoparticles makes DNA strands experience high local dielectric effect. There are also other factors that can increase the melting temperature of the DNA strand other than DNA surface density which are nanoparticle size, interparticle distance, and salt concentration.[56]

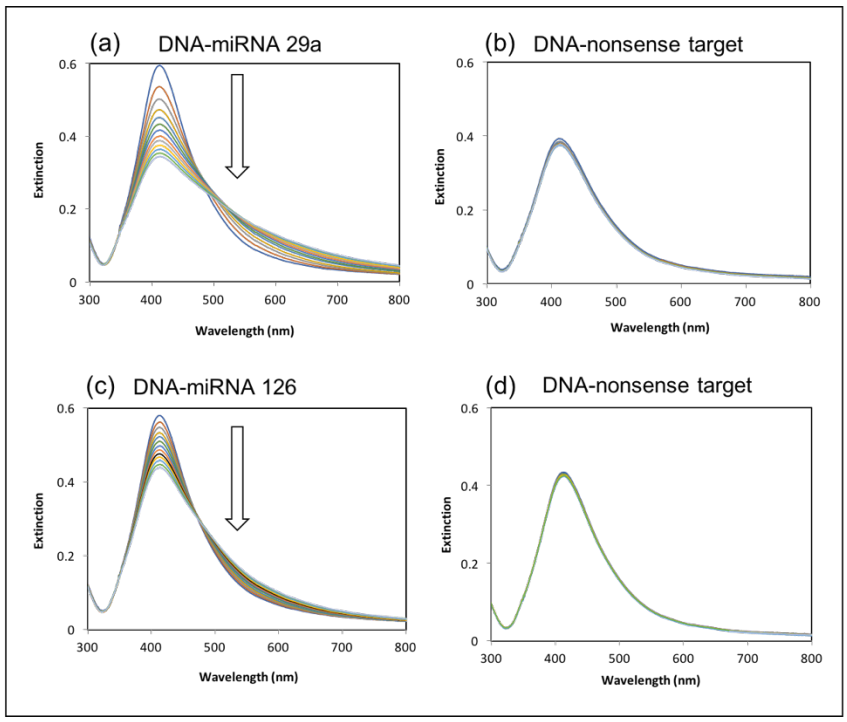

Figure 4.1: *Extinction spectra showing kinetic time studies.* ***a.*** *samples with miRNA-29a target present* ***b.*** *nonsense sequence present* ***c****. samples with miRNA-126 target present* ***d.*** *nonsense sequence present. All the spectra were collected over 120 minutes with each spectrum obtained at 10 minute intervals. The final concentration was 10 pM for each probe and 10 nM for the targets in a 400 µL sample.*

Ratios between absorbance values at 422 nm and 550 nm (indicative of conjugate dispersity) were calculated and plotted against time for the three targets (model RNA, miRNA-29a and miRNA-126) to compare the hybridisation efficiency of each target (Figure 4.2).

As the kinetics results show, duplex formation between the probes and miRNA126 target required a longer timeframe for completion of a full hybridisation event. In addition, model RNA was more efficient as compared to both miRNA targets.

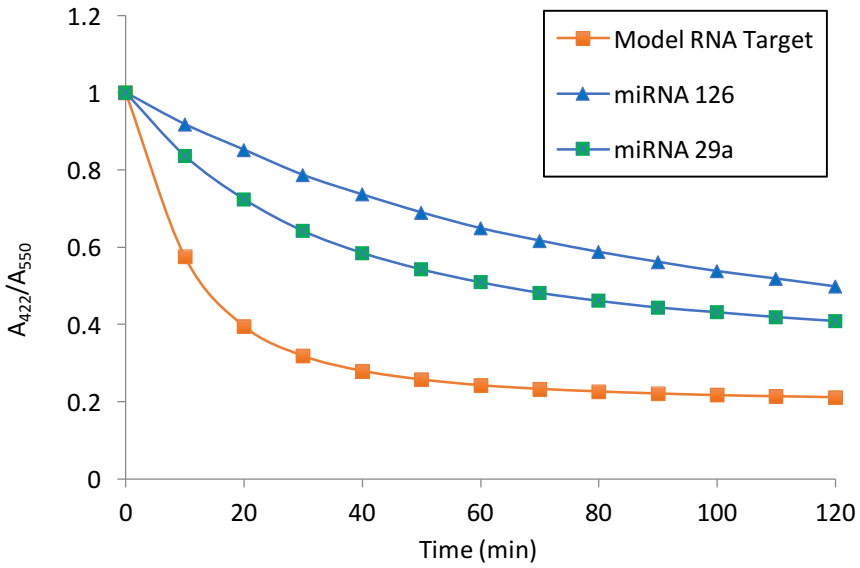

Figure 4.2: *Changes in nanoparticle assembly upon addition of different complementary targets over 120 min. The final concentration of targets was 10 nM and 10 pM for each probe in 400 µL samples using 0.3 M PBS buffer. The spectra were collected every 10 minutes using a UV-Vis spectrometer. The investigated targets were miRNA 29a, miRNA 126 and the model RNA that was used previously (chapter 3).*

The rate and extent of hybridisation whilst in the presence of complementary target depend on different conditions including temperature, concentration, length of the target sequence and hybridisation buffer.[91,56] As identified in the previous chapter, it was evident that increasing the concentration of the model RNA target to a specific threshold increased SERS signal which indicated an efficient concentration-dependant hybridisation event. In addition, the sequence complexity of the targets should also be considered for the potential to form a number of self-dimer configurations that may reduce discriminatory value (Table 4.3). This was considered and analysed *in silico* using the Oligoanalyzer application as available online, and it was identified that miRNA-126 had the highest propensity for dimer formation. This could be one of the reasons why the hybridisation event took longer as compared to the other targets investigated.

Table 4.3: *Complementary target names and number of associated homo-dimers that can be predicted by the Oligoanalyzer application.*

Target	Base-pairs
Model RNA Target	2
miRNA-29a Target	3
miRNA-126 Target	4

The buffer composition also has a great influence on the hybridisation process. The concentration and type of ions present facilitate hybridisation and can improve the kinetic efficiency with optimisation.

4.1.3 Buffer Study on the Hybridisation Experiment

Hybridisation experiments for silver nanoparticle conjugates with the addition of complementary miRNA target sequences was studied using different buffers to optimise the hybridisation efficiency. It was identified that use of 0.3 M PBS as a hybridisation buffer provided optimal results. The rate of hybridisation could be improved by increasing the salt concentration as this helped to screen the charges from the DNA sugar-phosphate backbone, allowing the oligo probe strands and the complementary DNA target to come close enough to hybridise.[56]

Dextran sodium sulfate (DSS) was selected for addition to the 0.3 M PBS hybridisation buffer because it is a known salt used for the enhancement of hybridisation kinetics and has been identified as an additive for the improvement of annealing rates.[92] This additive may also increase non-specific binding and the spectral background signal and therefore requires precise optimisation of concentration.[93-94] Addition of dextran sulfate increased the SERS background in the developed assay (Figure 4.3) and furthermore, induced probe hybridisation without target present which yielded a false-positive SERS signal. In the figure below, just 2% (w/v) dextran sulfate was used with 0.3 M PBS. However, the dextran polymer was reported to increase the rate of hybridisation of long target DNA sequences with oligonucleotide functionalised gold

nanoparticles,[92] but for this assay with the application of short target sequences, addition was not beneficial and increasing the salt concentration within the system affected the stability of the conjugates within this buffer, causing aggregation of the nanoparticles in the negative control suspension.

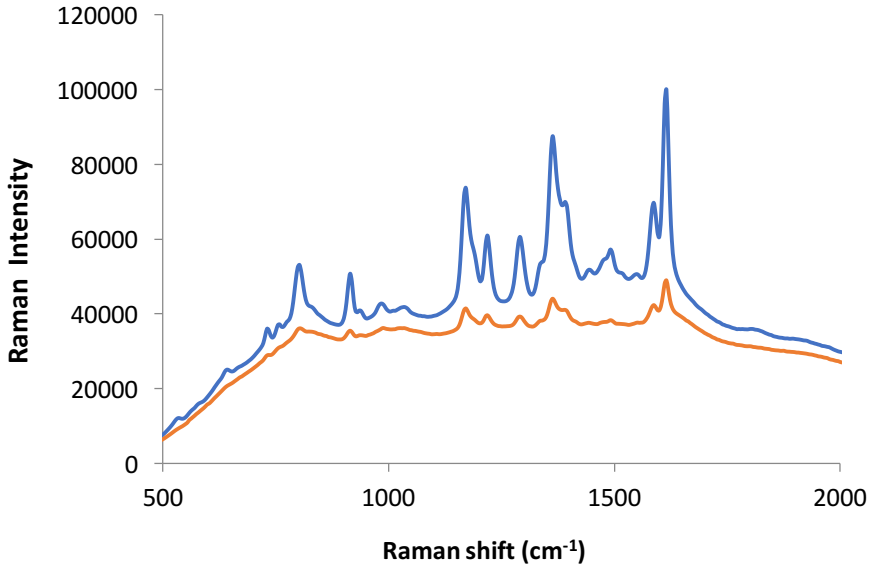

***Figure4.3**: SERS analysis for the detection of a complementary RNA target (blue line) and a non-complementary RNA sequence (red line) using MGITC-labelled oligonucleotide-hydroxylamine reduced silver nanoparticle conjugates and a 532 nm excitation wavelength with 5 × 5 s accumulations. The final probe concentration was 10 pM and 10 nM for the target with use of 2 % dextran sodium sulfate buffer (DSS) in 0.3 M PBS.*

An alternative buffer containing urea was also investigated as it is a known denaturation reagent and could help in preventing non-specific dimer formations, but this didn't improve the results with use of 0.3 M PBS and in addition gave a sharp SERS peak around 1000 cm^{-1} (Figure 4.4). The urea buffer contained 20 mM phosphate with 1.0 M NaCl and 6.0 M Urea.

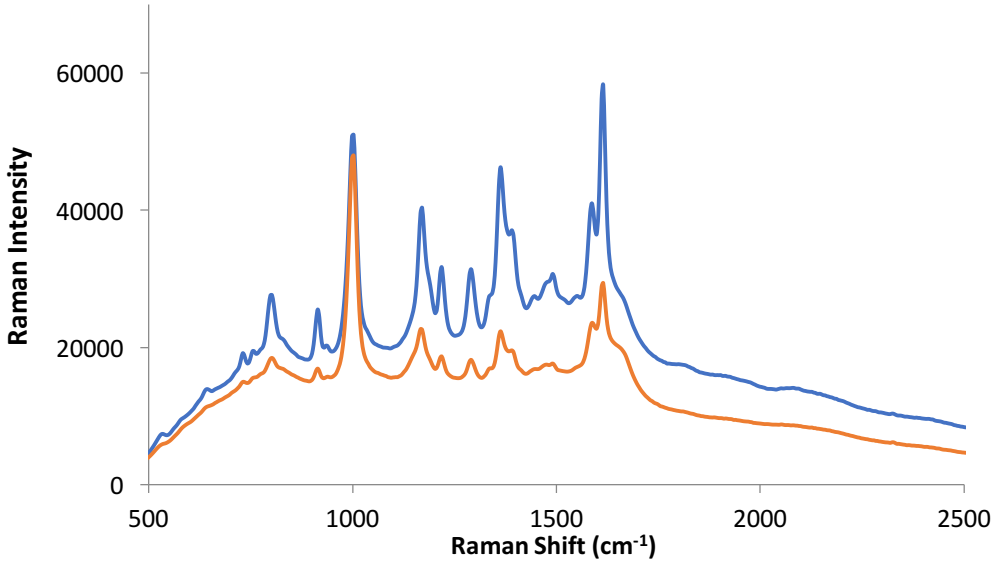

***Figure 4.4**: SERS analysis with a complementary RNA target (blue line) and non-complementary RNA target (red line) using MGITC-labelled oligonucleotide-hydroxylamine reduced silver nanoparticle conjugates and a 532 nm excitation wavelength with 5 × 5 s accumulations. The final probe concentration was 10 pM and 10 nM for the target with use of a urea buffer that consisted of 1.0 M NaCl, 20 mM phosphate, 6.0 M Urea.*

4.2 Monoplex Detection of miRNA-29a and 126 by SERS

Kinetic results showed that hybridisation occurred between the silver-nanoparticle conjugates and their corresponding targets. SERS was then used to demonstrate this and identify the SERS ON: OFF signal ratio. The MGITC Raman reporter was used at a concentration of 1×10^{-5} M for functionalisation of the silver conjugates as applied previously.

4.2.1 Monoplex Detection of miRNA-29a by SERS

The same experimental conditions as previously selected for use with the model RNA were applied again, although a reduced target concentration of 5 nM was added prior to the collection of SERS spectra. In the presence of the complementary target sequence, an increase in the SERS signal was obtained. The non-complementary and no target negative control samples showed no increase in SERS intensity and this

allowed for good discrimination between the presence and absence of target sequence (Figure 4.5). The enhancement of SERS spectra only occurred for a sample suspension that contained the miRNA-29a target, whilst the two negative control sample suspensions displayed no enhancement with comparably low SERS signal intensities.

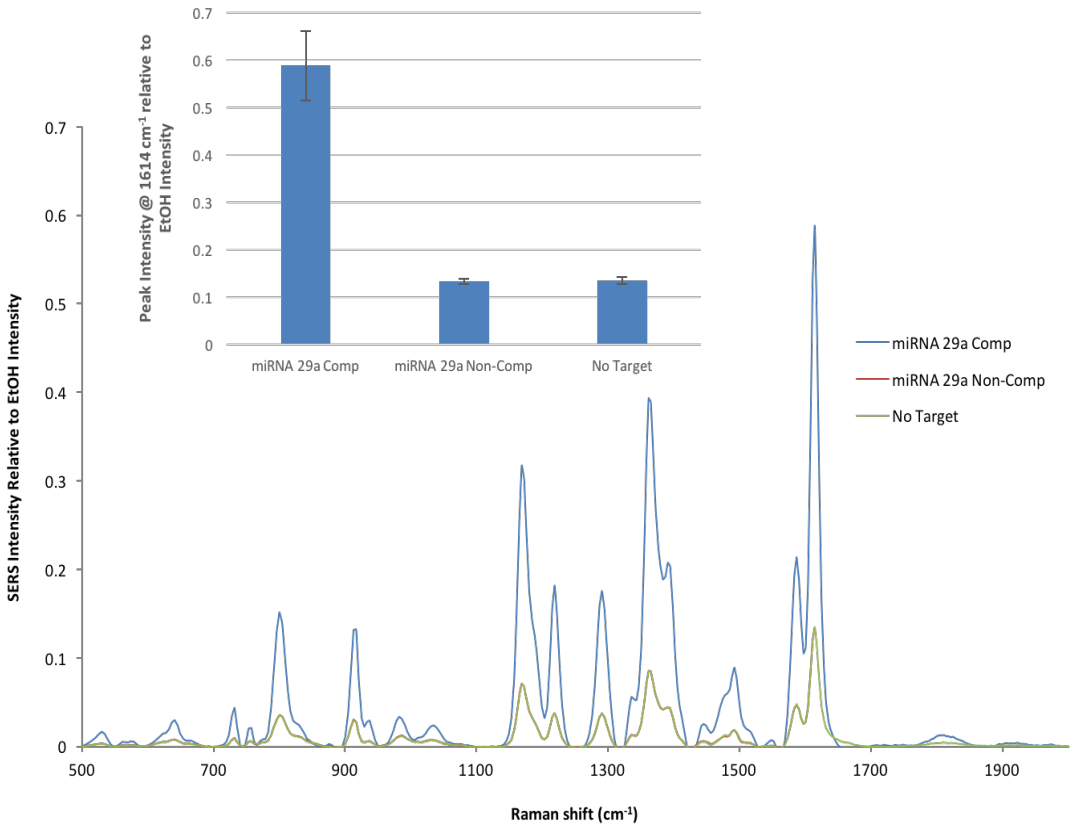

Figure 4.5: *SERS spectra for the miRNA-29a complementary target (blue line), non-complementary target (red line) and no target control (green line) were collected using an excitation wavelength of 532 nm. The spectra were collected using 3 × 3 s accumulations and the final concentration of each probe was 10 pM with 5 nM of target sequence. Inset: SERS intensity of the three suspensions for the 1644 cm^{-1} peak. Error bars represent the standard deviation from 4 replicates.*

The final concentration of the target sequence added was 5 nM because investigation of a concentration gradient ranging from 0 to 10 nM of complementary miRNA-29a indicated that the SERS signal started to decrease beyond a threshold of 5 nM final target concentration (Figure 4.6).

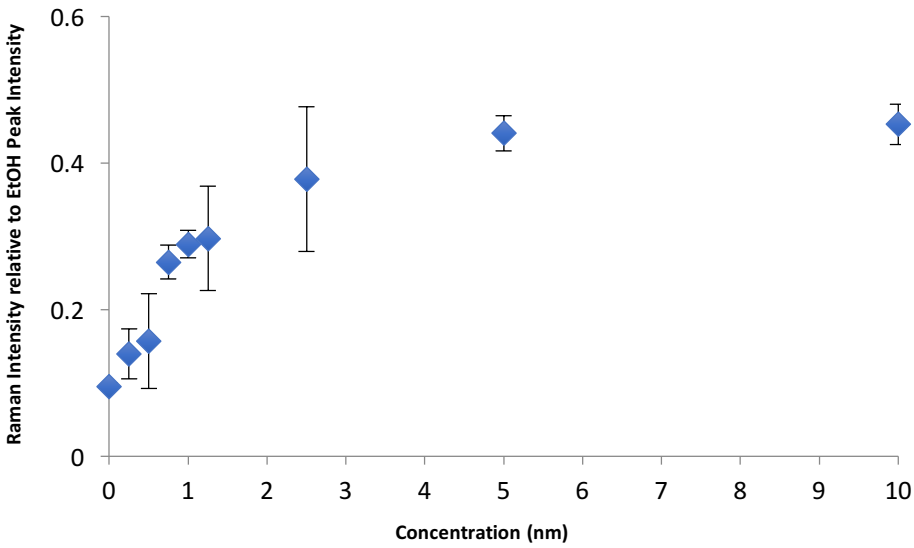

Figure 4.6: *Concentration study investigating miRNA-29a detection within a concentration range of 0 to 10 nM. MGITC was used as a Raman reporter with an excitation wavelength of 532 nm. The points represent the average of three replicates and the error bars indicate the standard deviation of the three replicates. The final concentration of each probe was 10 pM and the spectra were collected using 3 × 3 s accumulation times.*

4.2.2 Monoplex Detection of miRNA-126 by SERS

A significant ON: OFF discrimination ratio was also obtained with the addition of miRNA-126 target under the same experimental conditions and with the use of MGITC Raman reporter at a final concentration of 1×10^{-5} M (Figure 4.7).

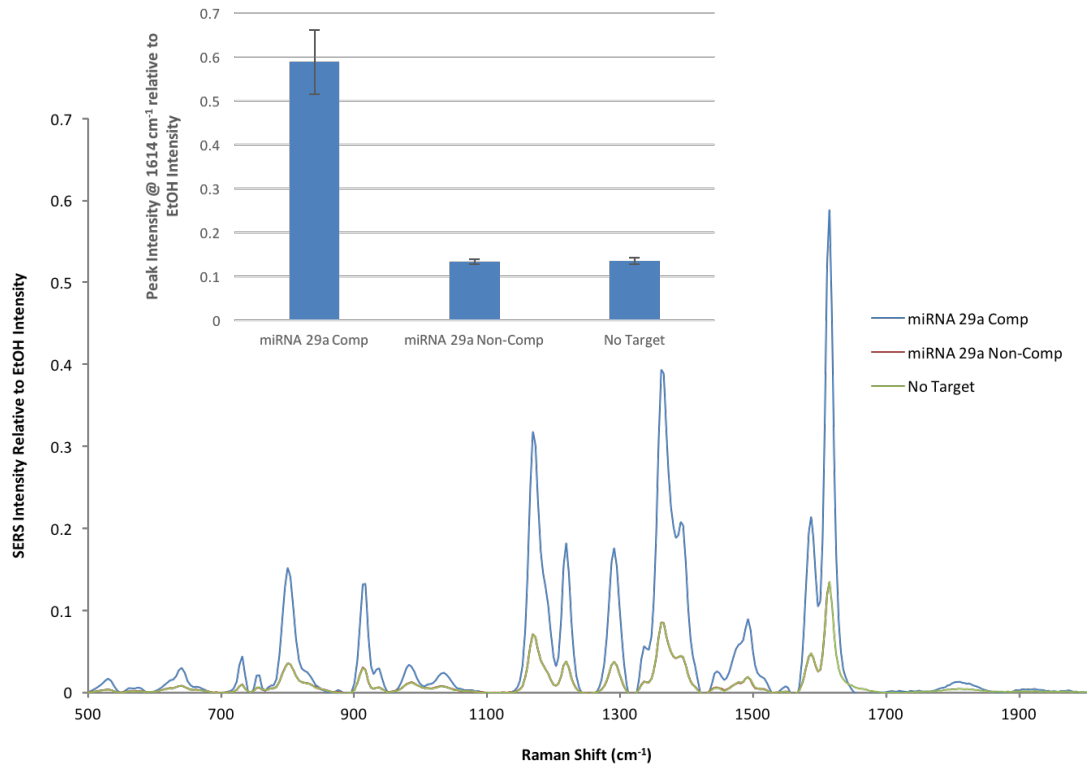

Figure 4.7: *SERS spectra for the miRNA-126 complementary target (blue line), non-complementary target (red line) and no target control (green line) were collected using an excitation wavelength of 532 nm. The spectra were collected using 3 * 3 s accumulation times and the final concentration of each probe was 10 pM with 5 nM of the target sequence. Inset: SERS intensity of the three solutions for the 1614 cm^{-1} peak. Error bars represent the standard deviation from 4 replicates.*

As identified for the previous target, a final concentration of 5 nM was added because investigation of a concentration gradient ranging from 0 to 10 nM of complementary miRNA-29a indicated that the SERS signal started to decrease beyond a threshold of 5 nM final target concentration (Figure 4.8).

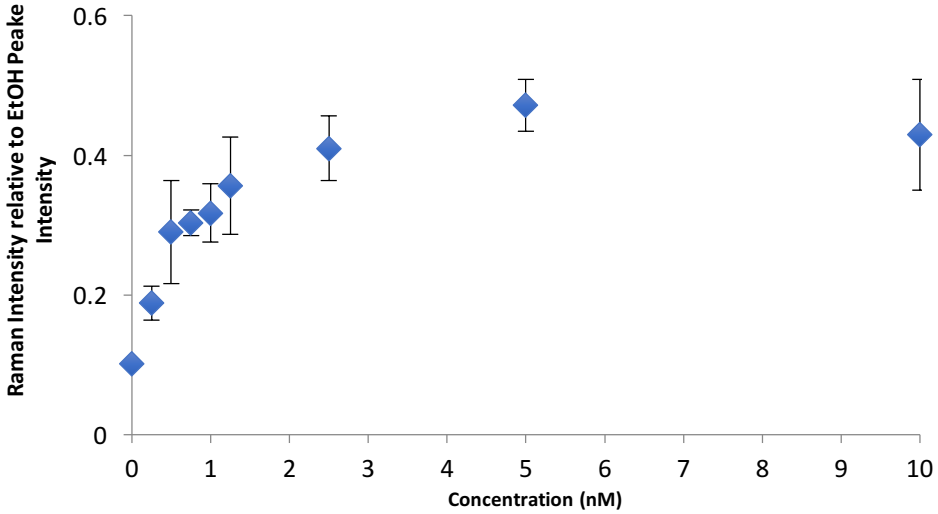

Figure 4.8: *Concentration study for miRNA-126 in the range of 0 to 10 nM. MGITC was used as a Raman reporter and spectra were collected using an excitation wavelength of 532 nm. The points represent the average of four replicates and the error bars show the standard deviation of the three replicates. The final concentration of each probe was 10 pM and the spectra were collected using 3 × 3 second accumulation times.*

SERS spectra identified with the addition of either miRNA-29a or miRNA-126 targets demonstrated distinctive ON: OFF ratios and produced a significant ON: OFF discrimination value. The solution-based assay developed was capable of confirming the presence or absence of a target sequence.

4.2.3 SERS Measurements of Hybridisation Kinetics Over Time

Hybridisation experiments for both the miRNA-29a and miRNA-126 targets were implemented for identification of the hybridisation rate associated with differing target duplexes and timeframe required for complete hybridisation (Figure 4.9). Investigation of both targets utilised identical experimental conditions, with a final probe concentration of 10 pM and target concentration of 5 nM selected as previously applied. MGITC Raman reporter (1×10^{-5} M) was used for all of the silver conjugate samples. The hybridisation rate increased over time as increasing numbers of

nanoparticles aggregated, although it was notable that the samples containing the miRNA-29a target aggregated at a faster rate as expected from the kinetic results. The SERS signal from the sample containing the non-complementary targets remained the same initially as no aggregation took place. However, after 180 min the signal began to increase suggesting that if the samples were left for too long, non-specific binding would occur. Therefore, the optimal hybridisation time was identified as two hours prior to implementation of SERS analysis, allowing for hybridisation to occur whilst avoiding interference from non-specific binding at longer timeframes.

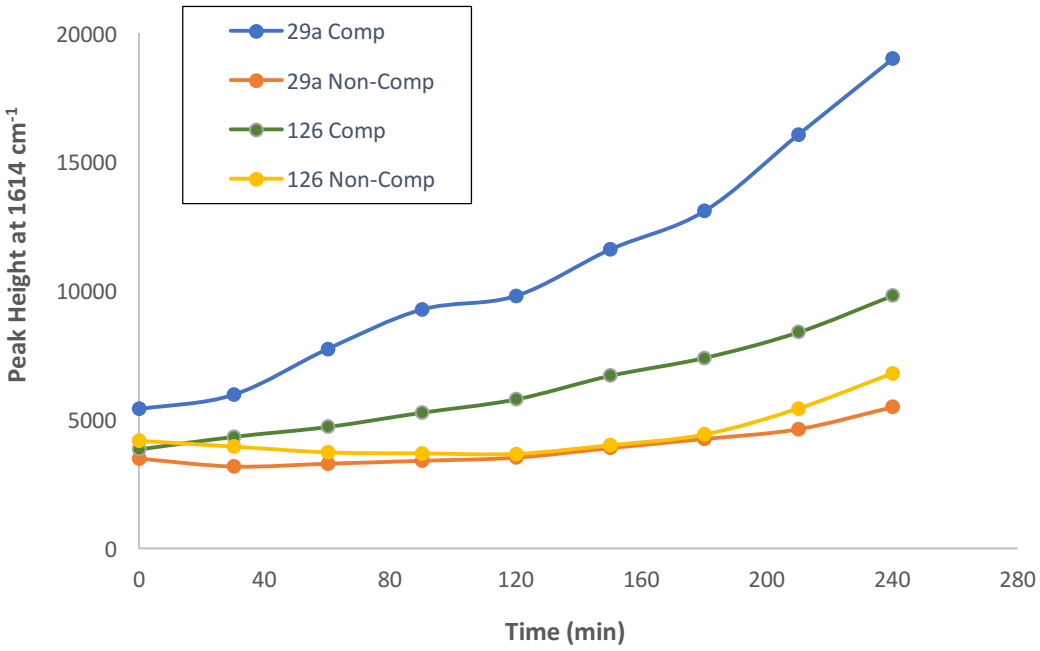

Figure 4.9: *MGITC peak at 1614 cm^{-1} plotted against time to highlight the differences in signal intensity from samples containing four different targets. Results demonstrated for each sample type show the mean values from four replicates collected using a 532 nm wavelength and 3 × 3 s accumulations. Final concentrations of silver-nanoparticle conjugates and targets were 20 pM and 5 nM respectively.*

4.2.4 Lower limit of detection for miRNA-29a & 126

A further concentration study for both of the miRNA targets was implemented within the range of 0 nM to 1 nM for determination of the lower limit of detection using SERS. The equation shown in Figure 4.10 was used to calculate the limit of detection which was found to be 463 pM for miRNA-29a and 320 pM for miRNA-126. MGITC reporter was used for detection of both targets and a final concentration of 10 pM was used for each conjugate.

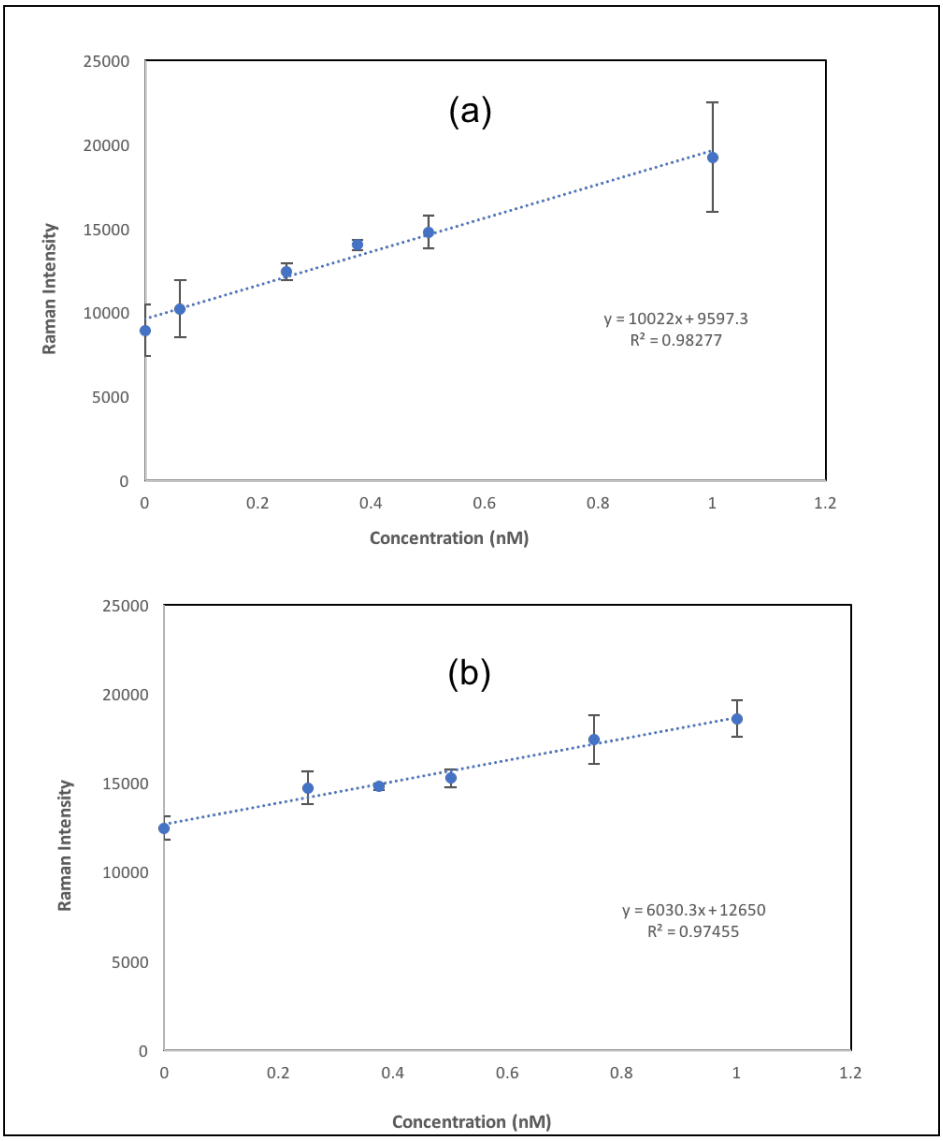

Figure 4.10: *Concentration studies conducted within the final target concentration range of 0 to 1 nM and final concentration of each probe was 10 pM using a 532 nm laser wavelength and 10 % laser power with 3 × 3 s replicate acquisitions. (a) miRNA-29a target concentration range and a calculated LOD of 463 pM (b) miRNA-126 concentration range and a calculated LOD of 126 pM.*

Following successful monoplex detection of each target with use of MGITC as a Raman reporter, a multiplex SERS format was developed. The probe conjugates for both targets were present in a single sample reaction mixture. Due to the multiplex basis of the assay, another Raman reporter was selected for the detection of the

secondary target. Rhodamine B isothiocyanate (RBITC) was selected for the detection of the miRNA-126 biomarker in addition to the MGITC reporter utilised for detection of miRNA-29a.

4.3 Multiplexing Experiment

4.3.1 Relative Dye Ratios

As it was necessary to detect two targets with the use two different Raman reporters, it was important to identify the appropriate concentration for each reporter. An insufficient concentration of dye could lead to weak Raman signals, whereas excess dye could increase the SERS signal background and therefore reduce the ON: OFF discriminatory value. A multiplex format additionally required experimental optimisation to identify a suitable dye concentration ratio, as differing concentrations are required for multiple Raman reporters to avoid saturation of one dye reducing discrimination from the other dyes used. The Raman reporter RBITC has a similar structure to that of MGITC and also attaches to the surface of silver nanoparticles through the isothiocyanate group.[95] RBITC is a fluorescent dye but fluorescence should be quenched when adsorbed to a AgNP surface. However, it has been reported that use of RBITC dye can result in high fluorescence background signal.[96] This may have been due to a proportion of Raman reporter remaining free in solution rather than adsorbing to the surface or dye may have dissociated from the surface following the conjugation process.

For optimisation of the multiplex experiment, a range of reporter molecule: AgNP ratios were investigated by application of differing numbers of dye molecules per nanoparticle. Reporter molecules: AgNP ratios investigated included 1000, 3000, 6000 and 9000 dye molecules per nanoparticle. Figure 4.11 indicates the differences in spectra obtained when varying ratios of MGITC dye were applied. There was an associated increase in peak intensity (1614 cm^{-1}) as the number of molecules increased from 1000-6000 molecules per nanoparticle, and subsequent decrease for 9000 molecules per nanoparticle. This was likely due to instability causing colloidal loss of suspension. Too low or too high dye ratios were not suitable for optimal ON: OFF

discrimination due to weak signal intensity or instability respectively, therefore the reporter molecule: AgNP ratio selected was 3000 dye molecules per silver nanoparticle.

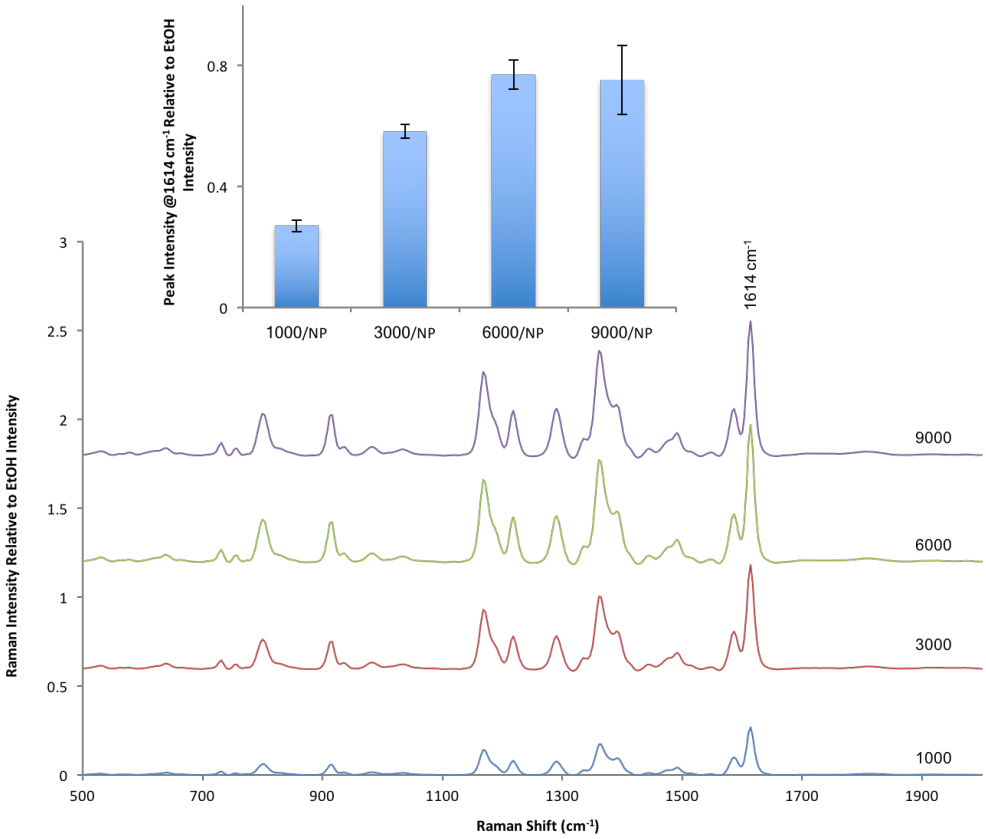

Figure 4.11: *SERS spectra for detecting of miRNA-29a complementary target with differing assumed numbers of dye molecules per nanoparticle used. MGITC was used to functionalise the DNA-conjugates in different ratios. The spectra were collected using an excitation wavelength of 532 nm and 3 × 3 s accumulations. The final concentration of each probe was 10 pM and 5 nM of the target. Inset: SERS intensity of the four suspensions for the 1614 cm^{-1} peak. Error bars represent the standard deviation from 4 replicates.*

For the detection of miRNA-126, RBITC dye was used and the same ratios were investigated. RBITC has a similar structure as compared to MGITC but has a distinctive peak that can be distinguished at 1642 cm^{-1}. The SERS peak increased as the number of dye molecules per nanoparticle increases (Figure 4.12) as expected, and

a ratio of 3000 RBITC molecules per nanoparticle was selected as this provided a comparable signal intensity to that of the MGITC dye at the same ratio. An increased intensity may have been achievable at higher ratios, but this would have overcome the MGITC signal for which higher intensities could not be achieved beyond 3000 reporter molecules per nanoparticle without some loss of suspension. Therefore, to maintain a balance in signal intensities between both dyes in a multiplex system, 3000 molecules per nanoparticle for both of the selected reporters was considered an appropriate concentration for multiplex discriminatory value.

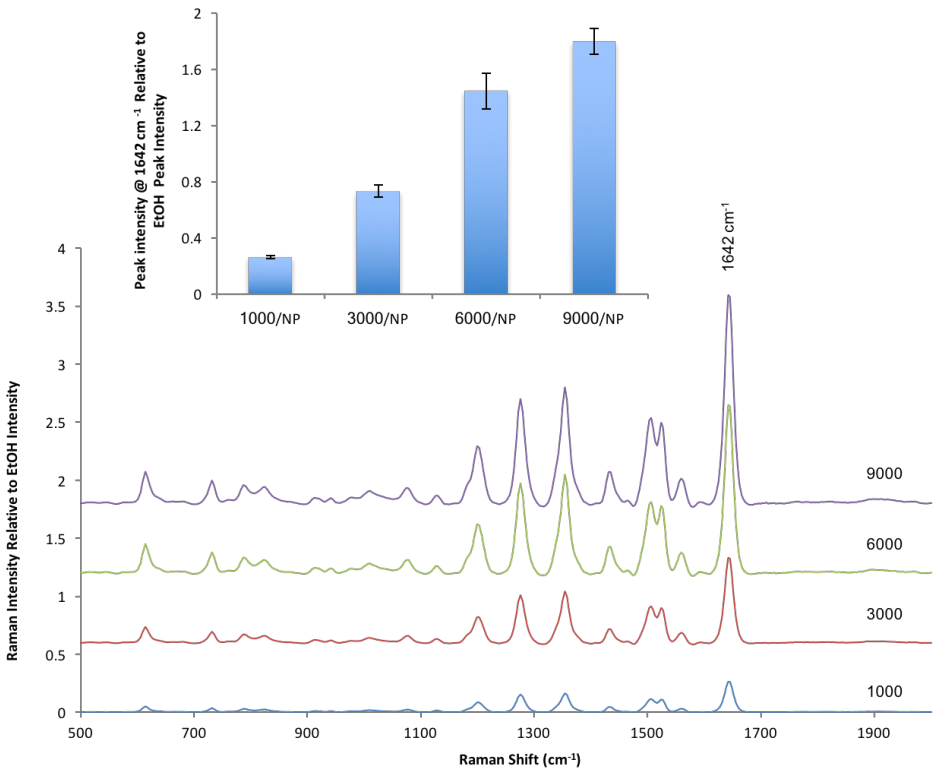

Figure 4.12: *SERS spectra for detecting of miRNA-126 complementary target with different amount of dye used. RBITC was used to functionalise the DNA-conjugates at different assumed ratios. The spectra were collected using an excitation wavelength of 532 nm and 3 × 3 s accumulations. The final concentration of each probe was 10 pM and 5 nM of the target. Inset: SERS intensity of the four suspensions for the 1642 cm^{-1} peak. Error bars represent the standard deviation from 4 replicates.*

Figure 4.13 shows overlapping singleplex detection of each target with use of 3000 dye molecules per nanoparticle with a comparable signal intensity ratio considered suitable for further development of a multiplex format.

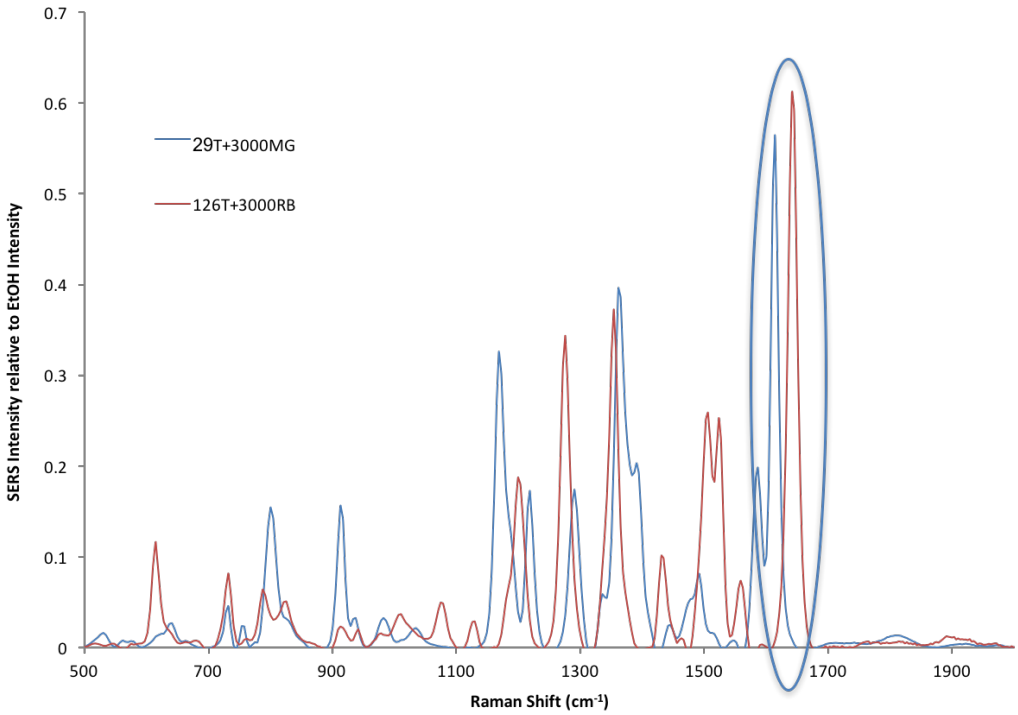

Figure 4.13: *SERS spectra obtained for the detection of miRNA-29a & 126 targets separately. miRNA-29a conjugates were functionalised with MGITC and a distinctive SERS peak was evident at 1614 cm^{-1} (blue line). RBITC was used to functionalise the DNA-conjugates for miRNA-126 target and a distinctive peak was evident at 1642 cm^{-1} (red line). Spectra were collected using an excitation wavelength of 532 nm and 3 × 3 s accumulations. Final concentration of each probe was 10 pM and 5 nM of the target.*

4.3.2 Detection of miRNA-29a & miRNA-126 by SERS in a Multiplex Format

For the application of the multiplex format experiment, all the required silver-nanoparticle probe conjugates were mixed with the targets within 0.3 M PBS hybridisation buffer. The final concentration for each probe remained at 10 pM with 5 nM of target addition. Five samples were prepared for comparison of signal intensities from MGITC as applied for the detection of miRNA-29a and RBITC as

applied for the detection miRNA-126 target (Figure 4.14). In the first sample both targets are present (a), whilst the second (b) and third (c) samples have only miRNA - 126 or miRNA-29a present respectively. For calculation of the ON: OFF ratio a sample with non-complementary target and a sample with no target was also included for analysis (d). The presence and absence of each target was demonstrated to significantly affect the SERS signal of the corresponding Raman reporter. The assay was applied for the detection of both targets using a mixture of the required probes, with a significant increase in MGITC signal intensity associated with samples containing miRNA-29a target, whilst RBITC signals also increased significantly in samples that contained miRNA-126 target. There was a small background observed from samples that had no target or non-complementary target present. However, discrimination between samples was evident due to the increase in associated MGITC and RBITC peaks at 1614 cm^{-1} and 1642 cm^{-1} respectively, as compared to the no target and non-complementary negative control samples (Figure 4.14).

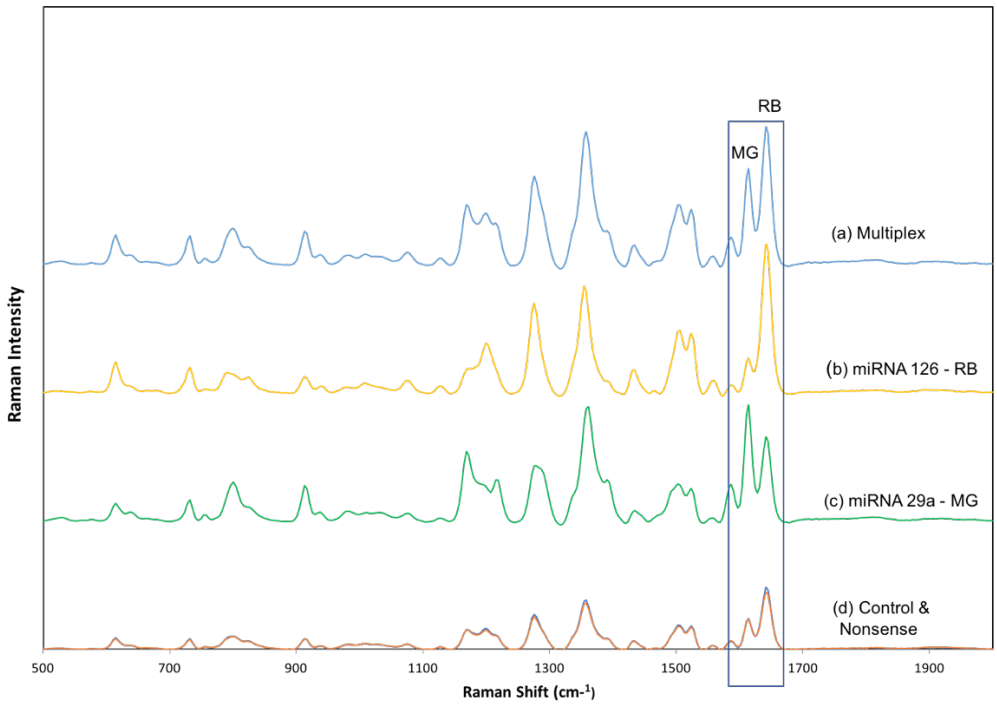

Figure 4.14: *SERS spectra obtained from different samples that contained mixed probes for the two targets. (a) Sample containing both target sequences (blue line), (b) Only miRNA-126 was present (yellow line), (c) Only miRNA-29a was present (green line), (d) Negative control samples containing no target (orange line) or non-complementary/nonsense target (blue line). Spectra acquired using a 532 nm wavelength with 3 × 3 s acquisitions. The final concentration of each probe in all samples was 10 pM with a 5 nM target concentration. A 0.3 M PBS hybridisation buffer was used for all the samples. MGITC and RBITC reporters were used to functionalise the corresponding conjugates at a ratio of 3000 molecules per nanoparticle.*

4.3.3 Principle Component Analysis (PCA) for the Multiplexing Experiment

To prove that the assay was capable of distinguishing between targets present within the multiplex hybridisation mix, principal component analysis (PCA) was implemented. PCA was performed for the samples as presented in Figure 4.15, with one sample containing both targets (miRNA-29a & miRNA-126), two samples containing only one target (only miRNA-29a or miRNA126) and two samples containing only a non-complementary target or no target control. The resulting PCA plot showed that the 5 samples were distinctively separate from each other and all were clearly distinguishable, although both the non-complementary and no target controls were closely aligned as expected for negative controls. The samples were analysed in

replicates of four which were closely grouped together, indicating the reproducibility of the assay. The sample that had both targets present was positioned between each grouping containing individual targets, which gave an indication that there was a contribution from both Raman reporters (MGITC and RBITC). If the results were not reproducible, the plot would show sample overlapping with associated difficulty in discrimination of individual group identities.

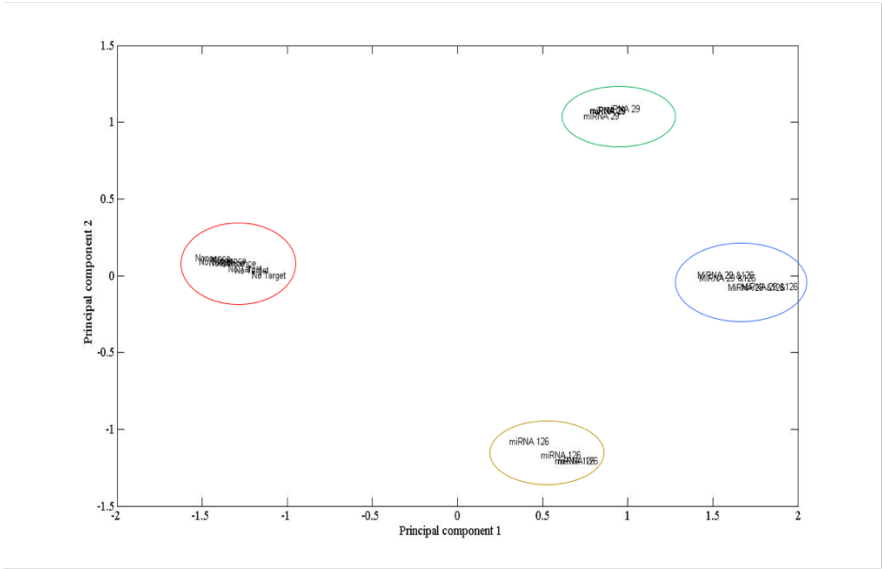

Red: control & Nonsense **Yellow**: miRNA 126-RBITC **Green**: miRNA 29a-MGITC **Blue**: Multiplex

Figure 4.15. *Principal component analysis (PCA) plot for the multiplex format. The sample containing both targets is circled in blue. The two negative control samples, (No target and non-complementary target) are circled in red. The sample containing only miRNA-126 target is circled in yellow, while the sample containing only miRNA-29a target is circled in green. Four replicates and one scan for each sample was performed using a laser wavelength of 532 nm. The acquisition time was 3 × 3 s using 532 nM laser wavelength. The final concentration of each probe in all samples was 10 pM with a target concentration of 5 nM. 0.3 M PBS hybridisation buffer was used for all samples.*

4.3.4 Detecting both miRNA-29a and miRNA-126 in a Multiplex Experiment at Different Target Concentration Ratios

4.3.4.1 Detecting miRNA-29a by SERS Within a Range of Target Concentrations

The multiplexing experiment for the detection of miRNA-29a and miRNA-126 was successful with a significant ON: OFF SERS discrimination observed for each target. The following investigation was implemented to assess the capability of the multiplex format for detection of the miRNA targets over a concentration range. This was performed by investigating one of the targets over a concentration range, whilst maintaining the other target at a fixed concentration. The multiplexing experiment was conducted at room temperature and the final concentration of probes was 10 pM. Initially the quantitative value for multiplex detection of miRNA-29a was investigated within a target range of 0-20 nM (Table 4.4), whilst the miRNA-126 target was maintained at a concentration of 5 nM. Nine samples were prepared with the same concentration of all probes and miRNA-126 target, whilst the concentration of miRNA-29a target was added at incremental increases of 2.5 nM.

Table 4.4: *Final concentration of miRNA-29a and miRNA-126 targets used for the multiplexing experiment.*

Sample No.	miRNA29a Target Conc. (nM) MGITC	miRNA126 Target Conc. (nM) RBITC
1	0	5
2	2.5	5
3	5	5
4	7.5	5
5	10	5
6	12.5	5
7	15	5
8	17.5	5
9	20	5

The MGITC-associated peak at 1614 cm^{-1} corresponded to the miRNA-29a target and the RBITC-associated peak at 1642 cm^{-1} corresponded to the miRNA-126a target. Figure 4.16 shows the SERS intensity of these two peaks for each sample. It was not expected that the SERS intensity would change for the miRNA-126 target as the concentration did not change and this what happened except for sample 9. There was a decrease in RBITC signal and this may have been due to the high concentrations of miRNA-29a present contributing to the dominance of the MGITC signal and associated reduction of the RBITC signal. The complementary miRNA-29a target sequence demonstrated a low signal intensity with no target present within sample 1. Subsequently, the signal increased with target addition but beyond a target concentration of 5 nM, the signal did not appear to increase significantly. The experiment could detect miRNA-29a at different concentrations.

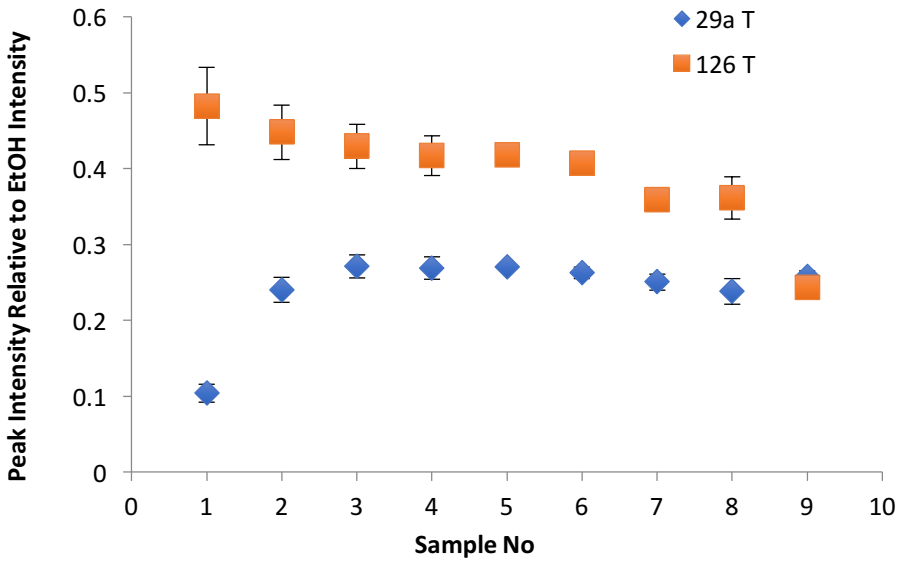

Figure 4.16: *SERS intensities at 1614 cm^{-1} and 1642 cm^{-1} for multiplexed samples hybridised in 0.3 M PBS buffer. Each sample is an average of four replicates. The spectra were collected using an excitation wavelength of 532 nm and 3× 3 s accumulations. The final concentration of each probe was 10 pM and with 5 nM of miRNA-126 target added. The final concentration of miRNA-29a was varied from 0 to 20 nM. MGITC and RBITC reporter was used to functionalise the DNA-conjugates at a ratio of 3000 molecules per nanoparticle. Error bars represent the standard deviation from 4 replicates.*

4.3.4.2 Detecting miRNA-126 by SERS within a Range of Target Concentrations

The same experimental conditions and criteria were applied for the detection of miRNA-126. The miRNA-29a target was maintained at a final concentration of 5 nM whilst the miRNA-126a concentration was changed in 2.5 nM incremental increases ranging from 0-20 nM. Table 4.5 shows the concentrations used for both targets within each sample:

Table 4.5: *Final concentration of miRNA-126 and 29a targets used within the multiplexing experiment*

Sample No.	**miRNA-126 Target Conc. (nM)** **(RBITC)**	**miRNA 29 Target Conc. (nM)** **(MGITC)**
1	0	5
2	2.5	5
3	5	5
4	7.5	5
5	10	5
6	12.5	5
7	15	5
8	17.5	5
9	20	5

A similar behaviour was observed when the concentration of miRNA-126 target was varied in samples containing a fixed concentration of miRNA-29a. In sample 1 there was no miRNA-126 target present as indicated by the low SERS signal obtained, with a subsequent increase in signal for sample 2 with addition of a final target concentration of 2.5 nM (Figure 4.17). As observed previously, the signal did not increase significantly beyond this threshold, and there was a slight decrease in signal intensities for both targets as the concentration increased further, inducing loss of colloidal suspension as the aggregate size increased.

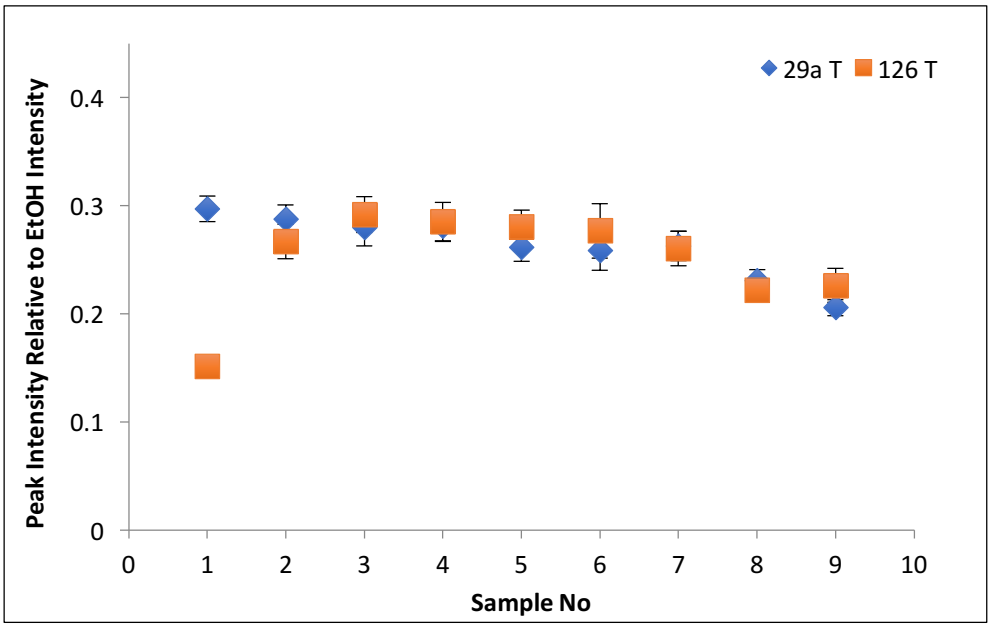

Figure 4.17: *SERS intensities at 1614 cm^{-1} and 1642 cm^{-1} for multiplexed samples hybridised within 0.3 M PBS buffer. Each sample is an average of four replicates. The spectra were collected using an excitation wavelength of 532 nm and 3 × 3 s accumulations. The final concentration of each probe was 10 pM and 5 nM of miRNA-29a target added. The final concentration of miRNA-126 was varied from 0 to 20 nM. MGITC and RBITC reporter was used to functionalise the DNA-conjugates at a ratio of 3000 molecules per nanoparticle. Error bars represent the standard deviation from 4 replicates.*

4.3.4.3 Detecting miRNA-29a & miRNA-126 Using a Range of Conjugate Concentrations

For this experiment, both targets were maintained at a final concentration of 5 nM, whilst the silver nanoparticle conjugates specific to each target were added at different ratios as shown in Table 4.6. The miRNA-126 specific probes were maintained at the same concentration but the concentration of the miRNA-29a specific probe pair was doubled incrementally.

Table 4.6: *Ratios of Silver-Nanoparticle conjugates for miRNA-29a & 126 Target.*

Sample No	(126P: 29P)
1	1:1
2	1:2
3	1:4
4	1:6
5	1:8

The final concentration of probes for miRNA-126 was maintained at 10 pM, whilst the concentration of miRNA-29a conjugates was increased in concentrations of 10 pM, 20 pM, 40 pM, 60 pM and 80 pM. As the concentration of miRNA-29a probes increased, there was an associated increase in reporter present within the suspension. The peak intensities correlating to MGITC at 1614 cm^{-1} and RBITC at 1642 cm^{-1} were selected for comparison. An increased MGITC peak signal was obtained each time the miRNA-29a probe concentration increased (Figure 4.18). However, there was a dramatic decrease in SERS signal observed for sample 5 that could be attributed to signal saturation. The signal from RBITC was expected to remain the same as the concentration did not change but instead there was a notable decrease in signal. Sample 1 contained probe sets specific to each target at the same concentration and a comparable intensity was observed. As the miRNA-29a probe concentration increased, MGITC dye present within the sample suspension was dominant. The total volume in all the samples was kept fixed throughout the experiment.

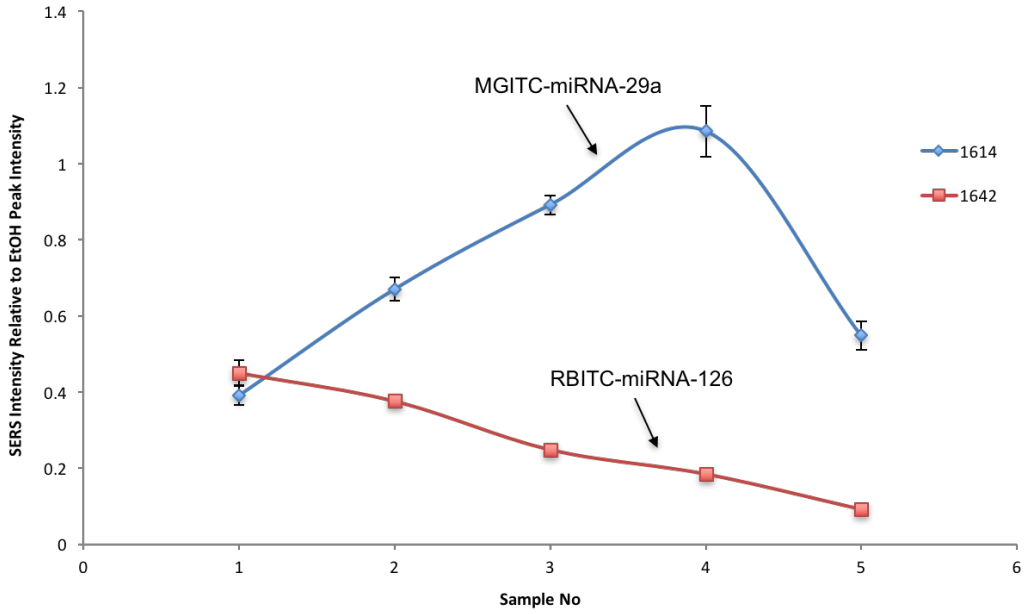

Figure 4.18: *SERS spectra intensities at 1614 cm^{-1} (blue line) and 1642 cm^{-1} (orange line) obtained using excitation wavelength of 532 nm and 3 * 3 s accumulations. The final concentration of miRNA-126 probes was 10 pM and 5 nM of miRNA-29a & miRNA-126 target sequences were added to the 0.3 M hybridisation buffer. The final concentration of miRNA-29a probes increased at concentrations of 10 pM, 20 pM, 40 pM, 60 pM and 80 pM respectively. MGITC and RBITC reporter was used to functionalise the DNA-conjugates in a ratio of 3000 molecules per nanoparticle. Error bars represent the standard deviation from 4 replicates.*

4.3.5 Serum Experiment

As determined from the previous results, the developed assay for miRNA biomarker detection demonstrated great promise for ON: OFF SERS discrimination of miRNA sequence specificity. As the ultimate objective of this research was to detect miRNA biomarkers that naturally exist within the circulatory system or specifically the serum component of blood, it was desirable to detect the selected biomarkers directly from this biological sample matrix. miRNA molecules are considered to be remarkably stable biomarkers and therefore it was feasible to develop a direct method to detect miRNA sequences with applicability in real-life situations. This would demonstrate great promise for implementing this method within a biomedical context. Thus, a synthetic serum (fetal bovine serum) was used to mimic a clinical sample and

investigate the capability of this method to detect the target within a biological sample matrix.

The miRNA-29a target was added at a final concentration of 5 nM to the corresponding silver nanoparticle conjugates at a final concentration of 10 pM. A total of six samples were prepared, five of which were positive samples containing complementary target within varying sample matrices that were added to the 0.3 M PBS hybridisation buffer. Additionally, a negative control sample with non-complementary target was added for comparison of the ON: OFF discrimination ratios. In addition to the positive and negative control samples containing respective complementary and non-complementary targets, three samples spiked with different % (v/v) concentrations of serum (10%, 5% and 1%) were hybridised with complementary target in 0.3 M PBS buffer. Finally, a sample containing addition of 1% serum and 2% dextran within the 0.3 M PBS hybridisation buffer was analysed in consideration that this may improve the discrimination value. The results are shown in Figure 4.19.

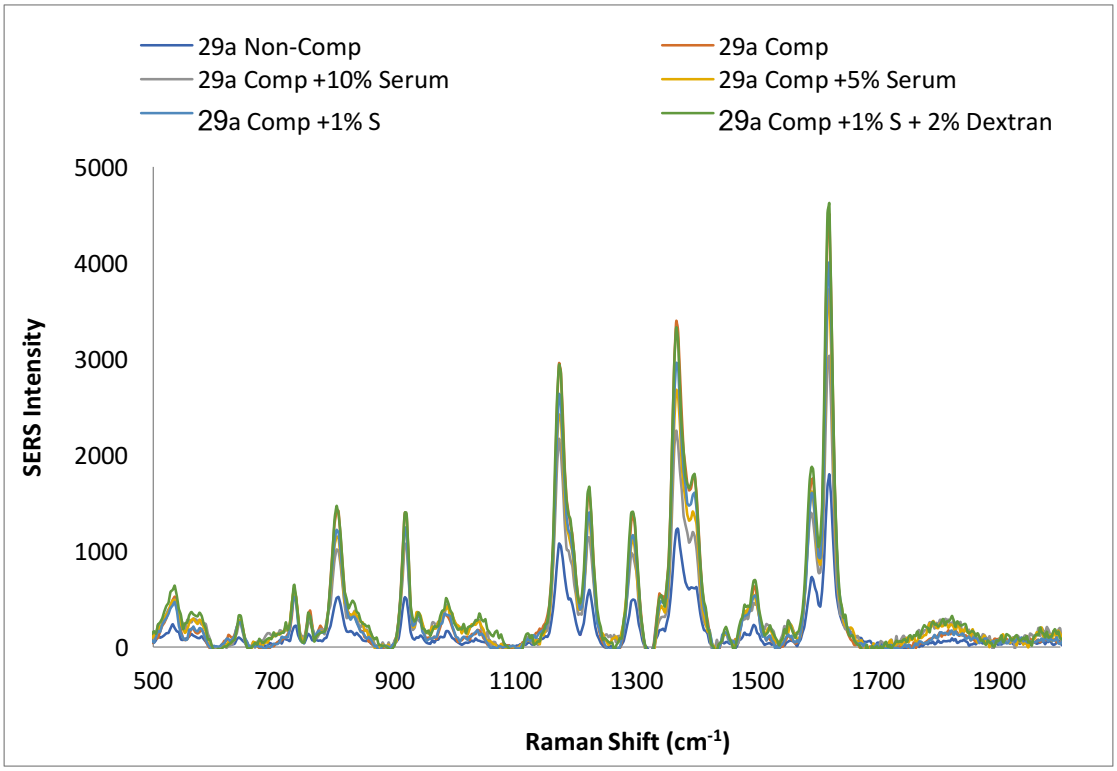

Figure 4.19: *SERS spectra obtained for the six samples hybridised with and without addition of serum and dextran using an excitation wavelength of 532 nm and 3 * 3 s accumulations. Unmodified PBS buffer with non-complementary target (dark blue line) and complementary target (orange line). PBS buffer spiked with serum (v/v) at 10% (grey line), 5% (yellow line), 1% (light blue line) and 1% serum with 2% dextran (green line). Final concentration of miRNA-29a specific probes was 10 pM each and 5 nM of the miRNA-29a target within the varying hybridisation buffers. MGITC was used to functionalise the miRNA-29a specific DNA-conjugates in a ratio of 3000 molecules per nanoparticle.*

As the amount of serum increased, the SERS signal decreased, although the addition of 2% dextran sulfate to the hybridisation buffer increased the signal to a comparable intensity as observed for the positive control. However, dextran buffer can also increase the signal intensity without target addition. It was not possible to detect the target in samples containing a high % of serum as the discrimination value was significantly inhibited by background interference. Figure 4.20 demonstrates that it was still possible to detect the target when the sample was spiked with serum.

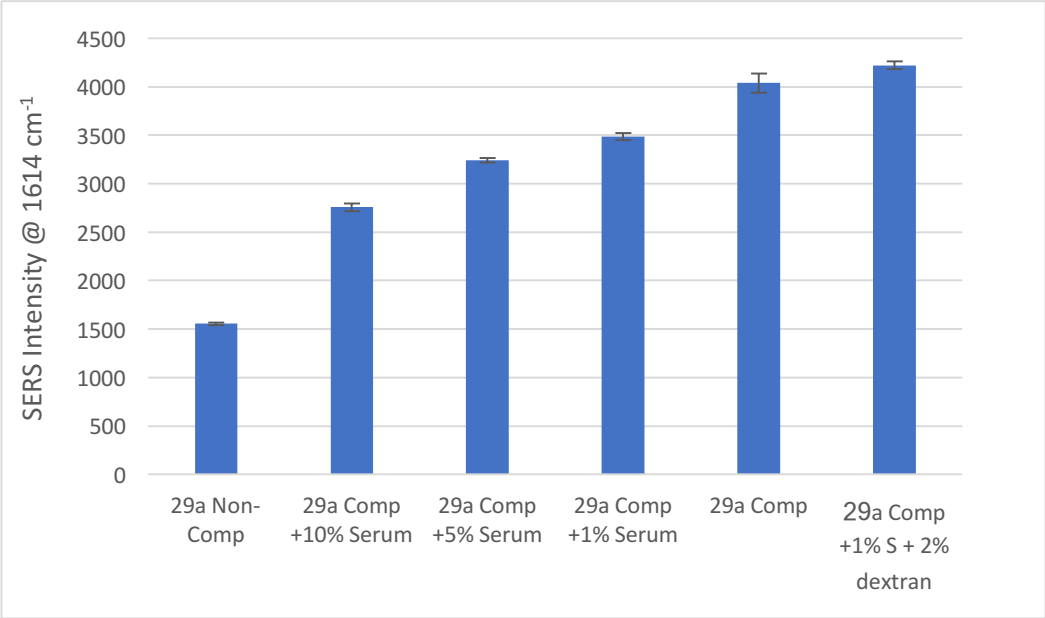

Figure 4.20: *SERS intensity at 1614 cm^{-1} as obtained for the five samples hybridised with and without the addition of serum and dextran using an excitation wavelength of 532 nm and 3 × 3 s accumulations. The final concentration of each miRNA-29a probe was 10 pM and with 5 nM of the miRNA- 29a target in 0.3 M PBS buffer. MGITC was used as a Raman reporter at a ratio of 3000 molecules per nanoparticle. Error bars represent the standard deviation from 3 replicates.*

It was notable from the investigation of miRNA detection within serum samples that reproducibility required further optimisation as compared to hybridisation within unmodified PBS buffer. Therefore, it was concluded that further experimentation should be considered for comparison of miRNA detection directly from biological serum samples and RNA extracts sourced from serum samples. However, in general, the method demonstrated potential for progression to analysis of miRNA detection sourced from clinical extracts.

4.4 Summary

Silver nanoparticles (AgNPs) with oligonucleotide probes were synthesised and used to detect specific miRNA biomarkers related to type 2 diabetes (miRNA-29a and miRNA-126) following successful detection of the model RNA sequences. Addition of miRNA target sequence to the probes resulted in the aggregation of the nanoparticles *via* hybridisation and changes in the kinetic and optical properties of the hybridised nanoparticle conjugates were observed. The dampening and broadening of the surface plasmon band (λ_{max}) due to the coupling of individual nanoparticles during aggregation resulted in a colour change to the suspension as observed by the naked eye. Adding a non-complementary miRNA sequence to the DNA nanoparticle conjugates resulted in no observed optical change as no hybridisation induced aggregation occurred. In addition, the assay could distinguish between different miRNA biomarkers in a one-pot approach by using different Raman reporters for each target. This demonstrated great promise for the use of oligonucleotide-nanoparticle conjugates and SERS for the detection of miRNA biomarkers related to type 2 diabetes and supporting the early detection, prevention and targeted treatment of many diseases by application of miRNA biomarker detection. The use of SERS for miRNA detection is particularly promising and provides a new nano-sensing approach for the detection of miRNA biomarkers. In turn, this could allow biologists and clinicians to detect and quantify miRNA levels, for use in medical diagnosis and early detection of type 2 diabetes and many other diseases. However, detecting miRNA in serum is still challenging as it is hard to see if any hybridisation occurred by SERS. Thus, another approach was developed using lateral flow strips that could help in detecting miRNA in serum.

CHAPTER 5: Lateral Flow Assay for the Detection of miRNA-29a using Silver Nanoparticles and SERS

5.1 Introduction to the Assay

With the application of SERS, miRNA targets were also detected using a solid-phase platform incorporating lateral flow strips. Lateral flow is already established for detecting nucleic acids,[97-99] and by using SERS, the sensitivity of this method can be increased for the detection of targets isolated from aqueous solutions and biological samples by paper-based chromatography. This technique is considered to be very attractive to many researchers because it is simple, rapid, low cost and doesn't require skilled operators or significant sample preparation.[100] However, some of the issues associated with this technique as compared to alternative analytical methods are the sensitivity and quantitative analysis limitations. Combining the visual detection of the target via the lateral flow (LF) strips with SERS will overcome these issues. In this work, a surface-based assay was developed using silver nanoparticle-conjugates for miRNA-29a detection via lateral flow strips.

A lateral flow strip has four main components (Figure 5.1), a sample pad, conjugate pad, nitrocellulose membrane and absorbent pad. In addition, it has an underlying backing card to support the strip and for ease of handling. The sample pad absorbs the sample solution and for this assay, it is immersed in the running buffer containing the target and the capture probe. The other probe is dispensed on the conjugate pad and as the sample solution migrates through the strip by capillary action, the nanoparticles are captured and aggregate on the test line (positive test) in the nitrocellulose membrane, presenting a clear green band that can be visually identified by eye. The excess solution continues to diffuse and is absorbed by the adsorbent pad. It is a quick test and the result can be observed within 15 min.

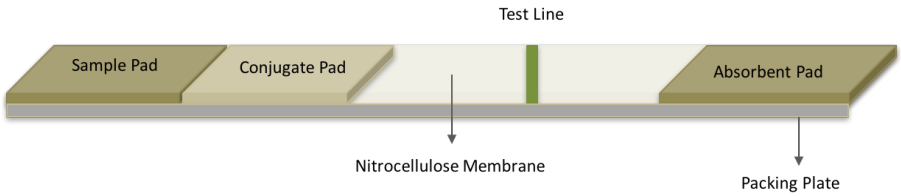

***Figure 5.1**: A schematic representation showing the main components of the lateral flow strip used in this assay.*

This assay relies on the same concept for the detection of miRNA target sequences upon hybridisation between the oligo-probe functionalised silver nanoparticles and complementary miRNA-29a target. Hydroxylamine silver nanoparticles were used for miRNA-29a detection using lateral flow strips. However, in this surface-based assay one of the miRNA-29a DNA conjugates has to be modified with biotin rather than a thiol functional group for immobilisation on the nitrocellulose membrane and subsequent capture by streptavidin. The test line on nitrocellulose is pre-treated with streptavidin which has a high affinity for biotin. Table 5.1 shows the sequence of the probes and targets used in this assay.

***Table 5.1:** Sequences of miRNA-29a targets and probes used in the lateral flow assay*

Sequence Name	Sequence Details
miRNA-29a complementary	UAG CAC CAU CUG AAA UCG GUU A
miRNA-29a probe 1	5' THIOL-$(HEG)_3$-TAA CCG ATT TC 3'
miRNA-29a probe 2	5' BIOTINHEXYL-AGA TGG TGC TA 3'
miRNA non-complementary	ACU GAC GAC GGC ACA UAU CUA C

Hybridisations between the biotin-modified DNA conjugate (probe 2), complementary miRNA-29a target, and oligo-probe (probe 1) functionalised nanoparticles were performed on the lateral flow strip to allow for SERS detection at low concentration. The running buffer used was 0.3 M PBS and the miRNA target with biotin modified oligo-probe (probe 2) was added to the buffer for subsequent application to the sample pad. The thiolated oligo-conjugate (probe 1) was pre-dispensed on to the conjugate pad. The test zone was pre-treated with streptavidin (2 mg/mL) for capturing the biotinylated oligo-probe. Buffer containing the target and biotinylated probe duplex migrated from the sample pad to the conjugate pad. Hybridisation then occurred between the oligo-probe functionalised nanoparticles deposited on the conjugate pad and the target with the associated biotinylated probe already hybridised. This completed the typical sandwich format with the biotin group and Raman-active nanoparticle at opposing ends of the target. Further migration of this complex to the nitrocellulose membrane allowed for capture on the test zone where the silver nanoparticles accumulated showing a clear green band. The concept for this assay is shown in Figure 5.2.

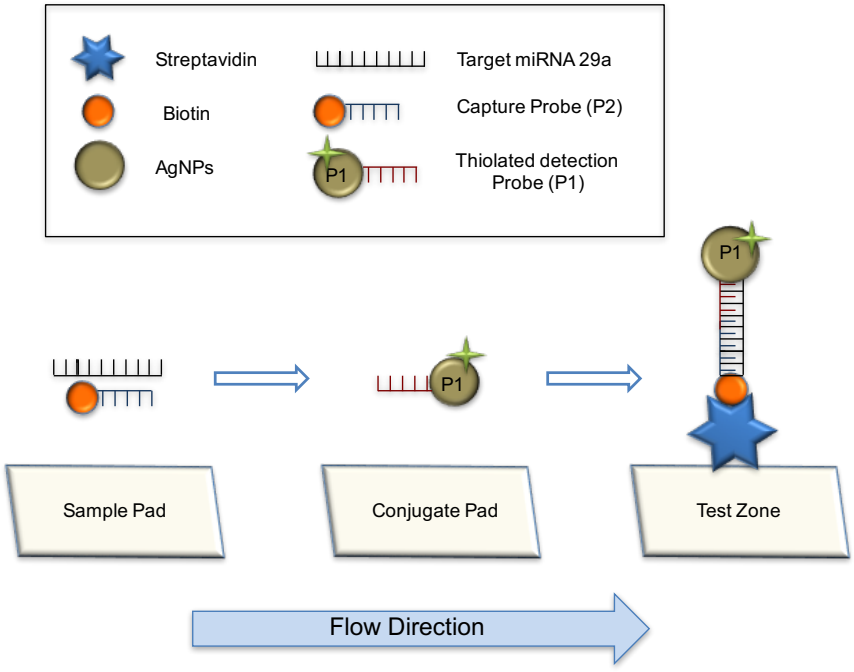

***Figure 5.2**: A schematic representation for the lateral flow assay used to detect miRNA sequences.*

5.2 Hybridisation Experiment

5.2.1 Approaches used for the Hybridisation Experiment

The sample volume prepared for the lateral flow test was 100 µL which could be absorbed by the absorbent pad and without saturating the strip which could inhibit the capillary action if overloaded. The probe and target concentration had to be optimised for the experiment but initially miRNA-29a target (4 µL, 250 nM) and biotinylated-oligo conjugate (1.0 µL, 5 µM) was added to the 0.3 M hybridisation buffer to produce a total sample volume of 100 µL. The thiolated oligo-probe functionalised nanoparticles (2.5 µL, 2.5 nM) were deposited on to the conjugate pad. The strip was then washed with 100 µL of 0.1 M PBS to remove any excess and unbound silver nanoparticles from the test zone to prevent inhibition of the capturing process. Additionally, a further two approaches were considered with the application of probes and target in a different order for comparison of different operating procedures (Figure 5.3). For the second approach, the target only was added to the running buffer and the biotinylated-oligo conjugate (1 µL, 5 µM) was dispensed on to the test zone. For the third approach, the sample containing only the biotinylated-oligo conjugate (1 µL, 5 µM) was initially run on the strip. The strip was left to dry for 12 h and the oligo-probe functionalised nanoparticles were deposited on the conjugate pad. The miRNA-29a target was then added to the 0.3 M PBS running buffer and subsequently run on the strip. The strips were examined and the first approach was selected for the proceeding experiments as it was the most rapid approach with optimal results demonstrated from this method.

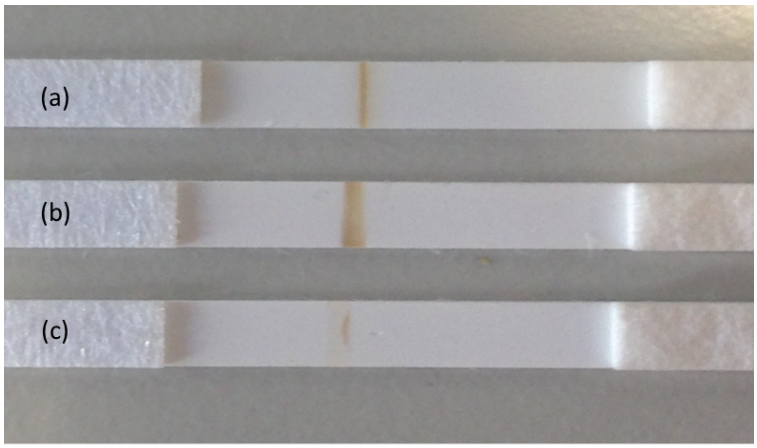

Figure 5.3: *Visual image showing the results gained from different approaches investigated applied for the hybridisation experiment on lateral flow strips. In all approaches miRNA-29a (4 µL, 250 nM) target was added to the 0.3 M PBS running buffer and the thiolated DNA (2.5 µL, 2.5 nM) was dispensed on to the conjugate pad. (a) Biotinylated-oligo conjugate (1.0 µL, 5 µM) was added to the test zone (second approach) (b) Biotinylated-oligo conjugate (1.0 µL, 5 µM) was added to the running buffer (first approach) (c) Biotinylated-oligo conjugate (1.0 µL, 5 µM) was added to the running buffer first and the strip left to dry for 12 h before performing the experiment (third approach).*

5.2.2 Analysis of the Lateral Flow Test Line by SERS

The thiolated oligo-silver nanoparticle (probe 1) was functionalised with the Raman reporter RBITC (2.5 µL, 1 x 10^{-5} M) to increase the sensitivity of the assay and allow for quantitative analysis by SERS. The thiolated oligo-silver nanoparticle conjugate (probe 1) was centrifuged twice to remove any excess dye left in the conjugate suspension. The first step of the hybridisation event occurred within the running buffer (0.3 M PBS) as the miRNA-29a target and biotinylated oligo-conjugate capture probe (probe 2) was added together to the running buffer and absorbed by the sample pad. Probe 2 was deposited on the conjugate pad and streptavidin (2 mg/mL) was pre-immobilized on the nitrocellulose membrane to form the test line. The sample solution (100 µL) containing the target and probe 2 migrated through the strip towards the absorption pad and when it is passed through the conjugate pad containing the deposited oligo- silver nanoparticle conjugate (probe 1), the second hybridisation step with the target occurred forming nanoparticle aggregates which continued to migrate along the strip. The test line consisted of streptavidin which captured the biotinylated

probe and formed a visible green band due to the accumulation of silver nanoparticles. The excess oligo-conjugates continued to migrate and absorbed within the absorbent pad. After 10-15 minutes, the strip was washed with 0.1 M PBS.

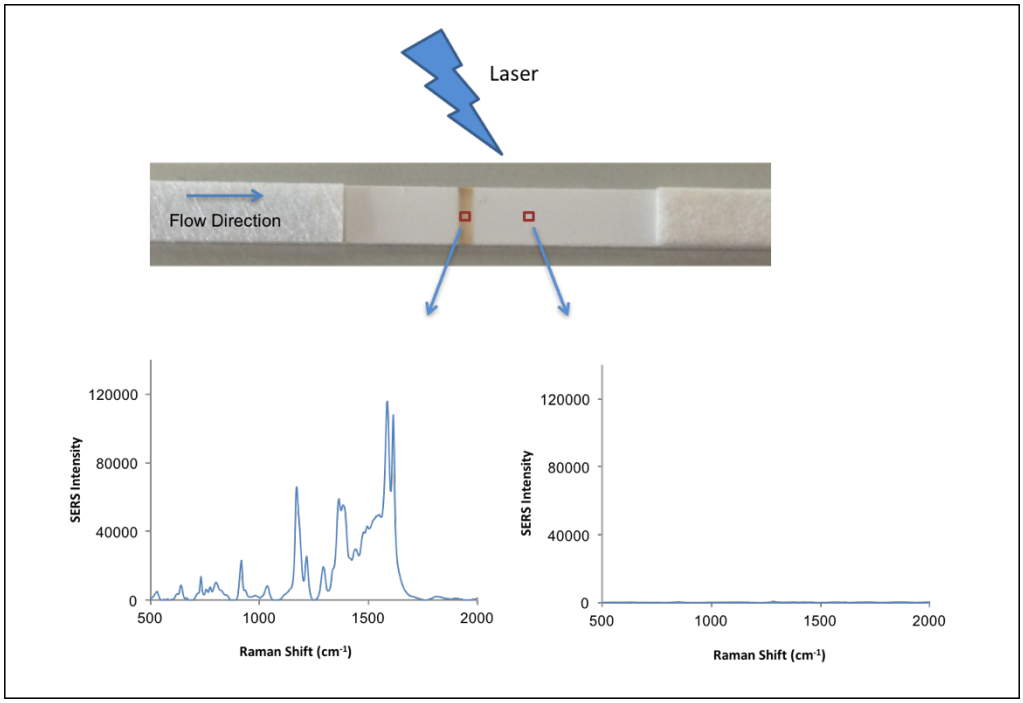

Figure 5.4: *The SERS spectra obtained from a lateral flow strip on the test line (left) and from a spot after the test line (right). The laser wavelength used was 532 nm, laser power 10% and 1 * 1 s accumulation times. The dye used was MGITC (2.5 µL, 1 x 10^{-5} M) and the final concentration of miRNA target was 5 nM. Each measurement was averaged from 50 measurements.*

It is clear from Figure 5.4 that the SERS spectrum obtained from the test line shows an intense SERS signal due to the aggregation of nanoparticles. Different areas on the nitrocellulose membrane were examined to see if there was any non-specific binding occurring but no SERS signal was obtained. A further investigation was carried out to see how specific the method was when non-complementary target was used.

5.2.3 Lateral Flow Assay Specificity Experiment

A study was conducted to investigate how specific the method was and determine if nanoparticle capture and aggregation was dependant on the sequence-specific hybridisation of the complementary target with probes, causing the nanoparticles to aggregate on the test line, indicating a positive result. Four experimental conditions were applied for this investigation. Initially miRNA-29a target was hybridised with complementary probes. Secondly, no target was added to the sample solution. Thirdly, a nonsense (non-complementary) miRNA target was used. Finally, a non-complementary thiolated probe (probe 1) specific to miRNA-126 was used with the miRNA-29a target and associated biotinylated-oligo conjugate. All the volumes applied and concentration of target was identical for all the conditions investigated with 0.3 M PBS used for the hybridisation buffer and 0.1 M PBS used for the washing buffer. The final concentration of the target was 5 nM.

Figure 5.5 shows the lateral flow strips for each experiment and only the initial experimental condition displayed a positive test line with a clear green band observed due to the presence of two complementary probes hybridising to the target. The other three experimental conditions did not display a test line indicating a negative result for the negative controls as expected, and confirming the sequence-specificity of the method, with a positive result obtained in the presence of target and complementary probes only.

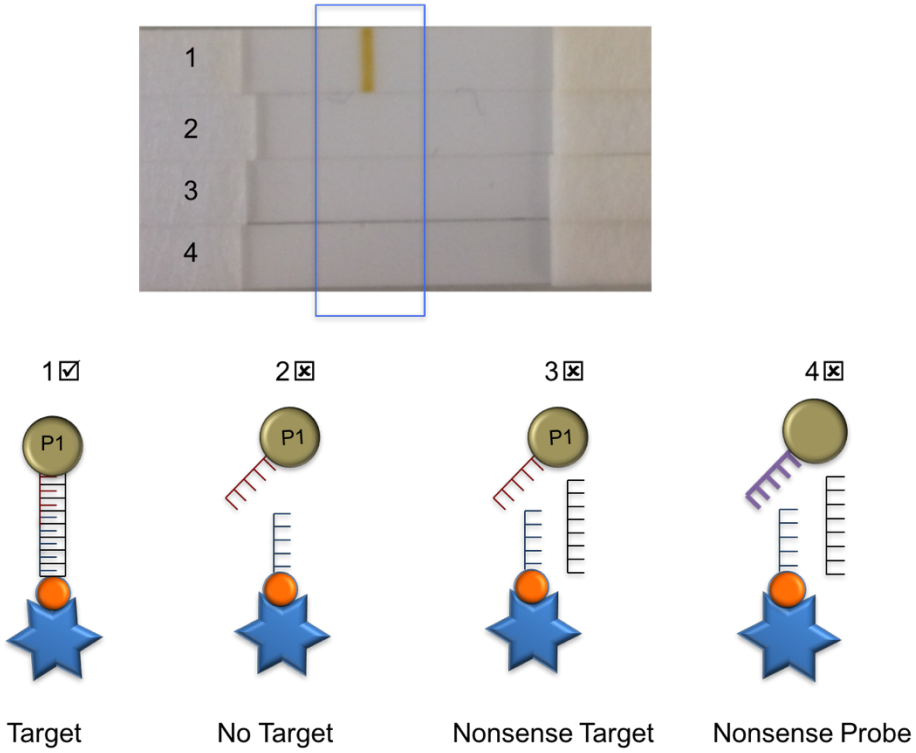

Figure 5.5: *Shows the lateral flow strips representing the four experimental conditions investigated where (1) target is complementary to the probes (2) no target was used (3) nonsense target was used (4) a nonsense probe 1 was used.*

5.2.4 Buffer Study for the Hybridisation Experiment

The hybridisation buffer has a strong effect on the efficiency of the assay and choosing the right buffer could improve the efficiency of the assay. In the literature it has been reported that use of BSA in the running buffer helped block non-specific binding.[97, 99] Therefore, 1 % BSA was added to 0.3 M PBS. However, the use of BSA in this assay resulted in blocking of the hybridisation between the target and probes which generated a weaker SERS signal as compared to the use of 0.3 M buffer only. Subsequently, 0.2 % BSA and 0.5 % Tween20 was added to the 0.1 M PBS washing buffer to investigate if this improved the signal intensity as compared to the use of 0.1 M PBS buffer washing buffer alone. The results did not prove beneficial with the addition of BSA or Tween20, so development continued with the use of 0.3 M PBS as the hybridisation buffer and 0.1 M PBS as the washing buffer. The final miRNA-29a

target concentration used for this experiment was 0.1 nM with 0.05 µM of probe 2 (biotinylated oligo-conjugate). The dye used was RBITC because it demonstrated a stronger SERS signal with application on the lateral flow strips. Figure 5.6 shows the spectra obtained with use of the 0.3 M PBS running buffer and 0.1 M PBS washing buffer. The spectra were obtained from a spot on the test line and a spot before and after the test line. Each spectrum displayed is an average of 50 measurements taken.

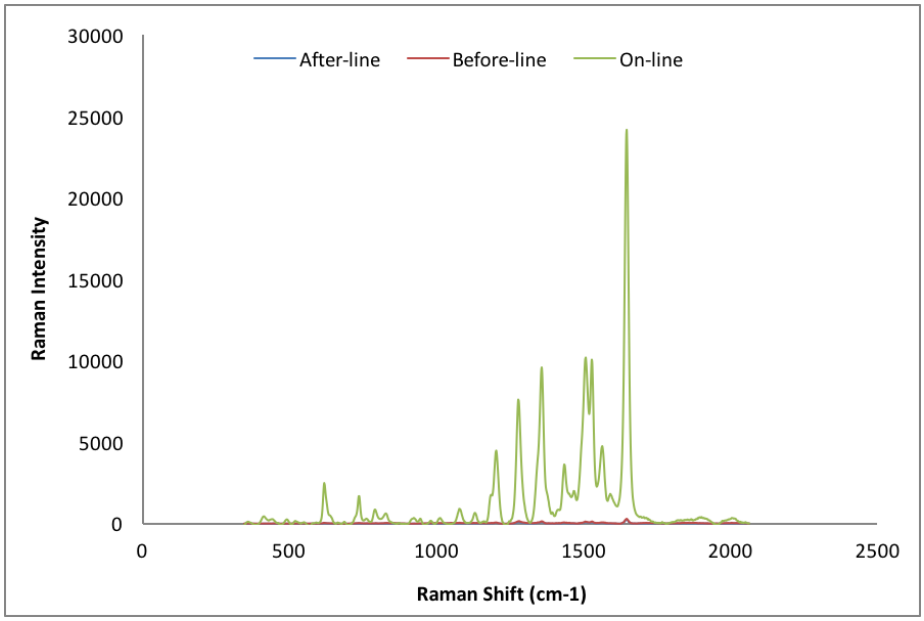

Figure 5.6: *The SERS spectra obtained from a lateral flow strip on the test line and from a spot before and after the test line with use of a 0.3 M PBS running buffer and 0.1 M PBS washing buffer. The laser wavelength was 532 nm, 10 % laser power and 1 * 1 s accumulation time. The dye used was RBITC (2.5 µL, 1 x 10^{-5} M) and the final concentration of miRNA-29a target was 0.1 nM. Each measurement was averaged from 50 spectra.*

The spectra obtained using the same experimental conditions as previously applied, with further addition of 0.2 % BSA and 0.5 % Tween20 in the 0.1 M PBS washing buffer are displayed in Figure 5.7. It was evident that the hybridisation event was affected by addition of BSA and Tween20 to the 0.1 M PBS washing buffer, with a weaker SERS signal obtained.

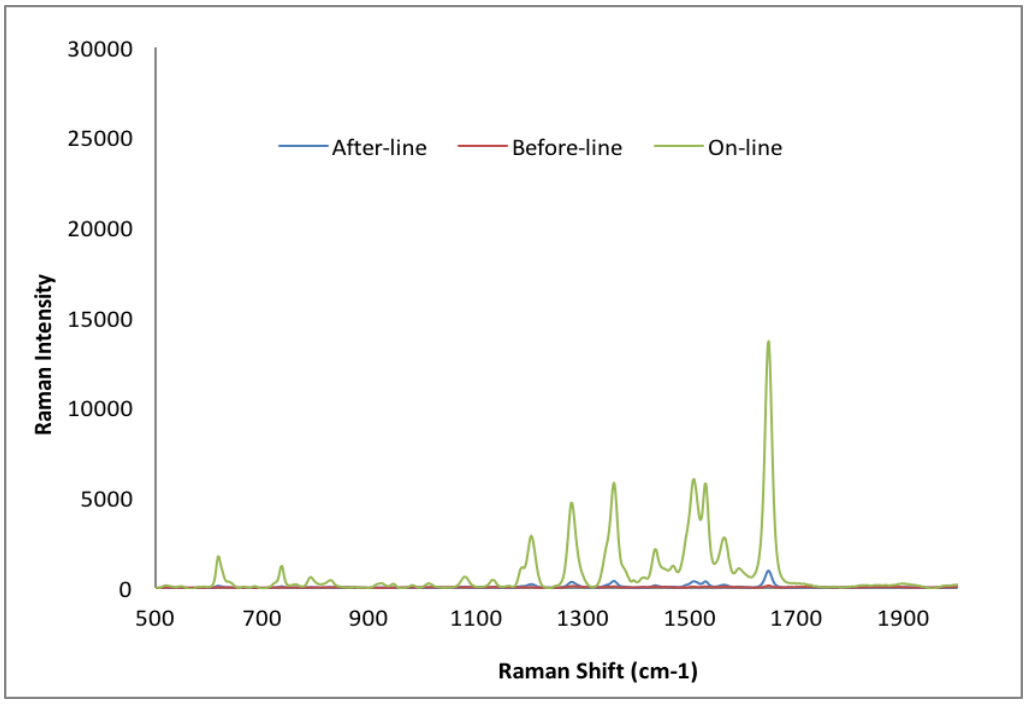

Figure 5.7: *The SERS spectra obtained from a lateral flow strip on the test line and from a spot before and after the test line with use of 0.3 M PBS running buffer and addition of 0.2 % BSA and 0.5 % Tween20 in the 0.1 M PBS washing buffer. The laser wavelength was 532 nm, 10% laser power and 1 * 1 s accumulation times. The dye used was RBITC (2.5 µL, 1 x 10^{-5} M) and the final concentration of miRNA-29a target was 0.1 nM. Each measurement was averaged from 50 spectra.*

5.3 Concentration Study for the Detection of miRNA-29a on Lateral Flow Strips

A study was conducted to identify the optimal experimental parameters for the hybridisation and detection of miRNA-29a on lateral flow strips. Probe 1 (2.5 µL, 2.5 nM) was spotted on to the conjugate pad of the lateral flow strip. The biotinylated oligo-conjugate (probe 2) was added to the 0.3M PBS running buffer and it was evident that 1 µL of 0.05 µM was sufficient for efficient hybridisation. The sample final volume used was 100 µL for all experiments. After all the other parameters were optimised, a concentration study of the miRNA-29a target was performed.

The study used different final concentrations of target miRNA-29a showing that the target could easily be detected visually down to a lower concentration limit of 125 pM, for which a green band was observable in the test zone (Figure 5.8). Below this concentration, SERS was required for confirmation of the target presence. When these samples were analysed by SERS, final target concentrations above a 1 nM threshold demonstrated signal saturation and was difficult to be determined. Therefore, the following experiments were conducted using miRNA-29a target concentrations below the 1.0 nM threshold to avoid signal saturation.

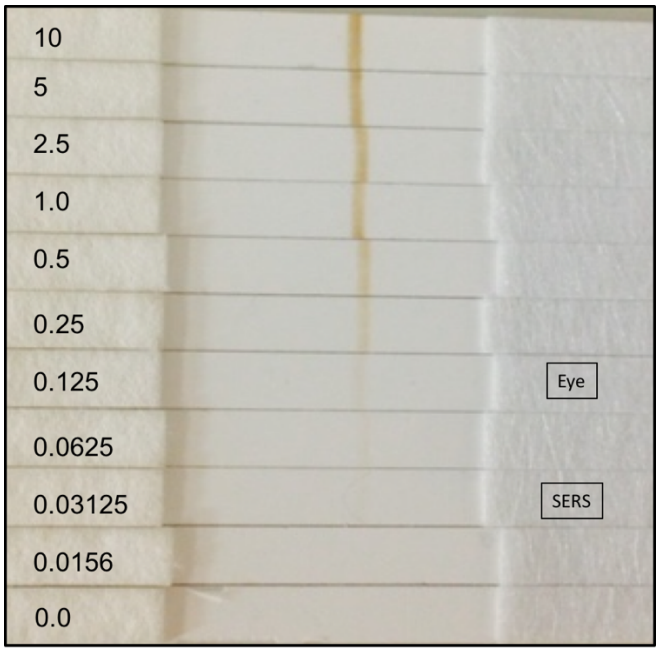

Figure 5.8: *Visual image of lateral flow strips using different final concentrations of the miRNA-29a target. All concentrations used for the target are listed on the left and listed in nM units of measurement. 2.5 µL of probe 1 (2.5 nM) was dispensed on to the conjugate pad and 1 µL of 5 µM probe 2 was added to the 0.3 M PBS running buffer.*

Figure 5.9 shows the SERS spectra obtained from one of the strips with a final target concentration of 0.1 nM. The short exposure time of 0.1 seconds was used to analyse the strip and each spectrum was averaged from 50 measurements taken from the chosen spot.

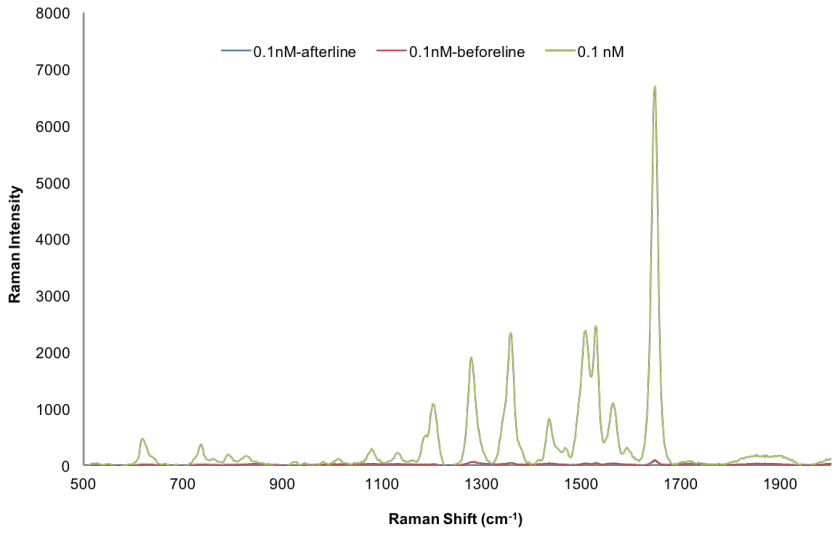

Figure 5.9: *Spectra generated from 50 points at the test line (green line) and at points before and after the test line. Renishaw InVia Raman microscope with a 532 nm laser wavelength, 5x lense, an exposure time of 0.1 s and 10 % laser power were used for this experiment. The final concentration of miRNA-29a target was 0.1 nM.*

A further concentration study was performed to determine a calibration curve for identification of the correlation between final target concentration and signal intensity at 1642 cm^{-1}. The highest target concentration studied was 0.4 nM to avoid any signal saturation. For this study, three lateral flow strips were prepared for each sample and three scans were performed per sample, with analysis applied using a Renishaw InVia Raman microscope and 532 nm laser. The calibration curve between final target concentration and the signal peak intensities is shown in Figure 5.10 and a visual image of the strips analysed (three replicates per sample) are shown in Figure 5.11.

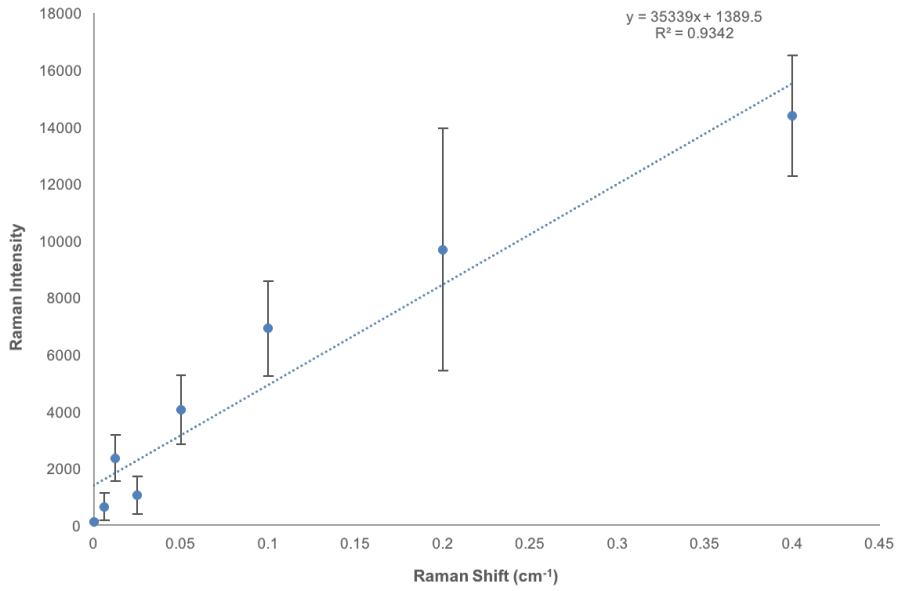

Figure 5.10: *A calibration curve between the final concentration of miRNA-29a and the peak intensity of RBITC at 1642 cm^{-1}. Three scans were taken for three replicates of each sample using Renishaw InVia Raman microscope with a 532 nm laser wavelength, 5x lens, an exposure time of 1 s and 10 % laser power were used. Each scan was an average of 50 points. The final target concentration was varied from 0 to 0.4 nM.*

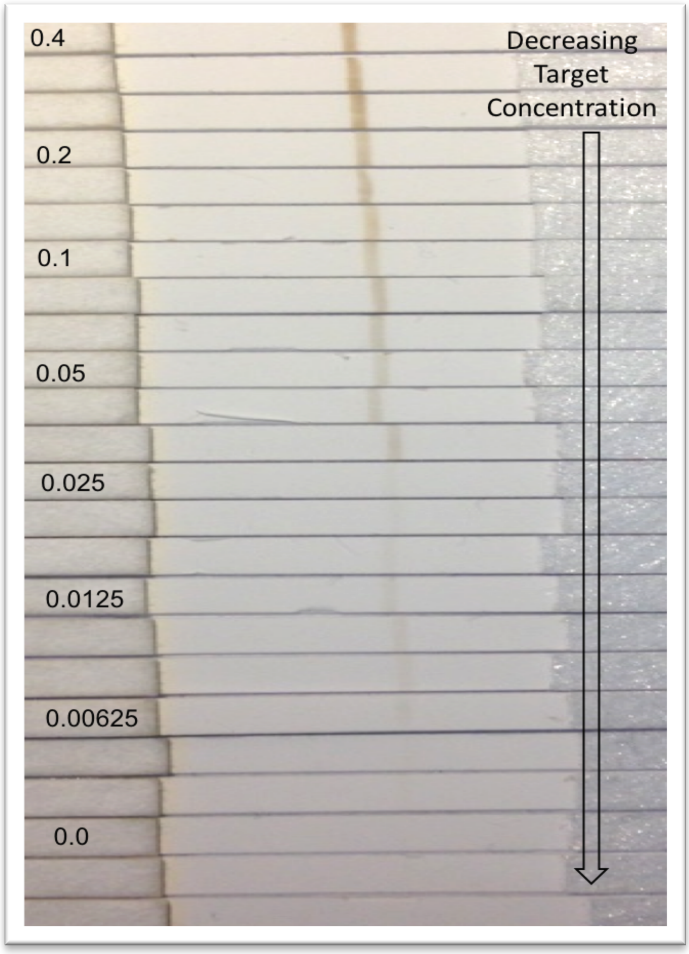

Figure 5.11: *Visual image of the lateral flow strips using different final concentrations of miRNA-29a target. All the concentrations used for the target are listed on the left in nM units of measurement. 2.5 µL of probe 1 (2.5 nM) was dispensed on to the conjugate pad and 1 µL of 5 µM probe 2 was added to the 0.3 M PBS running buffer. Three replicates were analysed for each concentration.*

The results displayed significant variation as obtained from the three strips for each sample concentration. This could be because a small area is selected on the test line for each strip and a map of 50 points was taken from this limited area. 50 points were measured from strip-to-strip, and although these points were taken from the test-lines of each, there was some inevitable variation in the positioning of the laser for each strip, which may also have contributed to variation.

The strips were also analysed using a Snowy Range Sierra 2.0 spectrometer with a 532 nm laser wavelength which is a relatively small and portable device suited for lateral flow SERS analysis, with the obtained calibration curve shown in Figure 5.12.

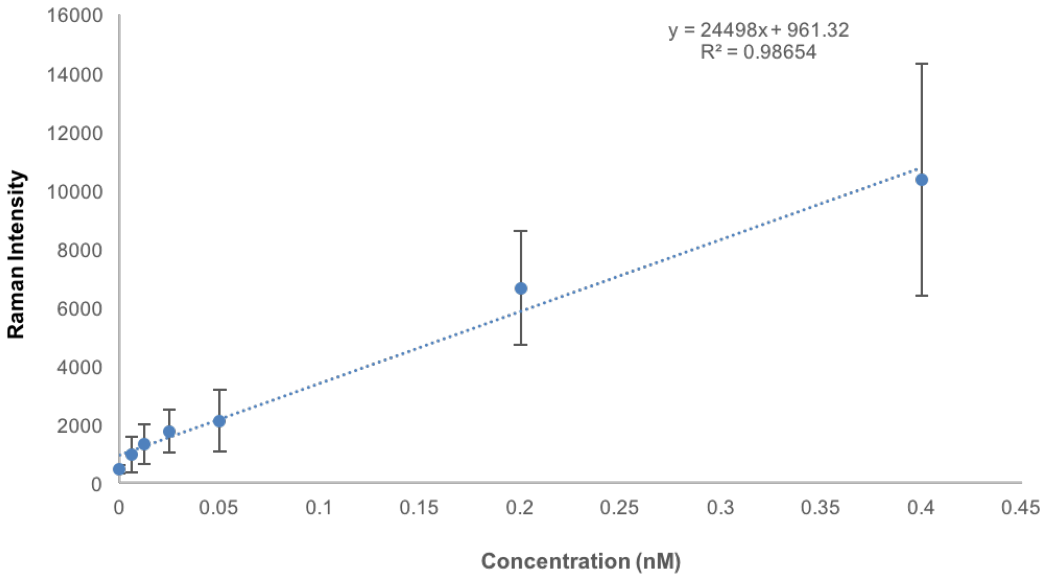

Figure 5.12: *A calibration curve indicating the relation between the final concentration of miRNA-29a and the peak intensity of RBITC at 1642 cm^{-1}. Each measurement is an average of three replicates and three scans of each sample were taken using snowy instrument with the wavelength of 532 cm^{-1}, exposure time of 1 s and 10% laser power. The final target concentration was varied from 0 to 0.4 nM and each scan was an average of 50 points.*

Using the Snowy instrument rather than the Raman microscope gave a better linearity between the final concentration of miRNA-29a target and Raman peak intensity at 1642 cm^{-1}. There was still a large variation amongst the replicates of each sample as the area detected by the laser on the test line could not be positioned to precisely the same point of the test line for each replicate. However, using snowy to obtain these results demonstrated great potential for the application of this assay format on a portable Raman spectrometer for rapid detection of miRNA targets. The limit of detection calculated from both graphs is highly comparable with a lower limit of 4 pM using the Raman microscope, and 18 pM using the portable Snowy spectrometer.

5.4 Double Sandwich Assay for miRNA-29a Detection.

As was observed previously, the assay was capable of detecting the target at low concentrations based upon the sandwich hybridisation format between the oligo-silver nanoparticle conjugates and the miRNA target. However, to increase the sensitivity of the assay an additional probe (probe 3) was used to form a double sandwich assay and in an attempt to intensify the SERS signal intensity from the silver nanoparticles. Probe 3 is a thiolated oligo-conjugate which is complementary to probe 1 with the following sequence: 5' GAA ATC GGT TA- $(HEG)_3$-thiol 3'. The assay was performed as previously, with the target and probe 2 added to the 0.3 M PBS running buffer and probe 1 dispensed on to the conjugate pad. As the buffer migrates through the lateral flow strip, hybridisation occurs and can be detected as a green band on the test line. After the test line formation, but prior to the 0.1 M PBS wash step, probe 3 was dispensed on to the conjugate pad, the strip was dried and the sample pad was then immersed in the 0.3 M running buffer and after 10 minutes, the strip was washed with 100 µL of 0.1 M PBS. As probe 3 travelled along the strip, a hybridisation event took place between probe 1 and probe 3 due to their sequence complementary. A schematic illustration that clarifies the concept of the double sandwich hybridisation format is shown in Figure 5.13.

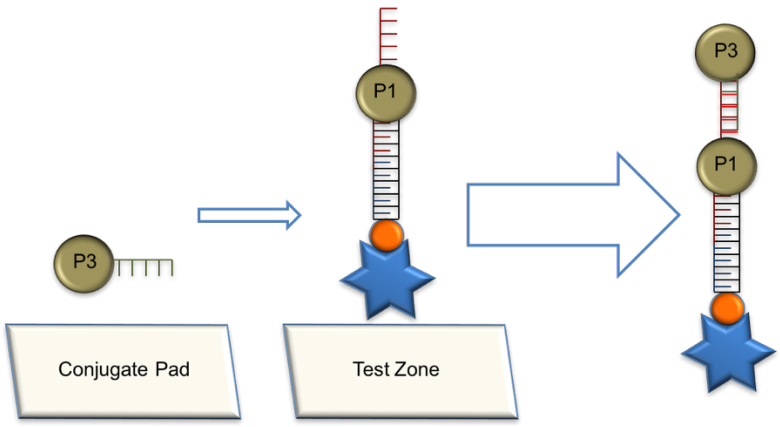

***Figure 5.13**: A schematic representation of the lateral flow assay using a double sandwich assay to detect miRNA-29a target. Probe 3 hybridised to probe 1 on the test zone.*

The double sandwich assay was applied for improvement of the SERS signal and to increase the assay's sensitivity. The experiment was performed as a proof-of-principle investigation founded upon the previous standard sandwich assay format with use of only two conjugates. In this instance, a third probe addition was applied to the strips and the strips were subsequently analysed by SERS (Figure 5.14).

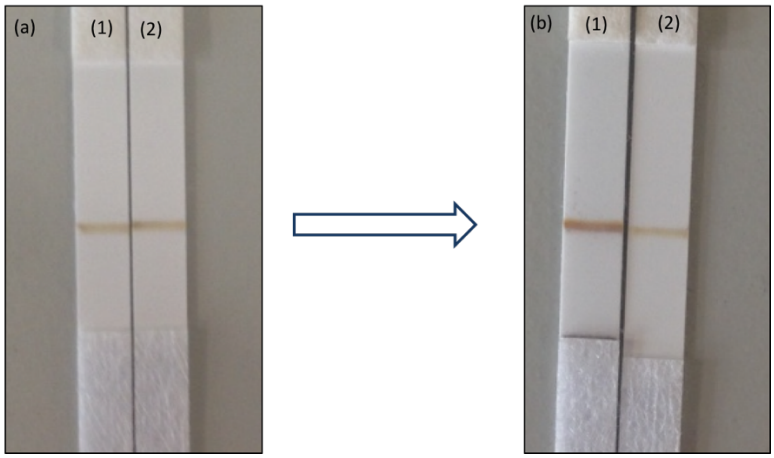

Figure 5.14: Image of lateral flow strips (a) a sandwich assay using probe 1 and 2 with target (0.4 nM) was performed on strip 1 and 2. (b) an additional probe (probe 3) was added to strip 1 to form a double sandwich assay with no additional probe added to strip 2.

Hybridisation occurred between miRNA-29a target and complementary probes (probe 1 and 2) on both strips 1 and 2. When the strips were dried, probe 3 was added to the conjugate pad of strip 1 only and then washed with 0.1 M PBS. 2.5 µL of probe 1 and 3 was used (2.5 nM) and 1 µL of 5 µM of the biotinylated oligo-conjugate (probe 2) was added to the 0.3 M PBS running buffer for all the strips. The final target concentration was 0.1 nM. It was evident from figure 4.14, that strip 1 displayed a significant increase in visual colouration on the test-line following treatment with probe 3. The intensity of colour on the test line increased which meant that addition of probe 3 was successful in terms of hybridisation and this in turn enhanced the extent of aggregation on the test-line. Both of the strips were then analysed by SERS (Figure 5.15).

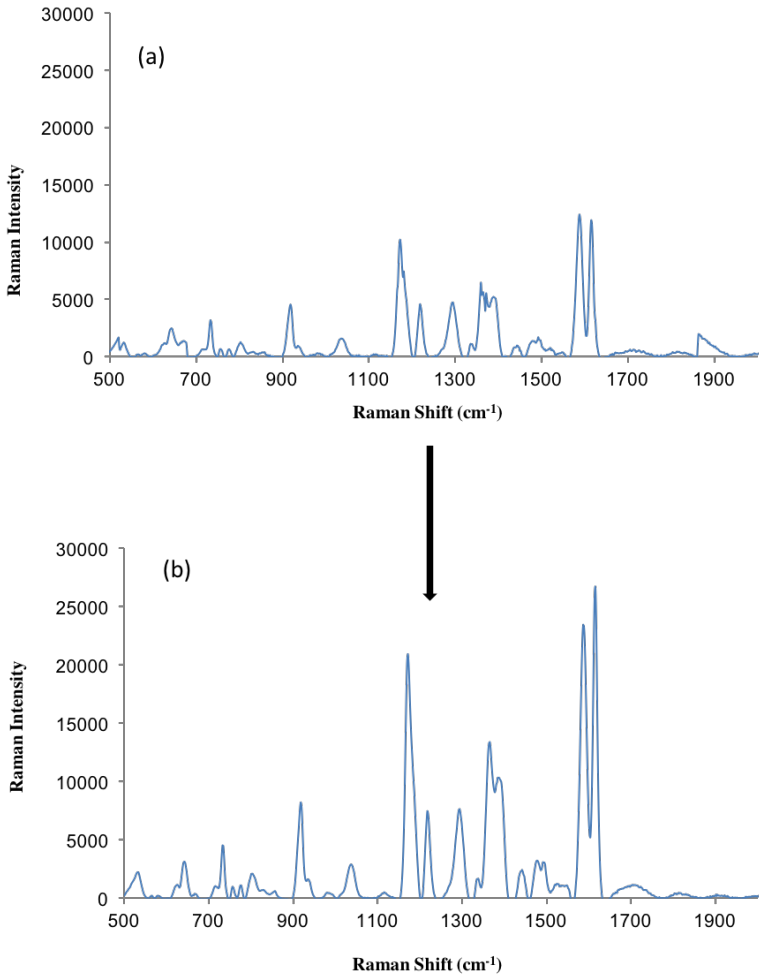

Figure 5.15: *(a) Spectrum obtained from the test line using miRNA-29a target with probe 1 and 2. (b) Spectrum obtained from the test-line using miRNA-29a target and probe 1, 2 and 3. The spectra were taken using a 532 nm wavelength, and exposure time of 1 second with 10% laser power. The final concentration of target used was 0.1 nM.*

If probe 3 was added without probe 1, no aggregation took place and the test result was negative (Figure 5.16). A positive result was only obtained if the target and complementary probes were present (probe 1 and 2) and the result was more intense if probe 3 was added which provided further enhancement with lower target concentrations for improved sensitivity.

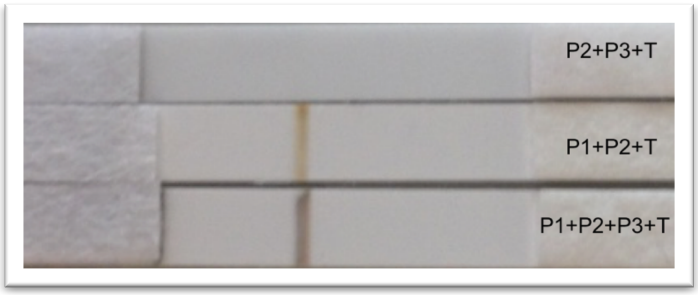

***Figure 5.16**: Visual image of three strips with use of different probes as listed on the right of the lateral flow strips displayed. Final target concentration was 0.4 nM.*

5.5 Serum Experiment

As mentioned in chapter 3, the ultimate objective was to develop an assay that could be used for biomedical application by rapid and sensitive detection of miRNA targets in biological samples. Therefore, to mimic a biological source, serum was added to the sample. Different % concentrations of serum (v/v) were spiked in to the running buffer containing miRNA-29a target (10 nM), probe 2 (0.05 µM), and probe 1 (2.5 µL, 2.5 nM) which was added to the conjugate pad of the lateral flow strips (Figure 5.17).

***Figure 5.17**: Visual image of lateral flow strips with different % concentrations of serum (v/v) were spiked into the 0.3 M PBS running buffer, as displayed on the left of the strips.*

As observed for the solution-based assay, there were difficulties in obtaining positive results with high concentrations of serum, in this instance beyond the threshold of 10% serum. However, with the solid-phase lateral flow platform for the detection of miRNA-29a, the results gained from the detection of the target were reproducible which was not the case for the solution-based assay. The lateral flow strip with application of samples spiked with 10% serum were analysed by SERS and demonstrated a significant SERS signal with associated discrimination ratio as obtained from the test line (Figure 5.18).

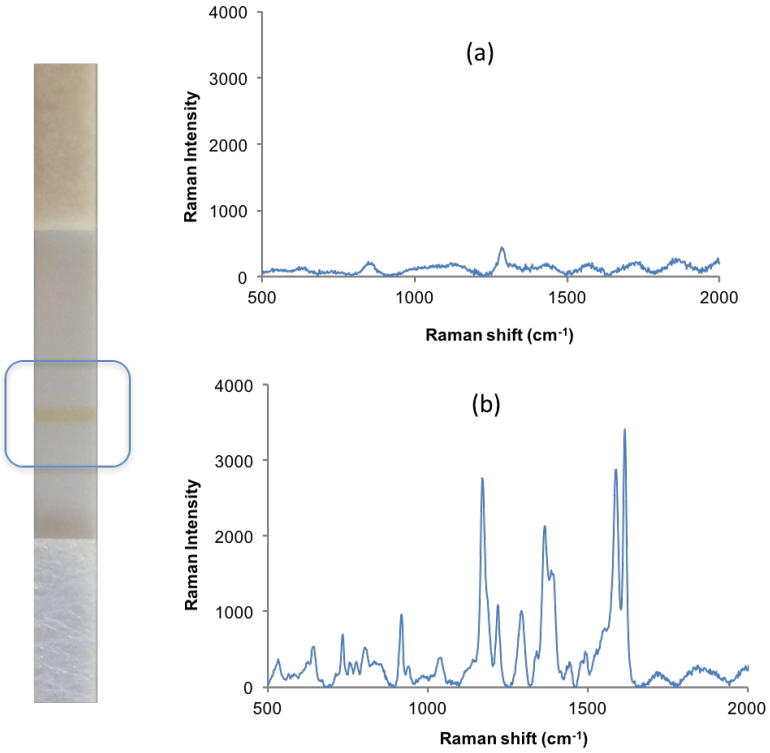

Figure 5.18: *The lateral flow strip with 10% serum spiked in to the running buffer (a) Spectrum obtained from a spot after the test line (b) Spectrum obtained from a spot on the test line. The final miRNA-29a target concentration used was 10 nM. The spectra were taken using a 523 nm wavelength and exposure time of 1 second with 10% laser power.*

The results obtained for quantitative detection of miRNA by naked eye and by SERS of the nanoparticles particles in aqoues solutions and a mimic biological sample show a high potential of using the assay clinically.

5.6 Summary of the Assay

A successful solid-phase platform for miRNA biomarker detection with use of lateral flow strips was developed. The assay allowed for visual detection of miRNA target presence and a quantitative analysis of detection by endpoint application of SERS. The lateral flow assay format provided a rapid, specific and sensitive method for miRNA detection. For development of the lateral flow format, a biotinylated DNA probe (probe 2) was used as a capture probe and added to the 0.3 M PBS running buffer with further addition of the target sequence. The thiolated DNA probe was deposited on the conjugate pad to act as a detection probe (probe 1). When the running buffer was added to the sample pad within a glass vial, the sample solution diffused through the strip by capillary action and hybridisation took place when absorbed by the conjugate pad. As the sample continued to diffuse through the nitrocellulose membrane, hybridisation complexes were captured by the streptavidin moiety of the biotin-streptavidin complex which formed the test zone, thus producing a visibly observable green band that indicated a positive result. When a non-complementary target or probe sequence was applied, no band was observed, indicating a negative result. Different concentrations of target were investigated and the assay could detect target concentrations as low as 18 pM. The assay was also able to detect the target in samples spiked with 10 % serum. This demonstrated that the assay had significant potential for use in future miRNA detection and diseases diagnostic technologies.

CHAPTER 6: Discussion and Conclusions

Oligonucleotide-silver nanoparticle conjugates have been investigated for their suitability as sensors to detect regulatory miRNAs associated with specific disease using surface enhanced Raman scattering (SERS). To achieve this, thiol modified oligonucleotides were conjugated to the surface of silver nanoparticles. To utilize the nanoparticle conjugates for SERS detection of RNA, a Raman reporter (isothiocyanate molecule) was added to a primary probe (probe 1), providing this conjugate with SERS active functionality, whilst a secondary probe (probe 2) consisted of a 12-base sequence with no Raman reporter. These probes contained different sequences, complementary to adjacent positions within the model RNA target. All of the oligonucleotides used to functionalise the silver nanoparticles were 5′ thiol- modified and upon hybridisation, a head-to-tail orientation was obtained. Hybridisation was initiated upon addition of a complementary model RNA target. This was composed of a 22-base oligonucleotide sequence which was added to the probe conjugates, resulting in the self-assembly of the nanoparticles and this could then be observed by a colour change within the nanoparticle suspension. Upon the addition of a non-complementary (nonsense) RNA sequence to the conjugates, no optical changes were observed and this confirmed the specificity of hybridisation to the complementary target sequence.

Hybridisation of the nanoparticle conjugates was monitored using extinction spectroscopy. Thermal and kinetic studies were implemented and the results obtained highlighted the successful development of a two-probe assay consisting of AgNP-oligonucleotide conjugates functionalised with dual hybridisation probes, that formed SERS active nanoparticle assemblies upon target addition. Melting experiments have shown that aggregation was a reversible process. When the conjugates were heated, DNA-RNA duplexes were denatured and at room temperature the duplex reformed. The results obtained from extinction spectroscopy and DLS confirmed the synthesis of stable conjugates and formation of nanoparticle assemblies due to sequence-specific RNA hybridisation. This resulted in an increased SERS response through the formation of “hotspots”, allowing clear discrimination between the target and

nonsense sequence using a final target concentration of 5 nM. The developed assay demonstrated great success for the detection of a model RNA target sequence, and the project progressed toward development and optimisation of an assay for the detection of miRNA biomarkers associated with diabetes.

miRNA has been repeatedly linked to a variety of diseases, and for this particular investigation miRNA-29a and miRNA-126 were selected as the gene expression profile of these miRNAs has been experimentally confirmed to be down-regulated within type 2 diabetes patients. The assay was able to distinguish between the presence or absence of the miRNA target and provided a significant On: Off SERS discrimination ratio. However, the rate and extent of hybridisation observed for the assays using miRNA targets was less efficient as compared to the model RNA. Samples were left for a time period between two and three hours prior to SERS analysis, to ensure a complete hybridisation event with the target miRNA. A range of hybridisation buffers were investigated for optimisation of the hybridisation efficiency with miRNA targets, with consideration of potential hybridisation enhancers such as dextran sulfate. However, using dextran sulfate buffer increased SERS spectra background interference and non-specific binding. Thus, in the developed assay 0.3 M PBS was used as the hybridisation buffer. In addition, the hybridisation process was found to be sensitive to variations in the final concentration of miRNA targets, with a specified concentration of 5 nM providing the optimal ON: OFF SERS discrimination. At concentrations above 5 nM, the SERS intensity signal started to drop and SERS discrimination was reduced. A background signal was present in the SERS spectrum obtained from the blank sample although this was to be expected as Raman reporter was also present in the blank sample. All spectra produced were baseline corrected and positive discrimination was successfully obtained.

Additionally, the assay was investigated for duplex detection of both targets in a one pot multiplex assay format. In this instance, two Raman reporters were used. MGITC was used for the detection of miRNA-29a and RBITC was used for the detection of miRNA-126. The assay was successful for detection of both targets in a duplex format. An increase in signal from the Raman reporter was observed when the corresponding target was present. When the target was absent, a reduced SERS signal was produced.

The final concentration of the targets in the multiplex experiment were maintained at 5 nM.

As the discrimination between SERS signals obtained with the addition of complementary and non-complementary targets was significant, the assay was extended to mimic a biological sample matrix. This was investigated to test the capability of the assay for potential clinical application. A synthetic serum was spiked into the samples at different % concentrations (w/v) and samples were then analysed by SERS. Unfortunately, the hybridisation process was inhibited by the presence of serum in the samples, even at low concentrations, and the results obtained were not satisfactorily reproducible. Further investigation would be required to identify if a pre-analytical extraction step to isolate miRNA from serum could eliminate the inhibitory effect of the biological sample matrix.

The solution based assay for miRNA detection was successful for the detection of synthetic miRNA targets and could be used for other targets that are associated with different diseases. Moreover, a surface-based assay for miRNA detection was developed for visual miRNA detection. This assay incorporated lateral flow strips which provide a rapid, sensitive and specific test for the presence of the target.

With application of this assay format, miRNA-29a target was investigated and RBITC Raman report was used. A sandwich hybridisation was performed on the lateral flow strip and formation of a visual green band was observed on the test line of the strip due to the aggregation of silver nanoparticles. The thiol conjugate (probe 1) served as the detection probe and probe 2 was functionalised with a biotin group to serve as the capture group. The test line on the strip was pre-treated with streptavidin, providing a capture moiety for the hybridisation complexes based upon the recognised strength of the avidin-biotin interaction. In the presence of a non-complementary miRNA target or DNA conjugate, no test line formation was observed as no silver nanoparticle aggregation occurred. When a reduced target concentration was applied, the visual line was not distinguishable. Thus, the strip was analysed by SERS for the determination of the target presence or absence, as deduced from the enhanced SERS signal intensity. This provided a lower detection limit as compared to visual analysis by eye alone.

The sensitivity of the assay was further increased with use of an additional thiol modified conjugate with sequence complementarity to probe 1. The strip was prepared as previously, and the additional probe was added to the conjugate pad and run through the strip with the running buffer. At the test line, this formed a double sandwich assay which intensified the colouration of the green band on the test line and this in turn improved upon the SERS signal intensity. This approach will provide diagnostic value in samples with very low target concentrations.

Additionally, this assay was also investigated with samples containing different % concentrations (w/v) of serum to test the capability for detection of miRNA target sequences in a biologically relevant sample matrix. At high concentrations of serum, no green band was visualised but at lower concentrations (below 50%), the results were promising and a green line was observed in a reproducible manner. Further investigation of the lateral flow nitrocellulose membrane porosity may be investigated in future to improve upon the isolation and capture of the miRNA target. Decreasing the pore size may improve the separation of larger interfering macromolecules from the miRNA analyte within the sample matrix, or increasing the pore size may improve the flow dynamics within the lateral flow test and allow for improved formation of test line aggregates. The optimal membrane materials for detection of miRNA by lateral flow test would have to be subjected to further experimentation to confirm optimal materials for use with serum samples. This may provide a means to eliminate the inhibitory effects associated with serum within this investigation. It has been shown that this biosensor provides a basis for the rapid, sensitive, specific and low-cost alternative for miRNA detection that could be further optimised for use in clinical practice.

However, challenges remain to be overcome for miRNA biomarker detection from biological samples in a clinical context. Translation of the assay described would require further validation of detection criteria in relation to biological parameters. For instance, the limit of detection achieved here would have to be validated against robust data quantified from multiple clinical samples to ensure suitable sensitivity. Such data may be obtained from clinical investigations conducted using alternative techniques such as RT-qPCR or microarray analysis. These could provide quantitative

confirmation of biological miRNA levels in serum samples. Matrix effects encountered from serum required further dilution, which would need to be accounted for as this could further decrease the target concentration detected. It is possible that strategies could be employed to circumvent the challenges associated with serum interference with SERS analysis, for instance use of different nanomaterials, laser wavelengths, or potentially more advanced SERS methods such as SESORS. Alternatively, pre-analytical adjustments could be made, such as inclusion of target separation by application magnetic beads, or further optimisation of lateral flow membrane material for improved chromatographic separation and capture. Finally, if satisfactory detection limits remained problematic prior to further advancement of SERS detection limits, it may be possible to improve the limit of detection by amplification of the target followed by SERS detection which could remain advantageous for multiplexing potential.

Overall, it can be concluded that silver-oligonucleotide nanoparticle conjugates were readily synthesised successfully, and demonstrated great potential and effectiveness as sensors for application to the SERS-based detection of miRNA sequences associated with indication of specific diseases.

REFERENCES

1. Crick, F., Central dogma of molecular biology. *Nature* **1970,** *227* (5258), 561-563.

2. An Introduction to Molecular Biology/RNA:The ribonucleic acid. https://en.wikipedia.org/wiki/RNA (accessed 2nd November).

3. Chen, X.; Ba, Y.; Ma, L.; Cai, X.; Yin, Y.; Wang, K.; Guo, J.; Zhang, Y.; Chen, J.; Guo, X., Characterization of microRNAs in serum: a novel class of biomarkers for diagnosis of cancer and other diseases. *Cell Research* **2008,** *18* (10), 997-1006.

4. Watson, J. D., Molecular structure of nucleic acids. *Nature* **1952,** *171*, 737-738.

5. CRICK, B. F. H. C., *ON PROTEIN SYNTHESIS*. Medical Research Council Unit for the Study of Molecular Biology,Cavendish Laboratory, Cambridge, 1958; Vol. 12.

6. Rich, A., A hybrid helix containing both deoxyribose and ribose polynucleotides and its relation to the transfer of information between the nucleic acids. *Proceedings of the National Academy of Sciences* **1960,** *46* (8), 1044-1053.

7. Hofacker, I. L.; Fontana, W.; Stadler, P. F.; Bonhoeffer, L. S.; Tacker, M.; Schuster, P., Fast folding and comparison of RNA secondary structures. *Monatshefte für Chemie/Chemical Monthly* **1994,** *125* (2), 167-188.

8. Yguerabide, J.; Yguerabide, E. E., Light-scattering submicroscopic particles as highly fluorescent analogs and their use as tracer labels in clinical and biological applications: I. Theory. *Analytical Biochemistry* **1998,** *262* (2), 137-156.

9. Verri, A.; Mazzarello, P.; Spadari, S.; Focher, F., Uracil-DNA glycosylases preferentially excise mispaired uracil. *Biochemical Journal* **1992,** *287* (3), 1007-1010.

10. Papachristodoulou, D.; Snape, A.; Elliott, W. H.; Elliott, D. C., *Biochemistry and molecular biology*. Oxford University Press: 2014.

11. Condorelli, G.; Latronico, M. V.; Dorn, G. W., microRNAs in heart disease: putative novel therapeutic targets. *European Heart Journal* **2010,** *31* (6), 649-658.

12. Filipowicz, W.; Bhattacharyya, S. N.; Sonenberg, N., Mechanisms of post-transcriptional regulation by microRNAs: are the answers in sight. *Nature Reviews Genetics* **2008,** *9* (2), 102-114.

13. Ambros, V., The functions of animal microRNAs. *Nature* **2004,** *431* (7006), 350-355.

14. Bartel, D. P., MicroRNAs: genomics, biogenesis, mechanism, and function. *Cell* **2004,** *116* (2), 281-297.

15. Sohel, M. H., Extracellular/circulating microRNAs: release mechanisms, functions and challenges. *Achievements in the Life Sciences* **2016,** *10* (2), 175-186.

16. Heneghan, H. M.; Miller, N.; Kerin, M. J., MiRNAs as biomarkers and therapeutic targets in cancer. *Current Opinion in Pharmacology* **2010,** *10* (5), 543-550.

17. Kosaka, N.; Iguchi, H.; Ochiya, T., Circulating microRNA in body fluid: a new potential biomarker for cancer diagnosis and prognosis. *Cancer Science* **2010,** *101* (10), 2087-2092.

18. Ahlqvist, E.; Storm, P.; Käräjämäki, A.; Martinell, M.; Dorkhan, M.; Carlsson, A.; Vikman, P.; Prasad, R. B.; Aly, D. M.; Almgren, P., Novel subgroups of adult-onset diabetes and their association

with outcomes: a data-driven cluster analysis of six variables. *The Lancet Diabetes & Endocrinology* **2018**.

19. Kong, L.; Zhu, J.; Han, W.; Jiang, X.; Xu, M.; Zhao, Y.; Dong, Q.; Pang, Z.; Guan, Q.; Gao, L., Significance of serum microRNAs in pre-diabetes and newly diagnosed type 2 diabetes: a clinical study. *Acta Diabetologica* **2011,** *48* (1), 61-69.

20. Arroyo, J. D.; Chevillet, J. R.; Kroh, E. M.; Ruf, I. K.; Pritchard, C. C.; Gibson, D. F.; Mitchell, P. S.; Bennett, C. F.; Pogosova-Agadjanyan, E. L.; Stirewalt, D. L., Argonaute2 complexes carry a population of circulating microRNAs independent of vesicles in human plasma. *Proceedings of the National Academy of Sciences* **2011,** *108* (12), 5003-5008.

21. Jiang, Q.; Wang, Y.; Hao, Y.; Juan, L.; Teng, M.; Zhang, X.; Li, M.; Wang, G.; Liu, Y., miR2Disease: a manually curated database for microRNA deregulation in human disease. *Nucleic Acids Research* **2008,** *37* (suppl_1), D98-D104.

22. Mitchell, P. S.; Parkin, R. K.; Kroh, E. M.; Fritz, B. R.; Wyman, S. K.; Pogosova-Agadjanyan, E. L.; Peterson, A.; Noteboom, J.; O'Briant, K. C.; Allen, A., Circulating microRNAs as stable blood-based markers for cancer detection. *Proceedings of the National Academy of Sciences* **2008,** *105* (30), 10513-10518.

23. Gilad, S.; Meiri, E.; Yogev, Y.; Benjamin, S.; Lebanony, D.; Yerushalmi, N.; Benjamin, H.; Kushnir, M.; Cholakh, H.; Melamed, N., Serum microRNAs are promising novel biomarkers. *PloS one* **2008,** *3* (9), e3148.

24. De Guire, V.; Robitaille, R.; Tétreault, N.; Guérin, R.; Ménard, C.; Bambace, N.; Sapieha, P., Circulating miRNAs as sensitive and specific biomarkers for the diagnosis and monitoring of human diseases: Promises and challenges. *Clinical Biochemistry* **2013,** *46* (10–11), 846-860.

25. Lombardi, G.; Perego, S.; Sansoni, V.; Banfi, G., Circulating miRNA as fine regulators of the physiological responses to physical activity: Pre-analytical warnings for a novel class of biomarkers. *Clinical Biochemistry* **2016,** *49* (18), 1331-1339.

26. Lawrie, C. H.; Gal, S.; Dunlop, H. M.; Pushkaran, B.; Liggins, A. P.; Pulford, K.; Banham, A. H.; Pezzella, F.; Boultwood, J.; Wainscoat, J. S., Detection of elevated levels of tumour-associated microRNAs in serum of patients with diffuse large B-cell lymphoma. *British Journal of Haematology* **2008,** *141* (5), 672-675.

27. Weber, J. A.; Baxter, D. H.; Zhang, S.; Huang, D. Y.; Huang, K. H.; Lee, M. J.; Galas, D. J.; Wang, K., The microRNA spectrum in 12 body fluids. *Clinical Chemistry* **2010,** *56* (11), 1733-1741.

28. Zampetaki, A.; Kiechl, S.; Drozdov, I.; Willeit, P.; Mayr, U.; Prokopi, M.; Mayr, A.; Weger, S.; Oberhollenzer, F.; Bonora, E., Plasma MicroRNA profiling reveals loss of endothelial MiR-126 and other MicroRNAs in type 2 DiabetesNovelty and significance. *Circulation Research* **2010,** *107* (6), 810-817.

29. Ortega, F. J.; Mercader, J. M.; Moreno-Navarrete, J. M.; Rovira, O.; Guerra, E.; Esteve, E.; Xifra, G.; Martínez, C.; Ricart, W.; Rieusset, J., Profiling of circulating microRNAs reveals common microRNAs linked to type 2 diabetes that change with insulin sensitization. *Diabetes Care* **2014,** *37* (5), 1375-1383.

30. Cissell, K. A.; Shrestha, S.; Deo, S. K., MicroRNA detection: challenges for the analytical chemist. ACS Publications: 2007.

31. Cissell, K. A.; Deo, S. K., Trends in microRNA detection. *Analytical and Bioanalytical Chemistry* **2009,** *394* (4), 1109-1116.

32. Chen, C.; Ridzon, D. A.; Broomer, A. J.; Zhou, Z.; Lee, D. H.; Nguyen, J. T.; Barbisin, M.; Xu, N. L.; Mahuvakar, V. R.; Andersen, M. R., Real-time quantification of microRNAs by stem–loop RT–PCR. *Nucleic Acids Research* **2005,** *33* (20), e179-e179.

33. Tang, F.; Hajkova, P.; Barton, S. C.; Lao, K.; Surani, M. A., MicroRNA expression profiling of single whole embryonic stem cells. *Nucleic Acids Research* **2006,** *34* (2), e9-e9.

34. Schmittgen, T. D.; Lee, E. J.; Jiang, J.; Sarkar, A.; Yang, L.; Elton, T. S.; Chen, C., Real-time PCR quantification of precursor and mature microRNA. *Methods* **2008,** *44* (1), 31-38.

35. Jiang, J.; Lee, E. J.; Gusev, Y.; Schmittgen, T. D., Real-time expression profiling of microRNA precursors in human cancer cell lines. *Nucleic Acids Research* **2005,** *33* (17), 5394-5403.

36. Varkonyi-Gasic, E.; Wu, R.; Wood, M.; Walton, E. F.; Hellens, R. P., Protocol: a highly sensitive RT-PCR method for detection and quantification of microRNAs. *Plant Methods* **2007,** *3* (1), 12.

37. Li, W.; Ruan, K., MicroRNA detection by microarray. *Analytical and Bioanalytical Chemistry* **2009,** *394* (4), 1117-1124.

38. de Planell-Saguer, M.; Rodicio, M. C., Detection methods for microRNAs in clinic practice. *Clinical Biochemistry* **2013,** *46* (10), 869-878.

39. Ferraro, J. R., *Introductory raman spectroscopy*. Academic Press: 2003.

40. Smith, E.; Dent, G., *Modern Raman Spectroscopy: a practical approach*. John Wiley & Sons: 2013.

41. Lee, P.; Meisel, D., Adsorption and surface-enhanced Raman of dyes on silver and gold sols. *The Journal of Physical Chemistry* **1982,** *86* (17), 3391-3395.

42. Smith, W., Practical understanding and use of surface enhanced Raman scattering/surface enhanced resonance Raman scattering in chemical and biological analysis. *Chemical Society Reviews* **2008,** *37* (5), 955-964.

43. Goulet, P. J.; Aroca, R. F., Surface-enhancement of fluorescence near noble metal nanostructures. *Radiative Decay Engineering* **2005**, 223-247.

44. Stacy, A.; Van Duyne, R., Surface enhanced raman and resonance raman spectroscopy in a non-aqueous electrochemical environment: Tris (2, 2′-bipyridine) ruthenium (II) adsorbed on silver from acetonitrile. *Chemical Physics Letters* **1983,** *102* (4), 365-370.

45. Rosi, N. L.; Mirkin, C. A., Nanostructures in biodiagnostics. *Chemical Reviews* **2005,** *105* (4), 1547-1562.

46. Leonhardt, U., Optical metamaterials: Invisibility cup. *Nature Photonics* **2007,** *1* (4), 207-208.

47. Daniel, M.-C.; Astruc, D., Gold nanoparticles: assembly, supramolecular chemistry, quantum-size-related properties, and applications toward biology, catalysis, and nanotechnology. *Chemical Reviews* **2004,** *104* (1), 293-346.

48. Privman, V.; Goia, D. V.; Park, J.; Matijević, E., Mechanism of formation of monodispersed colloids by aggregation of nanosize precursors. *Journal of Colloid and Interface Science* **1999,** *213* (1), 36-45.

49. Turkevich, J.; Stevenson, P.; Hillier, J., The size and shape factor in colloidal systems. *A General Discussion of the Faraday Society* **1951,** *11*, 55.

50. Frens, G., Controlled nucleation for the regulation of the particle size in monodisperse gold suspensions. *Nature* **1973,** *241* (105), 20-22.

51. Pillai, Z. S.; Kamat, P. V., What factors control the size and shape of silver nanoparticles in the citrate ion reduction method? *The Journal of Physical Chemistry B* **2004,** *108* (3), 945-951.

52. Van Hyning, D. L.; Zukoski, C. F., Formation mechanisms and aggregation behavior of borohydride reduced silver particles. *Langmuir* **1998,** *14* (24), 7034-7046.

53. Heard, S. M.; Grieser, F.; Barraclough, C. G.; Sanders, J. V., The characterization of Ag sols by electron microscopy, optical absorption, and electrophoresis. *Journal of Colloid and Interface Science* **1983,** *93* (2), 545-555.

54. Leopold, N.; Lendl, B., A new method for fast preparation of highly surface-enhanced Raman scattering (SERS) active silver colloids at room temperature by reduction of silver nitrate with hydroxylamine hydrochloride. *The Journal of Physical Chemistry B* **2003,** *107* (24), 5723-5727.

55. Ghosh, S. K.; Pal, T., Interparticle coupling effect on the surface plasmon resonance of gold nanoparticles: from theory to applications. *Chem. Rev* **2007,** *107* (11), 4797-4862.

56. Jin, R.; Wu, G.; Li, Z.; Mirkin, C. A.; Schatz, G. C., What controls the melting properties of DNA-linked gold nanoparticle assemblies? *Journal of the American Chemical Society* **2003,** *125* (6), 1643-1654.

57. Jain, P. K.; Huang, X.; El-Sayed, I. H.; El-Sayed, M. A., Review of some interesting surface plasmon resonance-enhanced properties of noble metal nanoparticles and their applications to biosystems. *Plasmonics* **2007,** *2* (3), 107-118.

58. Smith, B. D.; Dave, N.; Huang, P.-J. J.; Liu, J., Assembly of DNA-functionalized gold nanoparticles with gaps and overhangs in linker DNA. *The Journal of Physical Chemistry* **2011**, *115*(16), pp.7851-7857

59. Willets, K. A.; Van Duyne, R. P., Localized surface plasmon resonance spectroscopy and sensing. *Annu. Rev. Phys. Chem.* **2007,** *58*, 267-297.

60. McMahon, J. M.; Henry, A.-I.; Wustholz, K. L.; Natan, M. J.; Freeman, R. G.; Van Duyne, R. P.; Schatz, G. C., Gold nanoparticle dimer plasmonics: finite element method calculations of the electromagnetic enhancement to surface-enhanced Raman spectroscopy. *Analytical and Bioanalytical chemistry* **2009,** *394* (7), 1819-1825.

61. Kleinman, S. L.; Sharma, B.; Blaber, M. G.; Henry, A.-I.; Valley, N.; Freeman, R. G.; Natan, M. J.; Schatz, G. C.; Van Duyne, R. P., Structure enhancement factor relationships in single gold nanoantennas by surface-enhanced Raman excitation spectroscopy. *Journal of the American Chemical Society* **2012,** *135* (1), 301-308.

62. Emamian, S.; Eshkeiti, A.; Narakathu, B. B.; Avuthu, S. G. R.; Atashbar, M. Z., Gravure printed flexible surface enhanced Raman spectroscopy (SERS) substrate for detection of 2, 4-dinitrotoluene (DNT) vapor. *Sensors and Actuators B: Chemical* **2015,** *217*, 129-135.

63. Mirkin, C. A.; Letsinger, R. L.; Mucic, R. C.; Storhoff, J. J., A DNA-based method for rationally assembling nanoparticles into macroscopic materials. *Nature* **1996,** *382* (6592), 607.

64. Alivisatos, A. P.; Johnsson, K. P.; Peng, X.; Wilson, T. E.; Loweth, C. J.; Bruchez, M. P.; Schultz, P. G., Organization of'nanocrystal molecules' using DNA. *Nature* **1996,** *382* (6592), 609-611.

65. Elghanian, R.; Storhoff, J. J.; Mucic, R. C.; Letsinger, R. L.; Mirkin, C. A., Selective colorimetric detection of polynucleotides based on the distance-dependent optical properties of gold nanoparticles. *Science* **1997,** *277* (5329), 1078-1081.

66. Storhoff, J. J.; Elghanian, R.; Mucic, R. C.; Mirkin, C. A.; Letsinger, R. L., One-pot colorimetric differentiation of polynucleotides with single base imperfections using gold nanoparticle probes. *J. Am. Chem. Soc* **1998,** *120* (9), 1959-1964.

67. Pan, W.; Zhang, T.; Yang, H.; Diao, W.; Li, N.; Tang, B., Multiplexed detection and imaging of intracellular mRNAs using a four-color nanoprobe. *Analytical Chemistry* **2013,** *85* (21), 10581-10588.

68. Thompson, D. G.; Enright, A.; Faulds, K.; Smith, W. E.; Graham, D., Ultrasensitive DNA detection using oligonucleotide− silver nanoparticle conjugates. *Analytical Chemistry* **2008,** *80* (8), 2805-2810.

69. Giljohann, D. A.; Seferos, D. S.; Prigodich, A. E.; Patel, P. C.; Mirkin, C. A., Gene regulation with polyvalent siRNA− nanoparticle conjugates. *Journal of the American Chemical Society* **2009,** *131* (6), 2072-2073.

70. Kneipp, K.; Kneipp, H.; Kartha, V. B.; Manoharan, R.; Deinum, G.; Itzkan, I.; Dasari, R. R.; Feld, M. S., Detection and identification of a single DNA base molecule using surface-enhanced Raman scattering (SERS). *Physical Review E* **1998,** *57* (6), R6281.

71. Cao, Y. C.; Jin, R.; Mirkin, C. A., Nanoparticles with Raman spectroscopic fingerprints for DNA and RNA detection. *Science* **2002,** *297* (5586), 1536-1540.

72. Kang, T.; Yoo, S. M.; Yoon, I.; Lee, S. Y.; Kim, B., Patterned multiplex pathogen DNA detection by Au particle-on-wire SERS sensor. *Nano letters* **2010,** *10* (4), 1189-1193.

73. Hao, E.; Schatz, G. C., Electromagnetic fields around silver nanoparticles and dimers. *The Journal of Chemical Physics* **2004,** *120* (1), 357-366.

74. Faulds, K.; Littleford, R. E.; Graham, D.; Dent, G.; Smith, W. E., Comparison of surface-enhanced resonance Raman scattering from unaggregated and aggregated nanoparticles. *Analytical Chemistry* **2004,** *76* (3), 592-598.

75. Harper, M. M.; McKeating, K. S.; Faulds, K., Recent developments and future directions in SERS for bioanalysis. *Physical Chemistry Chemical Physics* **2013,** *15* (15), 5312-5328.

76. Park, S.-J.; Taton, T. A.; Mirkin, C. A., Array-based electrical detection of DNA with nanoparticle probes. *Science* **2002,** *295* (5559), 1503-1506.

77. Graham, D.; Thompson, D. G.; Smith, W. E.; Faulds, K., Control of enhanced Raman scattering using a DNA-based assembly process of dye-coded nanoparticles. *Nature nanotechnology* **2008,** *3* (9), 548-551.

78. McKenzie, F.; Ingram, A.; Stokes, R.; Graham, D., SERRS coded nanoparticles for biomolecular labelling with wavelength-tunable discrimination. *Analyst* **2009,** *134* (3), 549-556.

79. Zhang, X.; Servos, M. R.; Liu, J., Fast pH-assisted functionalization of silver nanoparticles with monothiolated DNA. *Chemical Communications* **2012,** *48* (81), 10114-10116.

80. Rogers, W. B.; Shih, W. M.; Manoharan, V. N., Using DNA to program the self-assembly of colloidal nanoparticles and microparticles. *Nature Reviews Materials* **2016,** *1*, 16008.

81. Kleinman, S. L.; Frontiera, R. R.; Henry, A.-I.; Dieringer, J. A.; Van Duyne, R. P., Creating, characterizing, and controlling chemistry with SERS hot spots. *Physical Chemistry Chemical Physics* **2013,** *15* (1), 21-36.

82. Barrett, L.; Dougan, J. A.; Faulds, K.; Graham, D., Stable dye-labelled oligonucleotide-nanoparticle conjugates for nucleic acid detection. *Nanoscale* **2011,** *3* (8), 3221-3227.

83. Nikolova, E. N.; Goh, G. B.; Brooks III, C. L.; Al-Hashimi, H. M., Characterizing the protonation state of cytosine in transient G· C Hoogsteen base pairs in duplex DNA. *Journal of the American Chemical Society* **2013,** *135* (18), 6766-6769.

84. Liu, J., Adsorption of DNA onto gold nanoparticles and graphene oxide: surface science and applications. *Physical Chemistry Chemical Physics* **2012,** *14* (30), 10485-10496.

85. Hurst, S. J.; Lytton-Jean, A. K.; Mirkin, C. A., Maximizing DNA loading on a range of gold nanoparticle sizes. *Analytical chemistry* **2006,** *78* (24), 8313.

86. McKenzie, F.; Graham, D., Controlled assembly of SERRS active oligonucleotide–nanoparticle conjugates. *Chemical Communications* **2009,** (38), 5757-5759.

87. Keir, R.; Sadler, D.; Smith, W., Preparation of stable, reproducible silver colloids for use as surface-enhanced resonance Raman scattering substrates. *Applied Spectroscopy* **2002,** *56* (5), 551-559.

88. Faulds, K.; McKenzie, F.; Smith, W. E.; Graham, D., Quantitative Simultaneous Multianalyte Detection of DNA by Dual-Wavelength Surface-Enhanced Resonance Raman Scattering. *Angewandte Chemie* **2007,** *119* (11), 1861-1863.

89. Faulds, K.; Smith, W. E.; Graham, D., Evaluation of surface-enhanced resonance Raman scattering for quantitative DNA analysis. *Analytical Chemistry* **2004,** *76* (2), 412-417.

90. Fernandez-Valverde, S. L.; Taft, R. J.; Mattick, J. S., MicroRNAs in β-cell biology, insulin resistance, diabetes and its complications. *Diabetes* **2011,** *60* (7), 1825-1831.

91. Liu, J.; Huang, P.-J. J.; Dave, N.; Smith, B. D., *Assembly of DNA-Functionalized Gold Nanoparticles with Gaps and Overhangs in Linker DNA*. UWSpace: 2011.

92. Storhoff, J. J.; Lucas, A. D.; Garimella, V.; Bao, Y. P.; Müller, U. R., Homogeneous detection of unamplified genomic DNA sequences based on colorimetric scatter of gold nanoparticle probes. *Nature Biotechnology* **2004,** *22* (7), 883-887.

93. Wahl, G. M.; Stern, M.; Stark, G. R., Efficient transfer of large DNA fragments from agarose gels to diazobenzyloxymethyl-paper and rapid hybridization by using dextran sulfate. *Proceedings of the National Academy of Sciences* **1979,** *76* (8), 3683-3687.

94. Hoefler, H.; Childers, H.; Montminy, M. R.; Lechan, R. M.; Goodman, R. H.; Wolfe, H. J., In situ hybridization methods for the detection of somatostatin mRNA in tissue sections using antisense RNA probes. *The Histochemical Journal* **1986,** *18* (11), 597-604.

95. Doering, W. E.; Nie, S., Spectroscopic tags using dye-embedded nanoparticles and surface-enhanced Raman scattering. *Analytical Chemistry* **2003,** *75* (22), 6171-6176.

96. Kim, K.; Lee, H. B.; Lee, Y. M.; Shin, K. S., Rhodamine B isothiocyanate-modified Ag nanoaggregates on dielectric beads: A novel surface-enhanced Raman scattering and fluorescent imaging material. *Biosensors and Bioelectronics* **2009,** *24* (7), 1864-1869.

97. Mao, X.; Ma, Y.; Zhang, A.; Zhang, L.; Zeng, L.; Liu, G., Disposable nucleic acid biosensors based on gold nanoparticle probes and lateral flow strip. *Analytical Chemistry* **2009,** *81* (4), 1660-1668.

98. Hou, S.-Y.; Hsiao, Y.-L.; Lin, M.-S.; Yen, C.-C.; Chang, C.-S., MicroRNA detection using lateral flow nucleic acid strips with gold nanoparticles. *Talanta* **2012,** *99*, 375-379.

99. Fu, X.; Cheng, Z.; Yu, J.; Choo, P.; Chen, L.; Choo, J., A SERS-based lateral flow assay biosensor for highly sensitive detection of HIV-1 DNA. *Biosensors and Bioelectronics* **2016,** *78*, 530-537.

100. Gao, X.; Xu, H.; Baloda, M.; Gurung, A. S.; Xu, L.-P.; Wang, T.; Zhang, X.; Liu, G., Visual detection of microRNA with lateral flow nucleic acid biosensor. *Biosensors and Bioelectronics* **2014,** *54*, 578-584.